

BAND STRUCTURE OF
Fe BASED SUPERCONDUCTORS

TEH YEE LIN

DEPARTMENT OF PHYSICS
FACULTY OF SCIENCE
UNIVERSITY OF MALAYA
KUALA LUMPUR

2010

BAND STRUCTURE OF
Fe BASED SUPERCONDUCTOR

TEH YEE LIN

DISSERTATION SUBMITTED IN FULFILMENT
OF THE REQUIREMENTS
FOR THE DEGREE OF MASTER OF SCIENCE

DEPARTMENT OF PHYSICS
FACULTY OF SCIENCE
UNIVERSITY OF MALAYA
KUALA LUMPUR

2010

Abstract

Several iron containing superconductors are discovered in 2008. The discovery introduced a new class of high-temperature superconductors, which are iron-based. The iron-based superconductors do not resemble conventional superconductors and have properties on their own which differ from the cuprates. We have studied the iron selenium, FeSe compound by removing some Se atoms from the lattice forming Fe:Se = 2:1 and 8:6 and also by replacing the Se vacancy with tellurium, samarium and oxygen atoms forming Fe:Se:Te = 2:1:1 and 8:6:2, Fe:Se:O = 8:6:2 and 8:4:2, FeSeSmO, FeSeTeO, Fe₂SeSm₂O₂, FeSeTeSmO and FeTeSmO. The band structures for each lattice are calculated by using the density-functional theory (DFT) in the local density approximation (LDA). The calculation is done by using polarized as well as unpolarised orbitals. The density of states (DOS) of each compound is also calculated. It is found that the gap is highly anisotropic. There is a pronounced effect on the energy gap upon removing some Se atoms from the lattice as well as substitution of other atoms into the FeSe lattice. The energy gap is reduced by a large amount of energy compared to the pure FeSe lattice. It was also found that the normal state gap also reduces upon oxidation. The normal state energy gap reduction produced by doping is related to the increase in the transition temperature of the superconductor.

Abstrak

Beberapa superkonduktor yang mengandungi ferum telah ditemui pada tahun 2008. Penemuan ini memperkenalkan satu kelas baru bagi superkonduktor suhu tinggi yang berasaskan ferum. Superkonduktor yang berasaskan ferum ini tidak menyerupai superconductor konvensional dan mempunyai ciri-ciri tersendiri berbeza dengan superkonduktor kuprat. Sebatian ferum selenium, FeSe telah dikaji dengan mengeluarkan beberapa atom Se dari kekisi untuk membentuk Fe:Se = 2:1 dan 8:6 dan juga dengan mengganti kekosongan Se dengan atom-atom tellurium, samarium dan oksigen untuk membentuk Fe:Se:Te = 2:1:1 dan 8:6:2, Fe:Se:O = 8:6:2 dan 8:4:2, FeSeSmO, FeSeTeO, Fe₂SeSm₂O₂, FeSeTeSmO dan FeTeSmO. Struktur jalur bagi setiap kekisi dikira dengan menggunakan teori fungsi ketumpatan (DFT) dalam penghampiran ketumpatan tempatan (LDA). Pengiraan telah dibuat dengan menggunakan orbital terketub dan juga dengan orbital tak terketub. Ketumpatan keadaan (DOS) bagi setiap sebatian juga dikira. Didapati bahawa jurang tenaga adalah sangat anisotropik. Terdapat juga perubahan yang jelas pada jurang tenaga apabila beberapa atom Se dikeluarkan dari kekisi FeSe mahu pun diganti dengan atom-atom lain ke dalam kekisi FeSe. Jurang tenaga mengurang dengan besarnya berbanding dengan kekisi FeSe tulen. Jurang keadaan normal juga didapati mengurang semasa pengoksidaan. Pengurangan jurang tenaga untuk keadaan normal hasilan pendopan adalah berkaitan dengan peningkatan dalam suhu peralihan superkonduktor.

Acknowledgment

First and foremost I would like to thank God for giving me the strength and courage for completing this dissertation. Secondly, I would like to thank my parents and my dearest family members who have been supporting me all the way.

I am grateful to my main supervisor, Profesor Dr. Keshav N. Shrivastava for his encouragements, and also his support and teachings throughout the entire research. I wish to thank Prof. Madya Hasan Abu Kassim for his kind cooperation and discussions. I would also wish to thank my lab mates for sharing and discussing related research topics.

I would like to thank University of Malaya, Research University Status Grant (UMRG) and also UM fellowship for supporting me financially in this research. I thank the UMRG for the grant of travel support of participating in the AMNRE in Jakarta and PERFIK in Malacca.

TABLE OF CONTENTS

Abstract	i
Abstrak	ii
Acknowledgements	iv
List of Figures	viii
List of Tables	xii
Chapter 1: Theory	
1.1 Review	1
1.2 Superconductivity	
1.2.1 Introduction	3
1.2.2 Historical Background	5
1.2.3 Meissner Effect	8
1.2.4 BCS Theory of Superconductivity	11
1.2.5 Classification of Superconductors	17
1.2.6 Applications	20
1.3 Density Functional Theory	
1.3.1 Introduction	21
1.3.2 Hartee-Fock Approach	22
1.3.3 The Hohenberg-Kohn Theorem	24
1.3.4 Kohn-Sham Approach	28
1.3.5 Exchange-Correlation	32
1.3.6 Local Density Approximation (LDA)	33

1.3.7 Generalized Gradient Approximation (GGA)	35
1.4 Overview	37
Chapter 2: DFT Computation of the Electronic Band Structure of FeSe	39
2.1 Introduction	40
2.2 Band Structure	41
2.2.1 FeSe	41
2.2.2 Fe:Se = 2:1	45
2.3 Binding Energy	48
2.4 Conclusion	49
Chapter 3: Paramagnetic Meissner Effect in FeSe Superconductor	50
3.1 Introduction	51
3.2 The Meissner Effect	53
3.3 Band Structure	57
3.4 Conclusion	64
Chapter 4: Density-Functional Theory Computation of Oxidation of FeSe	65
4.1 Introduction	66
4.2 Methodology	67
4.2.1 Band structure of Fe ₈ Se ₆ O ₂	67
4.2.2 Band structure of Fe ₈ Se ₄ O ₄	71
4.3 Binding Energy	74
4.4 Conclusion	74
Chapter 5: Electronic Band Structure of FeSeTeO Superconductor	75
5.1 Introduction	76

5.2 The band structure	77
5.3 Conclusions	81
Chapter 6: Band Structure of FeSe with Layers of Samarium and Tellurium Atoms	82
6.1 Introduction	83
6.2 Methodology	84
6.2.1 FeSeSmO	84
6.2.2 Fe ₂ SeSm ₂ O ₂	88
6.2.3 FeSeTeSmO	92
6.2.4 FeTeSmO	96
6.4 Conclusion	100
Chapter 7: Conclusion	101
List of Publications	105
References	106

List of figures

Figure 1.1	The resistance, R versus temperature, T curve of Kamerlingh Onnes indicating the superconducting transition phase.	6
Figure 1.2	The diagram shows the exclusion of magnetic field of the Meissner effect. (a) Magnetic field in the sample before critical temperature (b) The exclusion of the interior magnetic field at critical temperature	6
Figure 1.3	Lattice distortion created by the single electron in the lattice.	12
Figure 1.4	The Feynman diagram in (a) and (b) are the mirror process of phonon emission and absorption between two electrons. k_1 , k_2 and q are the wave vectors.	13
Figure 1.5	The graphs show the magnetization curve of Type I and Type II superconductor with negative magnetization.	19
Figure 1.6	Figure shows the schematic diagram of the approximation used in (a) LDA and (b) GGA calculation	36
Figure 2.1	The figure shows the $P4/nmm$ lattice of FeSe with the Brillouin Zone path	42
Figure 2.2	The band structure of FeSe calculated by using unpolarized orbitals in DFT (LDA).	42
Figure 2.3	The band structure of FeSe calculated by using polarized orbitals.	43
Figure 2.4	The DOS of FeSe for unpolarized orbitals.	44

Figure 2.5	The DOS of FeSe for polarized orbitals	44
Figure 2.6	The polarized band structure of Fe:Se = 2:1 structure.	46
Figure 2.7	The unpolarized band structure of Fe:Se = 2:1 structure.	46
Figure 2.8	The density of states of Fe:Se = 2:1 for unpolarized orbitals	47
Figure 2.9	The density of states of Fe:Se = 2:1 for polarized orbitals	47
Figure 3.1	The susceptibility of the LiFeAs in zero-field cooled and in finite (10G) field cooled samples showing derivations from $-1/4\pi$	56
Figure 3.2	The susceptibility of $K_{0.4}Sr_{0.6}Fe_2Se_2$ as a function of temperature for the zero-field as well as the finite (10G) field cooled samples. The lower zero-field cooled (SCF) does not reach the $-1/4\pi$	56
Figure 3.3	The band structure of Fe_2SeTe calculated by using DFT(LDA)	59
Figure 3.4	The density of electron states (DOS) of Fe_2SeTe calculated from the first principles.	60
Figure 3.5	The band structure of Fe:Se = 8:8 calculated by using polarised orbitals in the DFT(LDA).	60
Figure 3.6	The density of states of Fe:Se = 8:8 calculated by using the polarised orbitals in the DFT(LDA)	61
Figure 3.7	The polarised band structure of 8:6 cell from which Se atoms have been removed.	61
Figure 3.8	The density of states of Fe:Se = 8:6 cell calculated from the DFT(LDA) with polarised orbitals.	62
Figure 3.9	The polarised band structure when vacant sites of Se are occupied by Te atoms so that the ratio of atoms is Fe:Se:Te = 8:6:2	62
Figure 3.10	The density of states (DOS) of Fe:Se:Te = 8:6:2 calculated by polarised orbitals.	63
Figure 4.1	The band structure of $Fe_8Se_6O_2$ calculated by using unpolarized orbitals	69

Figure 4.2	The band structure of $\text{Fe}_8\text{Se}_6\text{O}_2$ calculated by using polarized orbitals	69
Figure 4.3	The DOS of $\text{Fe}_8\text{Se}_6\text{O}_2$ for unpolarized orbitals.	70
Figure 4.4	The DOS of $\text{Fe}_8\text{Se}_6\text{O}_2$ for polarized orbitals.	70
Figure 4.5	The band structure of $\text{Fe}_8\text{Se}_4\text{O}_4$ calculated by using unpolarized orbitals	72
Figure 4.6	The band structure of $\text{Fe}_8\text{Se}_4\text{O}_4$ calculated by using polarized orbitals	72
Figure 4.7	The DOS of $\text{Fe}_8\text{Se}_6\text{O}_2$ for polarized orbitals.	73
Figure 5.1	The band structure of FeSeTeO calculated by using unpolarised orbitals	79
Figure 5.2	The band structure of FeSeTeO calculated by using polarised orbitals	89
Figure 5.3	The DOS of FeSeTeO for unpolarised orbitals.	80
Figure 5.4	The DOS of FeSeTeO for polarised orbitals.	81
Figure 6.1	The unit cell of FeSeSmO stack of atoms.	85
Figure 6.2	The band structure of FeSeSmO calculated by using unpolarised orbitals.	86
Figure 6.3	The band structure of FeSeSmO calculated by using polarised orbitals.	86
Figure 6.4	The DOS of FeSeSmO for unpolarized orbitals.	87
Figure 6.5	The DOS of FeSeSmO for polarized orbitals.	88
Figure 6.6	The unit cell of $\text{Fe}_2\text{SeSm}_2\text{O}_2$ stack of atoms.	89
Figure 6.7	The band structure of $\text{Fe}_2\text{SeSm}_2\text{O}_2$ calculated by using unpolarised orbitals.	90

Figure 6.8 The band structure of $\text{Fe}_2\text{SeSm}_2\text{O}_2$ calculated by using polarised orbitals.	90
Figure 6.9 The DOS of $\text{Fe}_2\text{SeSm}_2\text{O}_2$ for unpolarized orbitals.	91
Figure 6.10 The DOS of $\text{Fe}_2\text{SeSm}_2\text{O}_2$ for polarized orbitals.	91
Figure 6.11 The unit cell of FeSeTeSmO stack of atoms.	93
Figure 6.12 The band structure of FeSeTeSmO calculated by using unpolarised orbitals.	94
Figure 6.13 The band structure of FeSeTeSmO calculated by using polarised orbitals.	94
Figure 6.14 The DOS of FeSeTeSmO for unpolarized orbitals.	95
Figure 6.15 The DOS of FeSeTeSmO for polarized orbitals.	95
Figure 6.16 The unit cell of FeTeSmO stack of atoms.	96
Figure 6.17 The band structure of FeTeSmO calculated by using unpolarised orbitals.	98
Figure 6.18 The band structure of FeTeSmO calculated by using polarised orbitals.	98
Figure 6.19 The DOS of FeTeSmO for unpolarized orbitals.	99
Figure 6.20 The DOS of FeTeSmO for polarized orbitals.	99

List Of Tables

Table 2.1	The band gaps in FeSe in units of eV	43
Table 2.2	The energy gap at various k-points in Fe:Se = 2:1 crystal.	45
Table 3.1	The values of $H_{\text{zero}}/4\pi H$ for Fe containing superconductors (zero-field cooled = ZFC)	55
Table 3.2	The band gap in eV at various K point calculated by using DFT(LDA) (pol=polarised, unpol=unpolarised). The coordinates of the k points are Z(0, 0, 0.5), A(0.5, 0.5, 0.5), M(0.5, 0.5, 0), G(0, 0, 0), R(0, 0.5, 0.5) and X(0, 0.5, 0).	59
Table 3.3	The band gap in eV at various points with varying ratios of atoms calculated using DFT(LDA).	63
Table 3.4	The Fermi energy in eV for the three systems	63
Table 4.1	Coordinate of atoms in $\text{Fe}_8\text{Se}_6\text{O}_2$	68
Table 4.2	The band gap of for polarized as well as unpolarized orbitals	69
Table 4.3	Coordinate of atoms in $\text{Fe}_8\text{Se}_4\text{O}_4$	71
Table 4.4	The band gap of for polarized as well as unpolarized orbitals	72
Table 5.1	Coordinate of atom in FeSeTe	78
Table 5.2	Coordinate of atoms in FeSeTeO	78
Table 5.3	The energy gap of various point in FeSeTe	80
Table 5.4	The energy gap of various point	80

Table 6.1	Some of the Sm containing compounds which have a superconducting phase.	83
Table 6.2	The coordinates of FeSeSmO atoms in a unit cell.	86
Table 6.3	The energy gap for various k points.	87
Table 6.4	The coordinates of Fe ₂ SeSm ₂ O ₂ atoms in a unit cell.	89
Table 6.5	The energy gap for various k points	89
Table 6.6	The coordinates of FeSeTeSmO atoms in a unit cell.	93
Table 6.7	The band gap energies at various k points	93
Table 6.8	The coordinates of FeTeSmO atoms in a unit cell.	96
Table 6.9	The band gap energies at various k points	97
Table 6.10	Fermi energy decreases upon doping with Te and Sm atoms	97

CHAPTER 1

THEORY

1.1 Review

The high temperature superconductivity in cuprates was discovered by Bednorz and Muller in 1986 [1]. This superconductor was highly sought after by scientists until the year 2008, when the iron based superconductor was discovered by Hideo Hosono et al. of the Tokyo Institute of Technology. The lanthanum oxygen fluorine iron arsenide ($\text{LaO}_{1-x}\text{F}_x\text{FeAs}$) was found to superconduct at 26K [2]. Even though, the critical temperature of this new compound is lower than the cuprates with critical temperature higher than 90K, this discovery sparked new interest in many scientists to discover more properties in iron-based superconductors. The FeSe occurring in PbO-type structure, known as the α -FeSe was found to behave like a superconductor at 8K when the compound is deficient of Se atoms, α -FeSe_{1-x}[3-4] at normal pressure. The critical temperature of α -FeSe_{1-x} was raised up to 27 K under high pressure [5].

Later on, FeSe superconductor was found to have higher transition temperature when the Se vacancy is substituted with tellurium atoms. It was also found that FeSe also becomes superconducting upon oxidation [6]. With application of pressure, the

superconducting temperature was raised to ~ 37 K. The conduction in iron-based superconductor is not explained by the periodic symmetry of the lattice structure but by doping and non-stoichiometry of the compound. Hence, the BSC theory does not give a successful explanation to the conductivity in the iron-based superconductors. It is believed that the B.C.S. theory with a suitable consideration of Hubbard hopping terms and the Coulomb repulsion will provide the correct theory of superconductivity.

The Meissner effect theory gives a susceptibility of $-1/4\pi = -0.07961$. However, from the experimental results of Khasanov et al [7], it is found that the iron based superconductor samples give a negative susceptibility value of -0.0155emu/g . This shows the diamagnetic property in iron-based compound which predicts superconductivity. By multiplying the value of the mass density of $\rho = 5.22\text{ g/cm}^3$, the susceptibility becomes -0.08091emu/cm^3 which is slightly higher than the Meissner susceptibility. This suggests that the magnetic field in the samples is not entirely zero and it is represented by an incomplete Meissner effect.

The iron-based superconductors may be categorized as the high-temperature superconductors, but, the superconductor holds large magnetic moment in the normal state, as compared with the cuprate superconductors. The iron-based superconductor has a class of its own.

In this chapter, superconductivity will be discussed in section 1.2 followed by the density functional theory (DFT) in section 1.3. The density functional theory is used to study the properties of the interesting superconductor material. Even though it does not give accurate values, it is sufficient to predict the properties of the normal state of the material.

SECTION 1.2

Superconductivity

1.2.1 Introduction

It was found that certain materials will undergo a phase transition to a state with zero electrical resistance, $R = 0$, at a certain critical temperature, T_c . The electrical resistance is defined from the Ohm's law, resistivity, $R=V/I$, where V is the voltage and I is the current. The conductivity σ is the inverse of the resistivity, ρ , which is the resistance per unit length in a wire, $\sigma =1/\rho$. The current density $J= \sigma E$, where E is the electric field. In order to obtain zero resistance in the sample, the voltage across the sample must be zero. Then, this sample exhibits the character of a perfect conductor with a finite current flow without any energy loss. It was also found that at relatively low temperature, $T < T_c$, the magnetic field inside the sample is zero. Any applied magnetic field on the sample was also found to be deflected from the samples. The phenomenon of the perfect conduction with no applied voltage and the exclusion of magnetic field in a material is called as 'superconductivity' and the material that carries this phenomenon is known as a superconductor. Hence, superconductor can be distinguished from a perfect conductor by two very simple characteristics, which is the zero electrical resistance in the sample and the exclusion of the interior magnetic field.

Different materials superconduct at different critical temperatures and exhibit different phase transitions, while keeping the general properties. Hence, superconductors can be further classified into two different types, which can be easily distinguished by their unique electronic and magnetic properties, namely the Type I superconductor and the Type II superconductor. Type I superconductors generally superconduct at lower temperatures and lower critical field while the type II superconductors superconduct at a higher temperature range with higher critical field with two critical fields. Most of the pure metals in the periodic table such as mercury, tin and lead which are superconductors exhibit type-I superconductivity, whereas most alloys like lead-bismuth alloys, barium-copper-oxide ceramics and highly-doped semiconductors exhibit type-II superconductivity. Noble metals such as gold and silver do not exhibit superconductivity. It is found in Au but the transition temperature is in μK .

Superconductivity is a quantum mechanical phenomenon. Hence, the electronic and magnetic properties of superconductors cannot be understood simply by classical physics of “perfect conductivity”. The exclusion of the interior magnetic field can be explained by the Meissner effect, while the absence of the electrical resistance in a superconductor and the microscopic properties can be accurately explained through the electron pairing via the electron-phonon interaction in the crystal lattice as explained by John Bardeen, Leon Cooper, and Robert Schrieffer, (BCS theory).

1.2.2 Historical Background

In 1911, a Dutch physicist, Heike Kammerlingh Onnes did a study on the electronic property of metals at very low temperatures [8]. Upon studying the property of solid mercury, it was found that the resistance of the solid mercury in the liquid Helium drops gradually with the decrease of temperature. Upon reaching 4.2K, the electrical resistance of the solid Mercury drops abruptly to zero as shown in Fig.1.1. Hence, a perfect conductor that conducts current with zero resistance is found. Onnes named this phenomenon as ‘superconductivity’ and with this discovery which requires liquid helium; he was awarded with Nobel Prize for liquefying helium gas in 1913. Onnes' discovery ignited much interest among scientists to do more experimental work to study this phenomenon further as well as to understand theoretically the explanation of the physics behind the extraordinary discovery. Many more materials were found to be superconducting such as lead with superconducting transition temperature at 7.19K in 1913 and niobium nitride with superconducting transition at 16K in 1941.

The understanding of superconductivity was taken to another notch by Walther Meissner and Ochsenfeld in 1933. By setting the current to run in a circular motion in a superconducting material, an internal magnetic field is formed. When the sample is cooled to the critical temperature T_c , the magnetic field in the sample disappears and expels any external magnetic field as shown in Fig. 1.2. The exclusion of interior magnetic field is known as the Meissner effect [9].

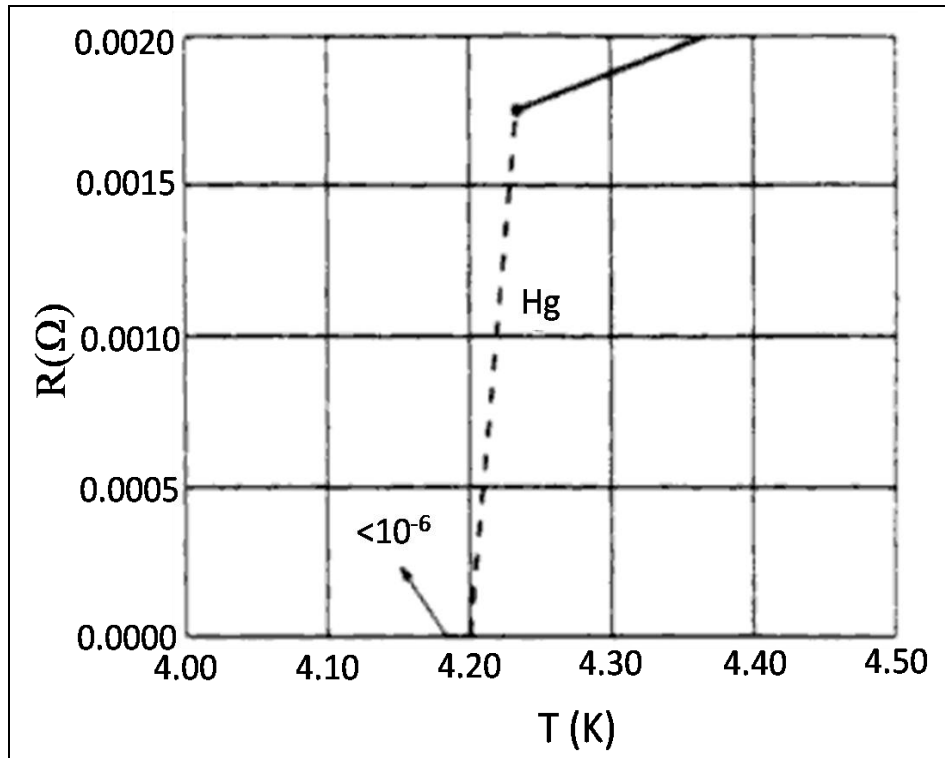
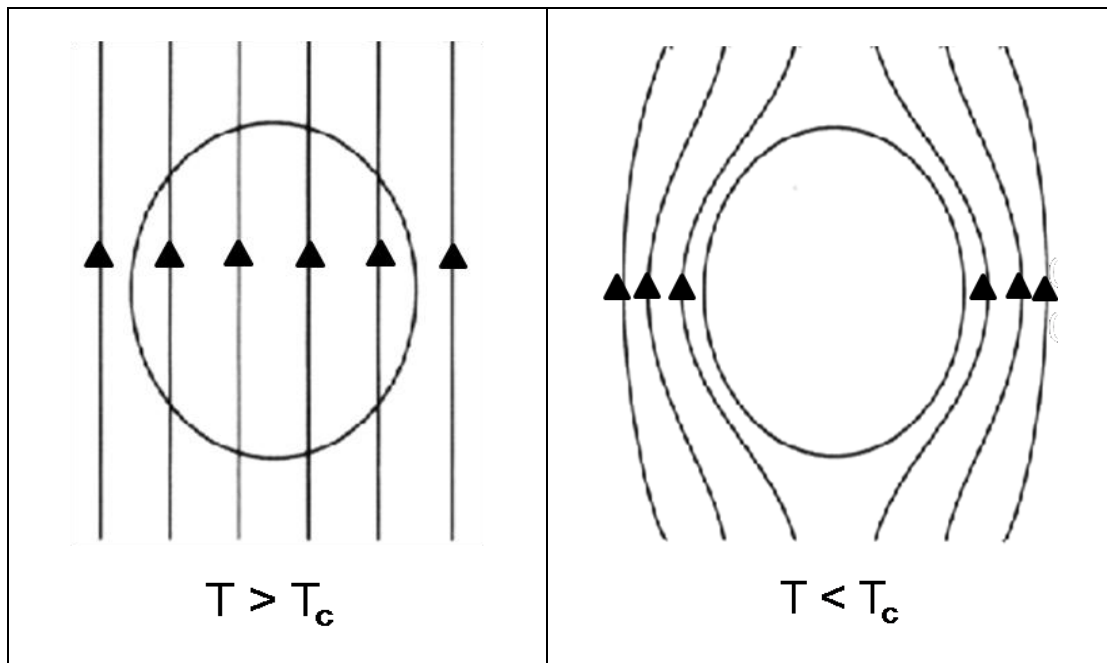


FIGURE 1.1.

The resistance, R versus temperature, T curve of Kammerlingh Onnes, Commun. Phys. Lab. Univ. Leiden, Nos. 122,124 (1911) indicating the superconducting transition phase in mercury.



(a) Magnetic field in the sample before critical temperature

(b) The exclusion of the interior magnetic field at critical temperature

FIGURE 1.2.

The diagram shows the exclusion of magnetic field of the Meissner effect.

Experimental results alone are not enough to explain the unusual phenomenon of superconductivity. Many scientists join in the race to explain their theories. In 1950 Landau and Ginzburg gave a macroscopic explanation for the properties of superconductors by using the thermodynamic arguments, such as the concept of free energy [10]. From there, Abrikosov predicted the two divisions of the superconductors, which is today's type I and Type II superconductors. He also explains the penetration of magnetic flux in the type II superconductors. Also in the same year, Maxwell and Reynolds et al. found that the critical temperature of a superconductor is dependent on the isotopic mass, M , of the constituent element, $T_c \propto 1/\sqrt{M}$.

Later in 1957, John Bardeen, Leon Cooper and Robert Schrieffer introduced the B. C. S. theory that unveils the explanation for the mysterious conductivity in the superconductor by explaining the microscopic properties of superconductors [11]. By modelling the superconducting current as superfluid of Cooper pairs, the zero resistivity conduction is explained by a pair of electrons interacting through the exchange of phonons. The authors of B. C. S. theory were later awarded the Nobel Prize in 1972.

The new era of superconductivity began in 1986 with the discovery of superconductivity in lanthanum-based cuprate perovskite material at 35K by Bednorz and Mueller [1]. The critical temperature was a lot higher than the previous record of 18 K in Nb_3Sn and 23 K for $NbGe$. Later in 1987, a perovskite ceramic material was found to superconduct at 92K. The increasing critical temperature of new material gives rise to the dawn of the high temperature superconductors. Since then the highest temperature superconductor was recorded in 1993, a ceramic material with critical temperature of 138K and 148 K under pressure.

In February 2008, the study of superconductivity shifted its focus from ceramic material to iron-based material. The new material was discovered by Hideo Hosono et al. of the Tokyo Institute of Technology when they found that lanthanum oxygen fluorine iron arsenide ($\text{LaO}_{1-x}\text{F}_x\text{FeAs}$) superconducts at 26K [2]. Subsequent research was done by other scientists after the discovery of Hosono. Substitution of different rare earth materials into $\text{LaO}_{1-x}\text{F}_x\text{FeAs}$ brings the superconducting temperature to 52K. Different type of iron-based materials such as FeS, FeSe and FeTe were also studied [3].

1.2.3 Meissner Effect

The magnetic properties of the superconductors are explained by the Meissner effect. Meissner effect was proposed by Meissner together with Ochsenfeld in 1933. It is also known as the Meissner-Ochsenfeld effect. When the sample is cooled to temperature T_c , any applied external magnetic field is expelled by the sample. This can be explained by Len's law, where the induced magnetic field in a sample tends to oppose the applied magnetic field. Hence, the superconductor is a diamagnetic material and this explains the negative magnetic susceptibility. However, the sample not only expels the applied external field but the original field in the normal sample was also expelled upon cooling. Therefore, a superconductor does not only behave as a diamagnetic material but also involves the Meissner effect. Actually, the spin of the electron gives rise to paramagnetism. If the pairs of electrons are formed, with one electron spin up and the other spin down, the spin of the pair is zero which explains the diamagnetism.

Diamagnetism can be explained by first looking at the Maxwell equation that explains the Faraday's Law of induction.

$$\nabla \times \vec{E} = -\frac{d\vec{B}}{dt} \quad (1.1)$$

The induced voltage is equal to the negative rate of change of magnetic induction, where E is the electric field and B is the magnetic induction. For a diamagnetic material, the magnetic field inside the sample must be constant as a function of time. Then, the rate of change of magnetic induction is then zero.

$$\frac{d\vec{B}}{dt} = 0 \quad (1.2)$$

Then the induced voltage will also be zero.

$$\nabla \times \vec{E} = 0 \quad (1.3)$$

Consider Ohm's Law, $V=IR$, is written as $\mathbf{E}=\rho\mathbf{j}$. Then, $E = 0$ gives zero resistivity. Hence, it is consistent with the definition of diamagnetism, where, zero electrical resistance give rise to zero magnetic fields inside the superconductor.

The equation of magnetic induction, B can be expressed as

$$\mathbf{B} = \mathbf{B}_o + 4\pi\mathbf{M} \quad (1.4)$$

Where, M is the magnetization. The final state of a sample is determined by the process of cooling the sample, which is either field-cooled sample or cooled-field sample. However, either way will give the exclusion of magnetic induction from the interior of the samples. In the case of magnetic superconductors or superconductors containing magnetic impurities, the zero field cooled magnetization is very different from the field-cooled values. The problem of field trapping can be solved separately and hence for the pure superconductors without magnetic impurities we can assume that the field inside

the sample is zero. Hence, assuming that the magnetic field inside the superconductor is zero, the equation becomes,

$$\mathbf{B}_o + 4\pi\mathbf{M} = 0 \quad (1.5)$$

Then, the susceptibility, χ for zero magnetic induction can be written as

$$\chi = \frac{\mathbf{M}}{\mathbf{B}_o} = -\frac{1}{4\pi} \quad (1.6)$$

Thus, susceptibility for zero induction gives a negative value. This is consistent with diamagnetism.

However, when an external magnetic field is applied to a superconducting material, the field is not instantly repelled. It penetrates into the material for a certain depth. As the fields decay exponentially to zero inside the superconducting material, the depth of penetration is called the London penetration depth λ_L and it is expressed as,

$$\nabla \times \vec{\mathbf{j}} = -\frac{\vec{\mathbf{B}}}{\mu_o \lambda_L^2}. \quad (1.7)$$

By taking the Maxwell equation for Ampere's circuit law,

$$\nabla \times \vec{\mathbf{B}} = \mu_o \vec{\mathbf{j}} \quad (1.8)$$

By adding curl to the both side of the equation, the Maxwell equation is now written as,

$$\frac{1}{\mu_o} [\nabla \times (\nabla \times \vec{\mathbf{B}})] = \nabla \times \vec{\mathbf{j}}$$

$$\frac{1}{\mu_o} [\nabla(\nabla \cdot \vec{\mathbf{B}}) - \nabla^2 \vec{\mathbf{B}}] = \nabla \times \vec{\mathbf{j}} \quad (1.9)$$

From Gauss's law of magnetism, $\nabla \cdot \vec{B} = 0$ then $\nabla(\nabla \cdot \vec{B}) = 0$. Then the magnetic induction in the superconductor must be identically zero lest the London penetration depth is infinite. Hence,

$$\frac{1}{\mu_0}(\nabla^2 \vec{B}) = \nabla \times \vec{j} \quad (1.10)$$

Equation (1.7) is then,

$$\frac{\nabla^2 \vec{B}}{\mu_0} = -\frac{\vec{B}}{\mu_0 \lambda_L^2}$$

$$\nabla^2 \vec{B} = \frac{\vec{B}}{\lambda_L^2} \quad (1.11)$$

This gives the fundamental approach to the Meissner effect.

1.2.4 BCS Theory of Superconductivity

The first successful microscopic explanation for the conduction in superconductivity was formulated by Bardeen, Cooper and Schrieffer in 1957. It is known as the BCS theory and it could quantitatively predict the properties of a superconductor. This theory is based on the formation of pairs of electrons of momenta k and $-k$ with one electron spin up and the other spin down, proposed by Leon Cooper, which shows that there is instability of the Fermi surface at the ground state upon the formation of pairs of 'bound' state electrons. This bound pairs of electrons are attracted to each other via the electron-phonon interaction and it is also known as the Cooper pairs.

The zero resistance in superconductivity can be explained by the movement of these Cooper pairs through the lattice unaffected by the thermal vibrations. This is because at low temperatures, the attractive phonon interactions between the electrons are stronger than the interactions between the electrons and ions. Hence, the electron-phonon interaction overcomes the Coulomb interaction. The formation of Cooper pairs can be explained by first explaining the distortion of the crystal lattice by a single electron in the lattice as shown in Fig. 1.3. This distortion of the crystal lattice will form a charge distortion (phonons) of positive charges around the electron. This charge distortion will eventually attract another electron at a certain distance in the lattice forming bound pairs of electrons.

The formation of bound pairs can also be described as the interaction of electrons due to the emission or absorption of lattice phonons. The emission and absorption process can be represented by the famous Feynman diagram as shown in Fig. 1.4.

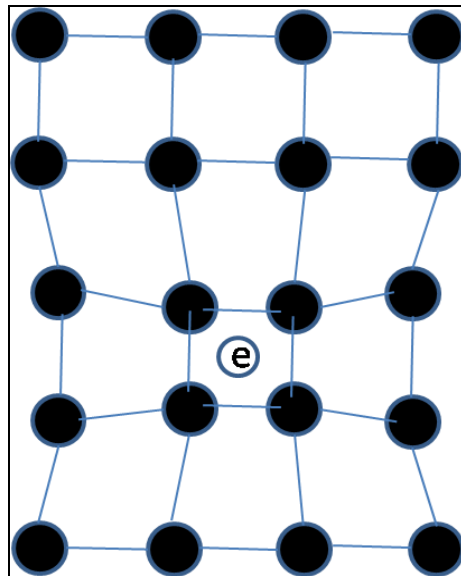


FIGURE 1.3.
Lattice distortion created by the single electron in the lattice.

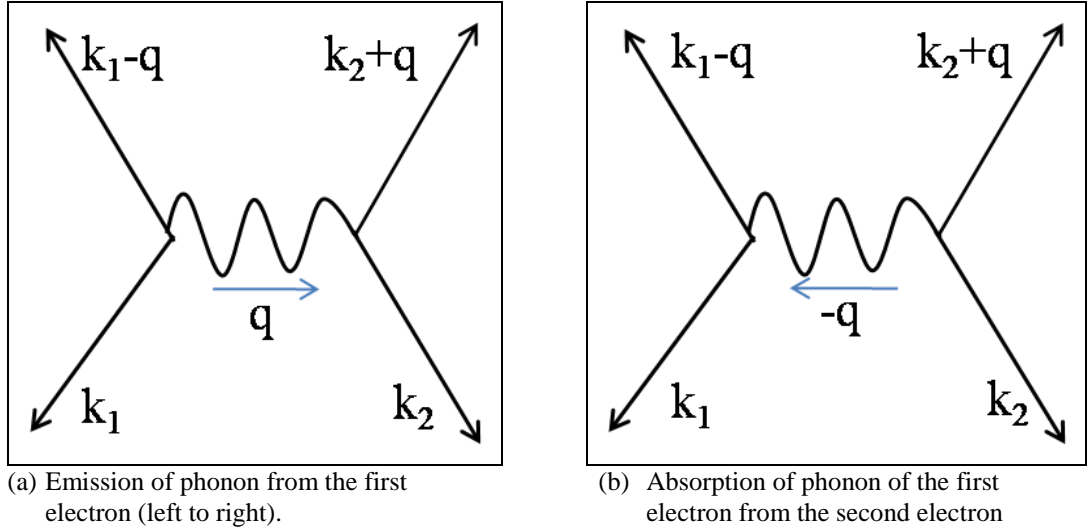


FIGURE 1.4

The Feynman diagrams in (a) and (b) are the mirror process of phonon emission and absorption between two electrons. k_1 , k_2 and q are the wave vectors.

Quantitatively, BCS theory can be explained through quantum mechanical method by the means of second order perturbation theory. The Hamiltonian without the Coulomb repulsion can be defined as

$$H = H_e + H_p + H_{e-p} \quad (1.12)$$

Where, H_e is the ground state Hamiltonian for single electrons. Electron at ground state only fills below the Fermi Energy E_F . Then the unperturbed Hamiltonian for single electron is written as

$$H_e = \sum_k (E_{k\sigma} - E_{F\sigma}) C_{k\sigma}^\dagger C_{k\sigma} \quad (1.13)$$

Where $E_{k\sigma}$ is the single particle energy for electrons and $C_{k\sigma}^\dagger$ ($C_{k\sigma}$) are the creation (annihilation) operators for electrons.

H_p is the unperturbed phonon Hamiltonian which can be defined by the creation a_q^\dagger operator and annihilation a_q operator of phonons and the single quasiparticle frequency $\hbar\omega_q$.

$$H_p = \sum_q \hbar\omega_q a_q^\dagger a_q \quad (1.14)$$

The Hamiltonian for electron-phonon interaction, H_{e-p} can be written as

$$H_{e-p} = \sum_{k_1, k_2, q} \lambda C_{k\sigma}^\dagger C_{k\sigma} (a_q + a_{-q}^\dagger) \delta(k'+q-k) + h.c \quad (1.15)$$

Where, λ is the dimensionless parameter.

The creation and annihilation operators for electrons can be written in the form of the number of particle n_k of a given wave vector k .

$$\begin{aligned} C_{k\sigma}^\dagger |n_1, \dots, n_k, \dots\rangle &= \theta_k (1 - n_k) |n_1, \dots, 1 - n_k, \dots\rangle \\ C_{k\sigma} |n_1, \dots, n_k, \dots\rangle &= \theta_k n_k |n_1, \dots, 1 - n_k, \dots\rangle \end{aligned} \quad (1.16)$$

where $\theta_k = (-1)^{\nu_k}$, $\nu_k = \sum_{j=1}^{k-1} n_j$. The second order perturbation energy for one phonon leaving the electron of wave vector k_1 with wave vector $k_2 = k_1 - q$ can be formulated as

$$\begin{aligned} E^{(2)} &= \sum_{k_1, k_2} \lambda^2 \frac{\langle n_{k_1} + 1, n_{k_2} | H | n_{k_1}, n_{k_2} + 1 \rangle \langle n_{k_1}, n_{k_2} + 1 | H | n_{k_1} + 1, n_{k_2} \rangle}{E_{k_1} - E_{k_2} - \hbar\omega_q} \\ E^{(2)} &= \sum_{k_1, q} \lambda^2 \frac{\langle n_{k_1} + 1, n_{k_1-q} | H | n_{k_1}, n_{k_1-q} + 1 \rangle \langle n_{k_1}, n_{k_1-q} + 1 | H | n_{k_1} + 1, n_{k_1-q} \rangle}{E_{k_1} - E_{k_1-q} - \hbar\omega_q} \\ E^{(2)} &= \sum_{k_1, q} \lambda^2 \frac{C_{k_1-q}^\dagger C_{k_1} C_{k_1}^\dagger C_{k_1-q}}{E_{k_1} - E_{k_1-q} - \hbar\omega_q} \end{aligned} \quad (1.17)$$

Similarly, the mirror process of phonon emission from the second electron can be written as

$$E^{(2)} = \sum_{k_2, q} \lambda^2 \frac{C_{k_2+q}^\dagger C_{k_2} C_{k_2}^\dagger C_{k_2+q}}{E_{k_2} - E_{k_2+q} - \hbar\omega_q} \quad (1.18)$$

By taking the 4 vector as conserved, three components of the wave vector and the complex frequency, the equation for the conservation of momentum and energy can be defined as,

$$k_1 = k_2 + q \quad (1.19)$$

$$E_{k_1} + E_{k_2} = E_{k_1-q} + E_{k_2+q} \quad (1.20)$$

Then the final effective interaction can be written by summing both equations of the mirror process, equation (1.17) and equation (1.18).

$$\begin{aligned}
H^{(2)} &= \sum_{k_1, q} \lambda^2 \frac{C_{k_1-q}^\dagger C_{k_1} C_{k_1}^\dagger C_{k_1-q}}{E_{k_1} - E_{k_1-q} - \hbar\omega_q} + \sum_{k_2, q} \lambda^2 \frac{C_{k_2+q}^\dagger C_{k_2} C_{k_2}^\dagger C_{k_2+q}}{E_{k_2} - E_{k_2+q} - \hbar\omega_q} \\
&= \sum_{k_1, k_2, q} \lambda^2 \frac{C_{k_2} C_{k_2+q}^\dagger C_{k_1} C_{k_1-q}^\dagger}{E_{k_1} - E_{k_1-q} - \hbar\omega_q} + \sum_{k_2, q} \lambda^2 \frac{C_{k_1} C_{k_1-q}^\dagger C_{k_2} C_{k_2+q}^\dagger}{E_{k_1-q} - E_{k_1} - \hbar\omega_q} \\
&= \sum_{k_1, k_2, q} \lambda^2 \frac{(E_{k_1} - E_{k_1-q} + \hbar\omega_q) - (E_{k_1} - E_{k_1-q} - \hbar\omega_q)}{(E_{k_1} - E_{k_1-q})^2 - (\hbar\omega_q)^2} (C_{k_2+q}^\dagger C_{k_2} C_{k_1-q}^\dagger C_{k_1}) \\
&= \sum_{k_1, k_2, q} \lambda^2 \frac{2\hbar\omega_q}{(E_{k_1} - E_{k_1-q})^2 - (\hbar\omega_q)^2} C_{k_2+q}^\dagger C_{k_2} C_{k_1-q}^\dagger C_{k_1}
\end{aligned} \tag{1.21}$$

When $E_{k_1} - E_{k_2} < \hbar\omega_q$ then the interaction becomes negative and thus, describes the attractive force between the electrons. Hence, the electrons will form pairs of zero spin and zero momentum which can be represented by

$$H^{(2)} = \sum_{k, -k, q} \lambda^2 \frac{2\hbar\omega_q}{(E_k - E_{-k})^2 - (\hbar\omega_q)^2} C_{k\uparrow}^\dagger C_{-k\downarrow}^\dagger C_{k\uparrow} C_{-k\downarrow} \tag{1.22}$$

This equation describes the bound state of the electrons in the BCS theory, where the pairs $(k\uparrow, -k\downarrow)$ are called the Cooper pairs. Hence, the electron pairs are correlated due to the Pauli Exclusion principles of electrons to form the Cooper pairs. In a full calculation, there will be other interactions in the Hamiltonian such as the Coulomb repulsive interaction between electrons which require the Bogoliubov transformation.

Superconductivity is destroyed when the electron-phonon interactions no longer exists. That happens when the Cooper pairs begin to break up at certain critical temperature and certain amount of energy is required in order to break the bound pair of electrons which are strongly correlated together. Hence, the BCS theory predicts an energy gap,

E_g at temperature T which is dependent on the critical temperature, T_c . The energy gap approaching the critical temperature, T_c can be defined as

$$E_g = 3.2k_B T_c \sqrt{1 - \frac{T}{T_c}} \quad (1.23)$$

Where, k_B is the Boltzmann's constant. The energy gap of the superconductor decreases as the transition temperature increases. However, the energy gap vanishes when the temperature, $T = T_c$. Hence, the increase in temperature will lessen the pair interaction energy which leads to the decrease of the energy gap. The Cooper pairs are formed below a transition temperature. Above that, the Cooper pair will break into two quasi-particles that behave almost like free electrons. This is when the superconductivity is destroyed. At absolute zero, $T = 0K$, the theory also predicts that the critical temperature, T_c is related to the energy gap, E_g by

$$E_g = 2\Delta(0) = 3.5k_B T_c \quad (1.24)$$

Where, Δ is the surface energy parameter which is defined by

$$\Delta = 2\hbar\omega e^{-1/N(0)V} \quad (1.25)$$

and, N is the density of states for electrons at the Fermi energy and V is the attractive potential for the one electron state at the Fermi energy.

By substituting equation (1.25) for Δ in equation (1.24), then,

$$3.5k_B T_c = 4\hbar\omega e^{-1/N(0)V} \quad (1.26)$$

This shows that the transition temperature is proportional to the phonon frequency, $\hbar\omega$.

In harmonic oscillator, frequency is expressed as

$$f = \hbar\omega = \frac{1}{2\pi} \sqrt{\frac{k}{M}} \quad (1.27)$$

Hence, the frequency is proportional to the inverse square root of mass of an atom.

Therefore, the transition temperature varies with the inverse square root of mass.

$$T_c \propto \frac{1}{\sqrt{M}} \quad (1.28)$$

Where, M is the isotopic mass. This explains the origin of the isotope effect. The transition temperature increases with decreasing isotopic mass.

1.2.5 Classification of Superconductors

Superconductors can be classified into two types, namely the Type I superconductor and the Type II superconductor. Both superconductors share many common properties but show different magnetic behaviour. Type I superconductor exhibits zero resistivity and exclusion of magnetic field from the interior of the superconductor (Meissner effect) at relatively low temperature, namely below the critical temperature, T_c . This superconductor only has one critical field, H_c , where superconductivity is destroyed when the applied magnetic field is beyond that critical field value. The critical magnetic field varies with temperature and it can be written as

$$H_c = H_c^0 \left(1 - \frac{T}{T_c}\right)^{1/2} \quad (1.29)$$

For any field below the critical field, the magnetization is negative, giving a diamagnetic material. The microscopic properties of Type I superconductors are accurately described by the BCS theory and it is also known as the conventional superconductor.

Type II superconductors are somehow much more complicated than the Type I superconductors. Besides sharing the similarity of zero resistivity below the transition temperature, Type II superconductors have two critical fields, one coming from the London penetration depth and the other from the coherence length. Due to scattering from the magnetic atoms, the transition temperature of the type-II superconductors is lower than those of type-I superconductors. The two critical magnetic fields which can be represented by

$$H_{c1} = \frac{\phi_0}{\pi\lambda_L^2}$$

$$H_{c2} = \frac{\phi_0}{\pi\xi^2} \tag{1.30}$$

where, λ_L is the London penetration depth and ξ is the coherent length. Below the lower critical field H_{c1} , superconductivity is formed with zero magnetic fields in the samples. This is known as the Meissner phase. When $H_{c1} < H < H_{c2}$, vortices are formed in the samples due to the small penetration of the magnetic field due to magnetic atoms. In this region, the superconductivity is maintained disregard of the field in the vortice. This region is also called the Abrikosov mixed phase region. Any applied magnetic field beyond the upper critical field H_{c2} , superconductivity is destroyed and the samples return to the normal phase. The magnetization is negative below the lower and the upper critical fields. Above the upper critical field, the normal magnetization is formed, where the superconductivity is suppressed. The magnetization curve is shown in Fig. 1.5.

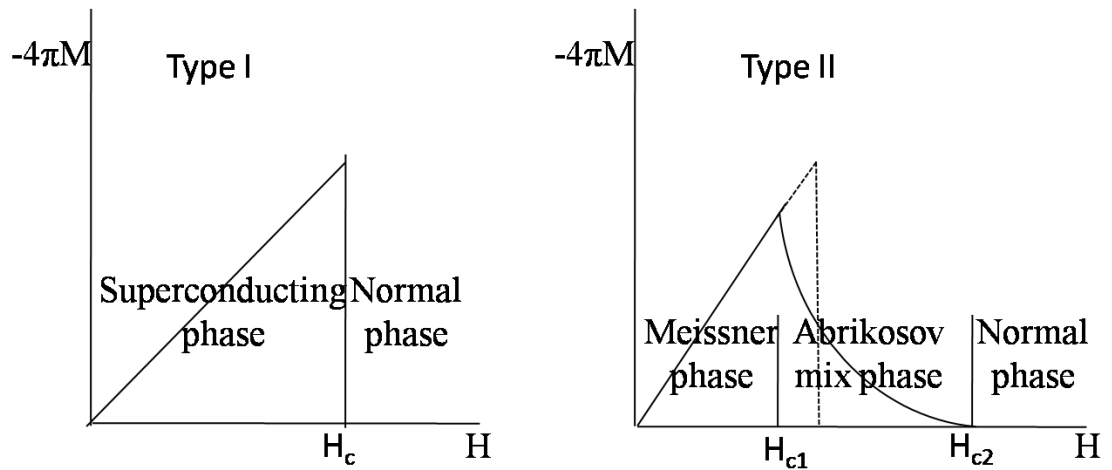


FIGURE 1.5.
The graphs show the magnetization curve of Type I and Type II superconductors with negative magnetization.

In the Abrikosov mixed phase, the high temperature superconductor allows certain amount of magnetic field to penetrate the sample. Hence, this explains the higher upper critical field in the type-II superconductors. The BCS theory is not sufficient to explain the conduction in the high-temperature superconductor and hence, Type II superconductors are also known as the unconventional superconductors.

1.2.6 Applications

After the discoveries of new superconducting materials and the gradual improvement in theoretical understanding, superconductor technology has eventually been put into applications. Since the critical temperature of the material obtained is moving toward a higher temperature, the cooling process has evolved from the expensive liquid helium to liquid hydrogen. Superconducting magnets are some of the most powerful magnets known today. It has been widely used in laboratories and hospitals all over the industrialised world. Some of the well known laboratories machines that adopt the application of superconductors are the, mass spectrometers and the beam-steering magnets in the particle accelerator. Magnetic Resonance Imaging, (MRI) is one of the most well known machines used in hospitals to make a thorough scanning of human bodies by using magnetic resonance. The powerful magnetic fields in these applications are generated by superconductors.

The discovery of high-temperature superconductors with transition temperature closer to the room temperature gives a new face lift to the superconductor technology. Upon approaching the room temperature, cooling system is becoming less important in order to maintain the superconducting state. When this is eliminated, future machines and more applications can be produced with much lower cost with higher efficiency. However, much more theoretical and experimental work has to be done to achieve the cost-effective room temperature superconductor.

SECTION 1.3

The Density Functional Theory

1.3.1 Introduction

Density functional theory (DFT) is one of the most popular methods used for “ab initio” calculation of the electronic properties of molecules and other finite systems. It is also important for quantitative studies. This method is first approached by Hartree-Fock wave functions by considering only the interaction of electrons with its closest neighbours. Hohenberg-Kohn then extends the approach to many-body systems of interacting particles by proving two theorems. However, Hohenberg-Kohn attempt was not sufficient to provide any information to understand the property of a given material. The Hohenberg-Kohn attempt is then improved by Kohn-Sham approach by replacing the many-body system of interacting particles with an auxiliary independent particle problem. The local density approximation (LDA) and the generalized gradient approximation (GGA) are the most widely used approximations to approximate the exchange-correlation energy functional. These two approximations provide the most promising approach for practical methods in the theory of material in DFT. Thus, the many-body particle problem becomes more feasible with a higher accuracy.

1.3.2 Hartree-Fock Approach

The earliest attempt to approximate a wave function of electrons is done by Hartree [12] by writing the many-electron wave function $\Psi(\mathbf{r})$ as a product of single particle functions $\Phi(\mathbf{r})$. This can be defined as

$$\Psi(\vec{r}_1, \vec{r}_2, \dots, \vec{r}_N) = \Phi_1(\vec{r}_1)\Phi_2(\vec{r}_2)\dots\Phi_N(\vec{r}_N) \quad (1.31)$$

Where \mathbf{r}_i is the positional coordinate and spin coordinate for the i^{th} electron. The individual one-electron function Φ_i is called the orbital and it describes each electron in the system. In the Hartree potential the electron does not interact with another electron one-by-one. They interact with the average density of the electrons. The many-body electron Schrödinger equation can be solved as N independent electron equations with a potential field arising from the average field of the other electrons. The equation can be defined as

$$\left(-\frac{\hbar^2}{2m}\nabla^2 + V_{\text{ext}} + \Phi_i \right) \Phi_i(\vec{r}) = \epsilon_i \Phi_i \quad (1.32)$$

From these orbitals, Φ , a many electron wave function, Ψ can be formed according to equation (1.29), and then the total energy, E of the ground state can be calculated. Since the electrons are interacting with an average density, then the Coulomb interaction is taken into account upon solving Φ_i and ϵ_i . However, there will be overlapping of interactions upon adding together the energies, i.e., the overlap of interaction between the orbitals of (1,2) and (2,1). This approximation is then corrected by “Hartree-Fock” approximation by taking the Pauli exclusion principle into consideration where each electron is described by a different wave function because each electron has different quantum numbers. With this, Hartree-Fock approximation uses the Slater determinant method to obtain the wave function rather than the product of orbitals. Hence, the

method for finding the best single determinant wave function for a system is known as the Hartree-Fock method.

$$\Psi(\vec{r}_1, \vec{r}_2, \dots, \vec{r}_N) = \frac{1}{\sqrt{N!}} \begin{vmatrix} \Phi_1(\vec{r}_1) & \Phi_2(\vec{r}_1) & \dots & \Phi_N(\vec{r}_1) \\ \Phi_1(\vec{r}_2) & \Phi_2(\vec{r}_2) & \dots & \Phi_N(\vec{r}_2) \\ \vdots & \vdots & \ddots & \vdots \\ \Phi_N(\vec{r}_1) & \Phi_N(\vec{r}_2) & \dots & \Phi_N(\vec{r}_N) \end{vmatrix} \quad (1.33)$$

The single determinant complicates the equation by an additional, non-local exchange term in the Schrödinger equation. However, the additional term improves the total energy. Hence, the Hartree-Fock equation is defined by

$$\left(\frac{\hbar^2}{2m} \nabla^2 + V_{\text{ext}}(\vec{r}_1) + \int \frac{e^2 d\vec{r}_2}{|\vec{r}_1 - \vec{r}_2|} \right) \Phi_i(\vec{r}_1) + \int v_x(\vec{r}_1, \vec{r}_2) \Phi_i(\vec{r}_2) d\vec{r}_2 = \varepsilon_i \Phi_i(\vec{r}_1) \quad (1.34)$$

where, v_x is the non-local exchange potential. The Hartree-Fock equations describe non-interacting electrons under the influence of a mean field consisting of the classical Coulomb potential and a non-local exchange potential. However, electrons do not interact with the average potential field but they interact in pairs. The electrons correlate their movements such that they are separated with the minimum amount of electrostatic repulsion. The Hartree-Fock method does not take into account for the dynamic correlations.

1.3.3 The Hohenberg-Kohn Theorem

In 1964, Hohenberg and Kohn made a fresh attempt to formulate the density functional theory as an exact theory of many-body systems by viewing the property of a system of many interacting particles as a function of the ground state density [13-17]. Hohenberg and Kohn formulated the theory by proving two theorems [13]. This attempt marks the beginning of the development of DFT and it provides a basic picture for the modern density functional method.

The first theorem from Hohenberg and Kohn is stated as:

For any system of interacting particles in an external potential $V_{\text{ext}}(\vec{r})$, the potential can be determined by the ground state density alone, $n_0(\vec{r})$ within an additive constant. Therefore, all properties of the system can be written as a functional of the ground state density.

The first theorem of Hohenberg-Kohn is proved by first assuming that there are two different external potentials $V_{\text{ext}}^{(1)}(\vec{r})$ and $V_{\text{ext}}^{(2)}(\vec{r})$ which differ by more than a constant.

These two potentials will eventually lead to the same ground state density, $n_0(\vec{r})$.

$$V_{\text{ext}}^{(1)}(\vec{r}) \neq V_{\text{ext}}^{(2)}(\vec{r}) \quad (1.35)$$

The two external potentials then lead to two different Hamiltonians and two different ground state wave functions.

$$\hat{H}^{(1)} = H_0 + V_{\text{ext}}^{(1)}(\vec{r}); H^{(1)}\Psi^{(1)} = E^{(1)}\Psi^{(1)} \quad (1.36)$$

$$\hat{H}^{(2)} = H_0 + V_{\text{ext}}^{(2)}(\vec{r}); H^{(2)}\Psi^{(2)} = E^{(2)}\Psi^{(2)} \quad (1.37)$$

Hence, the ground state energies, E_o , can be written as

$$E_o = \langle \Psi^{(1)} | H^{(1)} | \Psi^{(1)} \rangle \quad (1.38)$$

and

$$E_o = \langle \Psi^{(2)} | H^{(2)} | \Psi^{(2)} \rangle \quad (1.39)$$

respectively. The expectation value can be calculated by using the variational principles as shown in equation (1.38) by assuming that the ground state is non-degenerate.

$$E_o = \langle \Psi^{(1)} | H^{(1)} | \Psi^{(1)} \rangle \langle \Psi^{(2)} | H^{(1)} | \Psi^{(2)} \rangle \quad (1.40)$$

where,

$$\begin{aligned} \langle \Psi^{(2)} | \hat{H}^{(1)} | \Psi^{(2)} \rangle &= \langle \Psi^{(2)} | \hat{H}^{(2)} | \Psi^{(2)} \rangle + \langle \Psi^{(2)} | \hat{H}^{(1)} - \hat{H}^{(2)} | \Psi^{(2)} \rangle \\ &= E^{(2)} + \int d^3r [V_{ext}^{(1)}(\vec{r}) - V_{ext}^{(2)}(\vec{r})] n_o(\vec{r}). \end{aligned} \quad (1.41)$$

Hence,

$$E^{(1)} < E^{(2)} + \int d^3r [V_{ext}^{(1)}(\vec{r}) - V_{ext}^{(2)}(\vec{r})] n_o(\vec{r}) \quad (1.42)$$

Similarly, $E^{(2)}$ can be calculated by

$$E^{(1)} < E^{(2)} + \int d^3r [V_{ext}^{(1)}(\vec{r}) - V_{ext}^{(2)}(\vec{r})] n_o(\vec{r}) \quad (1.43)$$

By summing both equations (1.42) and (1.43) together,

$$E^{(1)} + E^{(2)} < E^{(2)} + E^{(1)} \quad (1.44)$$

Hence, it can be concluded that there cannot be two different external potentials that yield the same ground state density, $n_o(\vec{r})$. Therefore, the density uniquely determines the external potential to within an additive constant as stated by the Hohenberg-Kohn first theorem.

Since the Hamiltonian is uniquely determined by the ground state density, the wave function of any state is determined by solving the Schroedinger equation with this Hamiltonian. The unique ground state wave function is one that has the lowest energy. All the ground state properties including the kinetic energy of electron, T_e and the internal potential, V_{int} are also determined by the ground state density,

$$E(n) = T_e(n) + V_{\text{int}}(n) + V_{\text{ext}}(n) \quad (1.45)$$

where the Hohenberg-Kohn functional is defined as

$$F_{\text{HK}}(n) = T_e(n) + V_{\text{int}}(n) \quad (1.46)$$

Hence,

$$E(n) = V_{\text{ext}}(n) + F_{\text{HK}}(n) = \int n(\vec{r})V_{\text{ext}}(\vec{r})d\vec{r} + F_{\text{HK}}(\vec{n}) \quad (1.47)$$

The Hohenberg-Kohn second theorem states that:

The ground state energy and density can be determined by the variation method alone. For any particular $V_{\text{ext}}(\vec{r})$, the ground state density $n_0(\vec{r})$ minimises the functional giving a global minimum value.

The second theorem can be proved by first recalling the equation (1.47)

$$E(n) = \int n(\vec{r})V_{\text{ext}}(\vec{r})d\vec{r} + F_{\text{HK}}(\vec{n}) \quad (1.47)$$

where FHK is the Hohenberg-Kohn functional which is defined by $T(n) + E_{\text{int}}(n)$.

The ground state density $n^{(1)}(\vec{r})$ corresponds to the external potential, $V_{\text{ext}}^{(1)}(\vec{r})$. Hence,

the corresponding ground state wave function is $\Psi^{(1)}$.

The expectation value of the Hamiltonian is the unique ground state which can be written as

$$E^{(1)} = \langle \Psi^{(1)} | H^{(1)} | \Psi^{(1)} \rangle = E_{\text{HK}}[n^{(1)}]. \quad (1.48)$$

Next consider a new density of $n^{(2)}(\vec{r})$ which corresponds to a new wave function $\Psi^{(2)}$.

Hence, the new energy $E^{(2)}$ of this state can be written as

$$E^{(2)} = \langle \Psi^{(2)} | H^{(1)} | \Psi^{(2)} \rangle = E_{\text{HK}}[n^{(2)}]. \quad (1.49)$$

By comparing equations (1.48) and (1.49), it is clearly noted that $E^{(2)}$ is larger than $E^{(1)}$.

$$E^{(1)} = \langle \Psi^{(1)} | H^{(1)} | \Psi^{(1)} \rangle < \langle \Psi^{(2)} | H^{(1)} | \Psi^{(2)} \rangle = E^{(2)} \quad (1.50)$$

It can be concluded that the Hohenberg-Kohn functional evaluated for the correct ground state density is lower than the value for any other density. Hence, the second theorem of Hohenberg-Kohn is proved.

Now, with a known $F_{\text{HK}}(n)$, the exact ground state density can be determined by minimising the total energy of the system with respect to the variations in the density function $n(\vec{r})$. However, by only looking at the density, the density-functional theory does not provide an understanding of the electronic properties of the material. There is also no direct method to calculate the kinetic energy in equation (1.47) directly from the density. In conclusion, the Hohenberg-Kohn-Sham approach is correct in principle, but it is sufficient in practice to relate to the properties of a material.

1.3.4 Kohn-Sham Approach

Hohenberg-Kohn approach tried to solve the density functional theory (DFT) by taking the property of many-body system of interacting particles as a function of ground state density. The Hohenberg-Kohn approach can be expressed as equation (1.47)

$$E(n) = \int n(\vec{r})V_{\text{ext}}(\vec{r})d\vec{r} + F_{\text{HK}}(\bar{n}) \quad (1.47)$$

where, F_{HK} is the universal functional of ground state density, n , which comprise of the electron kinetic energy and the internal potential. This can be defined as

$$F_{\text{HK}} = \sum_i^N -\frac{\hbar^2}{2m} \nabla_i^2 + \frac{1}{2} \sum_{i \neq j} \frac{e^2}{|\vec{r}_i - \vec{r}_j|} \quad (1.51)$$

by using the Hartree atomic unit, $\hbar = m = e = 1$. Hohenberg-Kohn approach is correct in principle; however it is insufficient in practice. This is because it does not provide a way to understand the property of a material just by looking at the form of the density.

In 1965, Kohn and Sham proposed an improved approach to solve the density functional theory (DFT). Today, it is known as the Kohn-Sham ansatz. The Kohn-Sham approach replaces the many-particle problem with an auxiliary independent particle problem. This involves independent particles but an interacting density. Hence, this leads to exact calculation of the properties of many-body system by using independent particle method. This success becomes the basis of the most calculation that attempt to make “ab initio” prediction for the properties of a material.

The Kohn-Sham approach is derived upon two basic assumptions. Firstly, the exact ground state density can be represented by that of an auxiliary system of non-interacting

particles. This means the ground state density of interacting system is the same as that of the non-interacting system,

$$n_o(\vec{r}) = n_{\text{KS}}(\vec{r}). \quad (1.52)$$

This leads to the relation of the actual and auxiliary system as shown below.

$$V_{\text{ext}}(\vec{r}) \leftarrow n_o(\vec{r}) \Leftrightarrow n_{\text{KS}}(\vec{r}) \rightarrow V_{\text{KS}}(\vec{r}) \quad (1.53)$$

Secondly, the auxiliary Hamiltonian is chosen to have the usual kinetic operator and effective potential, $V_{\text{ext}}(\vec{r})$ acting on an electron of spin, s at point, \vec{r} . The Hamiltonian can be defined as

$$\hat{H} = \frac{\hbar^2}{2m} \nabla^2 + V_{\text{eff}}(\vec{r}) \quad (1.54)$$

By using the Hartree atomic unit, the Hamiltonian can be further simplified to

$$\hat{H} = -\frac{1}{2} \nabla^2 + V_{\text{eff}}(\vec{r}) \quad (1.55)$$

Hence, for N independent particles where $N = N(\uparrow) + N(\downarrow)$, each spin, s occupies respective orbitals, i , $\Phi_i^s(\vec{r})$ with the lowest eigenvalue $E_i^s(\vec{r})$ of the ground state. This can be represented by the Schrödinger equation.

$$\left[-\frac{1}{2} \nabla^2 + V_{\text{eff}}(\vec{r})\right] \Phi_i^s(\vec{r}) = E_i^s \Phi_i^s(\vec{r}). \quad (1.56)$$

In Hohenberg-Kohn (HK) approach, the universal functional F_{HK} comprises of the electron kinetic energy and the interaction potential. Kohn-Sham improved the Hohenberg-Kohn expression by separating the universal functional into three parts. The first two parts remain the same as for the Hohenberg-Kohn expression. Kohn-Sham

adds in the third part of the functional with the exchange-correlation functional. Hence, the Kohn-Sham approach can be expressed as

$$E[n(\vec{r})] = T_s[n] + E_{\text{Hartree}}[n] + E_{\text{xc}}[n] + \int n(\vec{r})V_{\text{ext}}(\vec{r})d\vec{r} + E_{11} \quad (1.57)$$

where, E_{11} is the nuclei-nuclei interaction and T_s is the independent particle kinetic energy which is defined by

$$T_s[n(\vec{r})] = -\frac{1}{2} \sum_{i=1}^N \int \Phi_i^* \nabla^2 \Phi_i d\vec{r} \quad (1.58)$$

E_{Hartree} is the Hartree energy which is the electron-electron interaction determined by the classical Coulomb interaction energy. It can be expressed as

$$E_{\text{Hartree}}[n(\vec{r})] = -\frac{1}{2} \iint \frac{n(\vec{r}_1)n(\vec{r}_2)}{|\vec{r}_1 - \vec{r}_2|} d\vec{r}_1 d\vec{r}_2 \quad (1.59)$$

The solution of this auxiliary system for ground state can be view as the problem of minimization with respect to density. Since, only T_s is expressed as a the function of orbitals, it can be differentiated directly with respect to $\Phi^*(\vec{r})$. All other term are expressed as a function of density. Hence, chain rule is used to derive the variational equation.

$$\frac{\delta E}{\delta \Phi^*} = \frac{\delta T_s}{\delta \Phi^*} + \left[\frac{\delta V_{\text{ext}}}{\delta n} + \frac{\delta E_{\text{Hartree}}}{\delta n} + \frac{\delta E_{\text{xc}}}{\delta n} \right] \frac{\delta n}{\delta \Phi^*} \quad (1.60)$$

Since,

$$T_s[n(\vec{r})] = -\frac{1}{2} \sum_{i=1}^N \int \Phi_i^* \nabla^2 \Phi_i d\vec{r} \quad (1.61)$$

then,

$$\frac{\delta T_s}{\delta \Phi^*} = -\frac{1}{2} \nabla^2 \Phi \quad (1.62)$$

From,

$$n(\vec{r}) = \sum_i |\Phi_i|^2 = \sum_i \Phi_i^* \Phi_i \quad (1.63)$$

Then,

$$\frac{\delta n(\vec{r})}{\delta \Phi^*} = \Phi(\vec{r}) \quad (1.64)$$

Hence, equation (1.60) can be written as

$$\frac{\delta E}{\delta \Phi^*} = -\frac{1}{2} \nabla^2 \Phi + [V_{\text{ext}} + V_{\text{Hartree}} + V_{\text{xc}}] \Phi \quad (1.65)$$

Where the effective potential V_{eff} is defined as

$$V_{\text{eff}} = V_{\text{ext}} + V_{\text{Hartree}} + V_{\text{xc}} \quad (1.66)$$

Therefore, equation (1.60) can be further simplified to be

$$\frac{\delta E}{\delta \Phi^*} = [-\frac{1}{2} \nabla^2 + V_{\text{eff}}] \Phi = \epsilon_i \Phi. \quad (1.67)$$

This is known as the Kohn-Sham equation of the auxiliary non-interacting system. The auxiliary Hamiltonian is given in equation (1.55) and it is also known as the effective Hamiltonian.

The effective potential, V_{eff} is dependent on the ground state density. The effective potential and the long range Hartree potential forms an independent particle potential and this can be solved by using the self-consistent method with the resulting density. However, the Kohn-Sham equation is not solved without solving the exchange-correlation energy density term. The exchange-correlation functional can be approximated which will be discussed in the following section.

1.3.5 Exchange-Correlation

In the previous section, Kohn-Sham replace the many-body particle problem with an auxiliary independent particle problem. Kohn-Sham splits the effective potential into three parts. First two parts consist of the non-interacting terms which are the kinetic energy of the independent particles, the Hartree long-range energy and the interacting term, which is the exchange-correlation term.

The kinetic energy can be determined exactly. The non-interacting term is easily solved by wave function represented by a Slater determinant of orbitals. This determinant can be solved by using a suitable software calculation, such as the Monte Carlo method. The unknown exchange-correlation energy term must be approximated in order to solve the Kohn-Sham equation.

The exchange-correlation term can be separated into the exchange energy and the correlation energy.

$$E_{xc} = E_x + E_c \quad (1.68)$$

The exchange energy is due to the interactions of any two electrons. The wave function is anti-symmetric and this is due to the exchange of the coordinates of the two electrons upon interaction. If the spin of the electrons are taken into consideration during the interaction, then it is known as the Heisenberg interaction. Hence, it can be represented as

$$E_x = \int \Psi_1[\vec{r}_1(\uparrow)]\Psi_2[\vec{r}_2(\downarrow)] \frac{e^2}{|\vec{r}_2 - \vec{r}_1|} \Psi_1[\vec{r}_2(\uparrow)]\Psi_2[\vec{r}_1(\downarrow)] \quad (1.69)$$

It is called the "Majorana interaction" when the exchange of spin is neglected.

The correlation energy is the difference between the interacting kinetic energy, E and the non-interacting Kinetic energy, E_s .

$$E_c = E - E_s \quad (1.70)$$

Hence, it is clear that the exchange-correlation energy term includes all the many-particle interactions.

The exchange-correlation energy can be approximated by several approximations. The local density approximation (LDA) and the generalized gradient approximation (GGA) are the most popular functionals used to approximate the exchange correlation functional. This will be discussed in the next section.

1.3.6 Local Density Approximation (LDA)

Approximate functionals are used to approximate the exchange-correlation functional, $E_{xc}(n)$. The local density approximation (LDA) is one of the simplest and most commonly used approximation to approximate the exact functional for the unknown exchange and correlation energies. LDA is derived from the concept of the homogeneous electron gas (HEG) model. This model is built by placing N interacting electrons which are placed in an infinite volume V and it is neutralised with a positive back ground charge.

To approximate the exchange-correlation functional, LDA assumes that the charge density varies slowly on an atomic scale. Then, the distribution of electrons in an atom is approximated to be homogeneous. Therefore, the electrons in this system are

subjected to a constant external potential and thus the density is constant. Hence, $E_{xc}(n)$ at any point \mathbf{r} can be expressed in terms of a local functions of the density. Then, the total exchange-correlation energy of an inhomogeneous system can be approximated by integrating over a local function of the charge density. The exchange-correlation energy functional $E_{xc}[n(\vec{r})]$ is defined as;

$$E_{xc}[n(\vec{r})] = \int n(\vec{r})\varepsilon_{xc}[n(\vec{r})]d\mathbf{r} \quad (1.71)$$

where, ε_{xc} is the exchange-correlation energy per electron in a uniform electron gas. The exchange-correlation energy per electron can be further simplified into two parts; the exchange term and the correlation term as shown in the equation below.

$$\varepsilon_{xc} = \varepsilon_x - \varepsilon_c \quad (1.72)$$

The exchange term can be derived analytically by Dirac's approximation in a homogeneous system.

$$\varepsilon_{xc}[n(\vec{r})] = -\frac{3}{4}\left(\frac{3}{\pi}\right)^{1/3}[n(\vec{r})]^{1/3} \quad (1.73)$$

However, the correlation part cannot be derived analytically, but it can be calculated accurately by using the Monte Carlo simulations.

1.3.7 Generalized Gradient Approximation

(GGA)

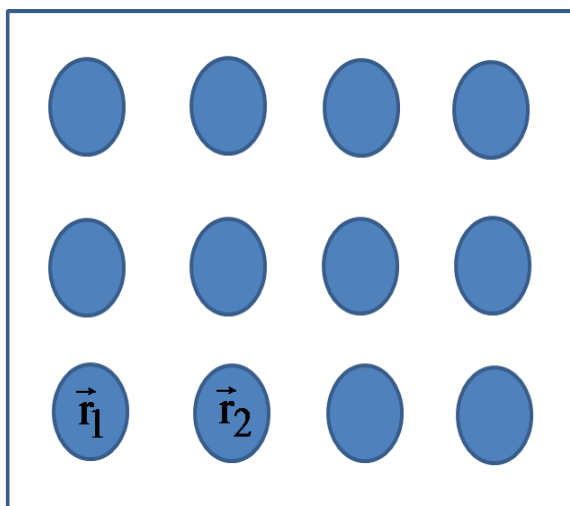
The local density approximation (LDA) assumes that the density of electrons in an atom is approximately homogeneous. However in real systems, the distribution of electrons in a system is far from being uniform. There is a density gradient, ∇n between two atoms. The difference of the two approximations are shown as Fig. 1.6.

Hence, the proper step to improve the accuracy of the exchange-correlation functional is to construct a functional that depends on the local density and the density gradient also.

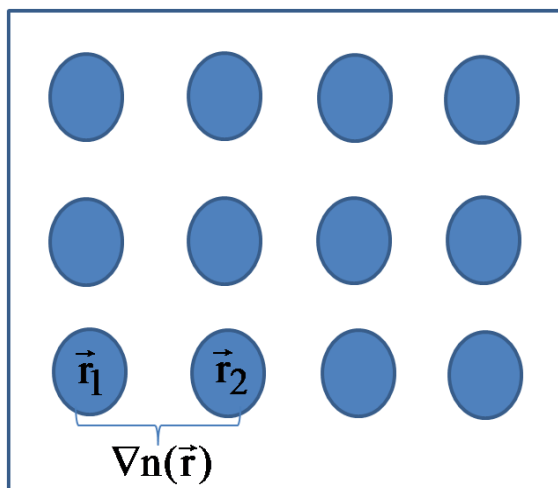
The new approximation can be constructed as

$$\varepsilon_{xc}^{GGA}[n, \nabla n] = \int n(\vec{r}) \varepsilon_{xc}[n(\vec{r}), \nabla n(\vec{r})] d^3r \quad (1.74)$$

LDA constructs the functional based on ‘local density’ which is derived from the uniform electron gas. GGA minimises the LDA error by including a semi-empirical functional which contains one or more parameters to satisfy various physical constraints according to the nature of the system of interest. Perdew-Wang 1991 (PW91) and Perdew, Burke and Ernzerhof (PBE) are the most popular GGA that is used to approximate the functional. With the small varying density gradient contribution, $E_{xc}^{GGA} < E_{xc}^{LDA}$. Hence, GGA reduces the binding energy compared to LDA. This improves the agreement with the experimental value.



(a) LDA approximate the exchange-correlation by considering only the local density at point \vec{r}



(b) GGA approximate the exchange correlation functional by considering both local density and the density gradient between two atoms.

FIGURE 1.6

Figure shows the schematic diagram of the approximation used in (a) LDA and (b) GGA calculations.

SECTION 1.4

Overview

The discovery of iron based superconductors in year 2008 has instilled various interests of many researchers around the world. The iron based superconductors does not resemble conventional superconductors and has a property on their own. Hence, it introduced a new class of high-temperature superconductor. In this research, first principle calculation of polarised and unpolarised electronic band structure of various types of iron based superconductors is calculated using the density functional theory (DFT) as provided in the Accelrys Material Studio commercial software.

The space groups of the interest lattices and the lattice parameters are determined before the lattice is built. The lattice will then undergo geometry optimization in order to obtain the equilibrium structure at the minimum potential energy, where the forces between the atoms are zero. The optimized structure is then used to calculate the polarised and the unpolarised band structures of the respective compounds. Both calculations are compared to obtain more accurate band-gap analysis.

In this calculation, the band structure is calculated by using the DFT method in the local density approximation (LDA) approach formed with the parameterization given by Perdew-Wang (PWC) functional. In the polarised calculation the spin orbitals are used in the DFT calculation. The basis set, double numerical with polarization (s, p and d orbitals for polarisation) are used to describe the valence electrons in the polarised orbital calculation.

This research is begin by studying the pure lattice of iron selenium, FeSe and the alloy of FeSe by removing the selenium atom forming Fe:Se = 2:1 as dicussed in chapter 2. The larger lattice of FeSe alloy is the built in chapter 3 forming Fe:Se = 8:6 and Tellurium atom is introduced to substitute the Se vacancy forming Fe:Se:Te = 2:1:1 and 8:6:2. In this chapter, the Meissner effect is discussed as well. In chapter 4, the oxidation of FeSe compound is discussed by adding oxygen into the FeSe lattice forming Fe:Se:O = 8:6:2 and 8:4:2. The oxidation of FeSeTe compound is then discussed in the following chapter and in chapter 6, the samarium atom is substitute into various FeSe compound forming FeSeSmO, FeSeTeO, Fe₂SeSm₂O₂, FeSeTeSmO and FeTeSmO. The conclusion of each chapter is then summarised in chapter 7.

CHAPTER 2

DFT COMPUTATION OF THE ELECTRONIC BAND STRUCTURE OF FeSe

The band structure of FeSe is calculated in the space group P4/nmm with unpolarized as well as with polarized orbitals. There is a tetrahedron of Se atoms inside the cell. The polarized Fermi energy is found to be -4.54 eV and the binding energy is -33.0 eV. The energy gap varies from 0.58 eV at Z point to 1.58 eV at R point. The gap is highly anisotropic. Next, a unit cell of FeSe with two Se atoms removed is made. There are 2 Se atoms in the perfect unit cell; and there is only one Se atom in the doped cell. There is a pronounced effect on the density of states. The band structure for the unit cell with only one atom of Se per unit cell is calculated by using polarized as well as unpolarized orbitals. It is found that the gap is reduced by a large amount of energy in the unit cell with 1 Se atom compared with that with 2 Se atoms. The gap for 1 Se cell varies from 0.45 eV at G point to 1.0 eV at Q point. This reduced gap is conducive to superconductivity.

SECTION 2.1

Introduction

Recently, it has been reported that FeSe becomes superconducting [7] when some Se atoms are removed. In particular, $\text{Fe}_{20}\text{Se}_{17}$ is superconducting at about 10K. The typical a.c. susceptibility was found to be -0.015 to -0.017 emu/g. The mass density is $\rho = 5.22$ g/cm³ so that the susceptibility is -0.08091 emu/cm³. The value of $-1/4\pi$ is -0.07961 . Hence, the experimental value is slightly deeper than expected for the perfect Meissner effect. This means that the field inside the superconductor is not zero but there is a small field. This small field may be parallel to the external field or may be oppositely directed. In the present case, it is parallel to the field. The electronic configuration of Fe is $3d^64s^2$ and that of Se is $4s^24p^4$. If 4 electrons of $4p^4$ will fill up the need of $3d^6$, it will provide a diamagnetic material. Apparently, it does not quite happen that way and there is something like a weak diamagnet which becomes a superconductor when some of the $4p^4$ electrons are removed altogether. The superconducting phase is found when the contribution of Se is less than that of Fe [7].

In the present work, the pure FeSe is studied as well as that alloy which is deficient in Se. The calculation of the electronic band structure of Fe:Se = 2:2 as well as Fe:Se = 2:1 are reported. The characteristic developments in the band structure when 1 Se is removed from the unit cell is found.

SECTION 2.2

Band Structure

2.2.1 FeSe

The density-functional theory in the local density approximation (LDA) is used to calculate the band structure. The effort to use the generalized-gradient approximation (GGA) were also made but the results of the two approximations were very close to each other. Hence, only LDA results are reported here.

The unit cell of FeSe in the space group $P4/nmm$ consists of 2 atoms of Fe and 2 atoms of Se. The 8 Fe atoms are on the eight corners and 2 Fe atoms are on the top and bottom face centered positions as shown in Fig 2.1. The 4 Se atoms form a tetrahedron with atoms on the faces so that there are only 2 Se atoms per unit cell. After optimization, the unit cell parameters are found to be $a = 3.7675\text{\AA}$ and $c = 5.7096\text{\AA}$. The coordinates of K-points are Z (0, 0, 0.5), A (0.5, 0.5, 0.5), M (0.5, 0.5, 0), G (0, 0, 0), R (0, 0.5, 0.5) and X (0, 0.5, 0). The band structure for the unpolarized orbitals is given in Fig. 2.2 and that for the polarized is given in Fig. 2.3. In between Z and A points the unpolarized calculation is showing a gap which vanishes when polarized orbitals are used. Usually, the spin up and spin down energies are clearly visible but in the present case, that is not happening showing lack of polarization is the FeSe.

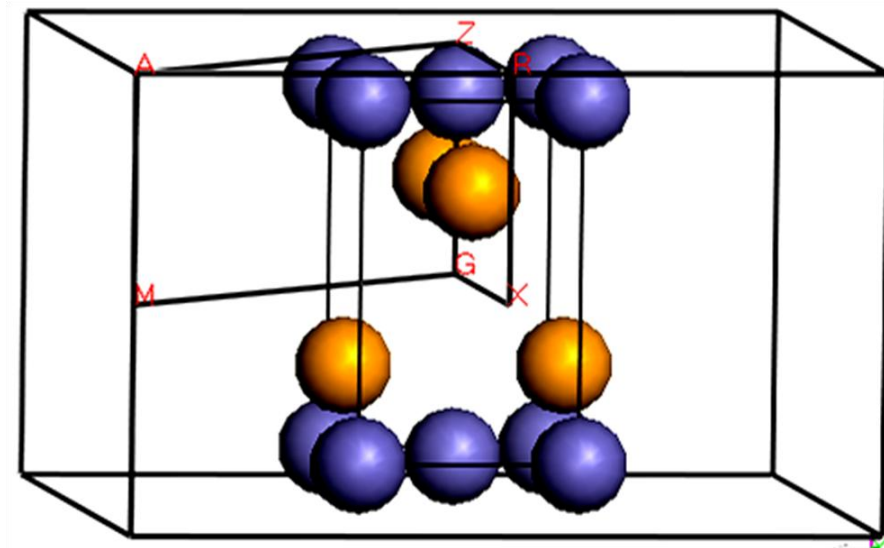


FIGURE 2.1
The figure shows the P4/nmm lattice of FeSe with the Brillouin Zone path

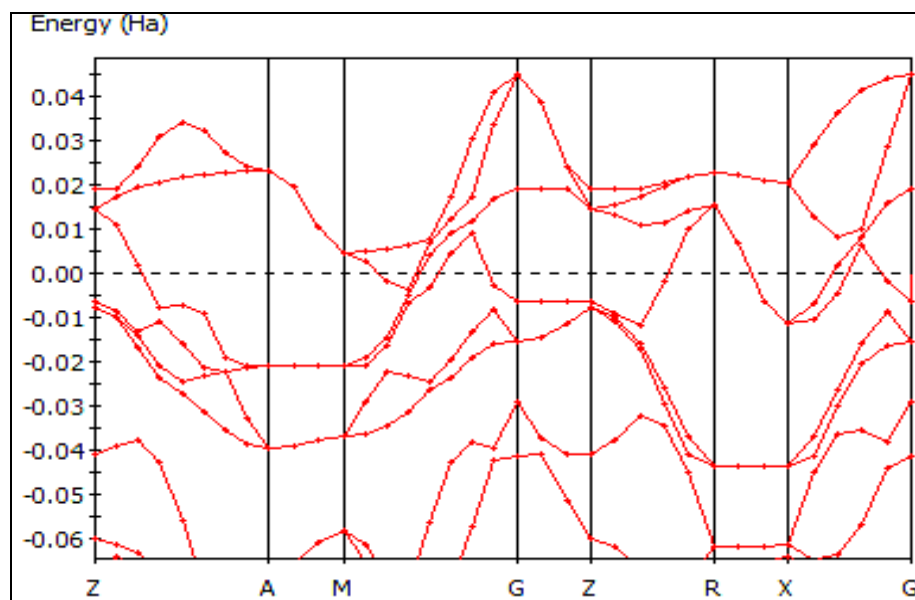


FIGURE 2.2.
The band structure of FeSe calculated by using unpolarized orbitals in DFT (LDA).

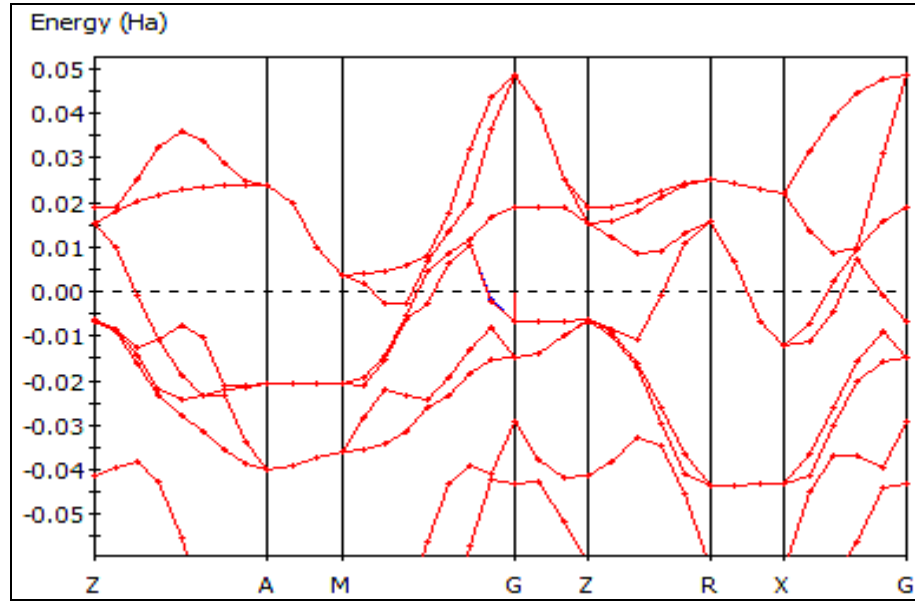


FIGURE 2.3.

The band structure of FeSe calculated by using polarized orbitals.

Most of the features in the unpolarized band structure are similar to those of polarized structure. The Fermi energy is -4.544 eV in the polarized case compared with -4.290 eV for the unpolarized case. The band gap at various k-points is given in Table 2.1. The polarized gap varies from 0.58 eV at Z point to 1.58 eV at R point. The density of states (DOS) for the unpolarized case is given in Fig. 2.4 and for the polarized case in Fig. 2.5. Somehow the chemical binding is such that the effect of spin polarization is quite small.

TABLE 2.1. The band gaps in FeSe in units of eV

K-point	Band Gap in FeSe (eV)	
	Polarized Orbitals	Unpolarized Orbitals
Z	0.58	0.60
A	1.21	1.20
M	0.66	0.71
G	0.68	0.69
Z	0.59	0.60
R	1.58	0.61
X	0.90	0.87
G	0.68	0.69

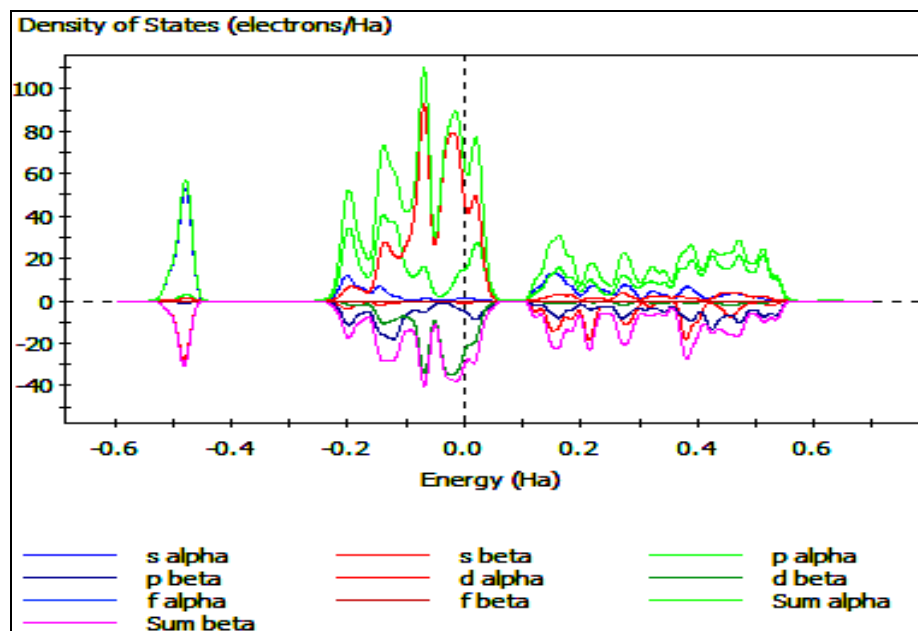


FIGURE 2.4.
The DOS of FeSe for unpolarized orbitals.

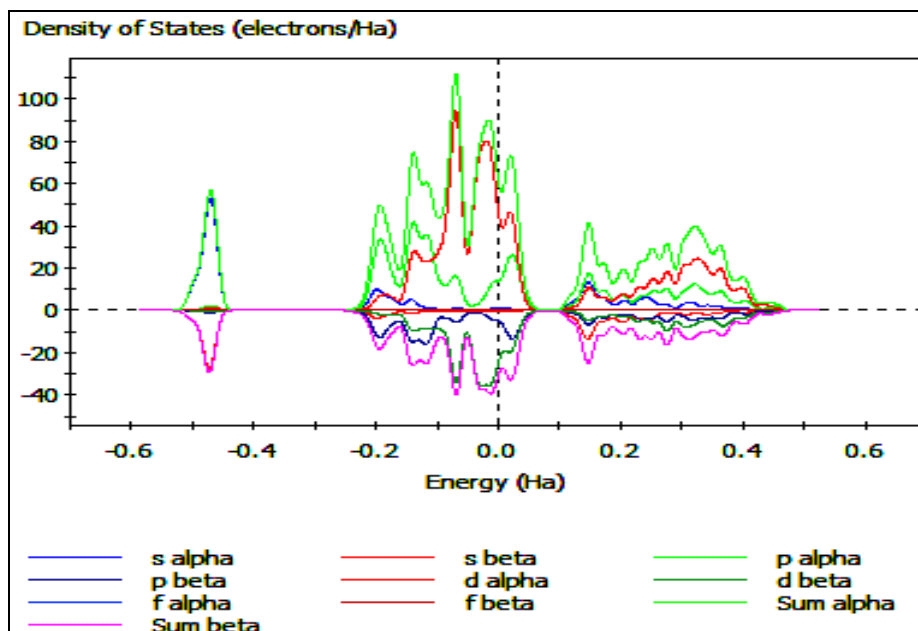


FIGURE 2.5.
The DOS of FeSe for polarized orbitals.

2.2.2 Fe:Se = 2:1

Usually, the doping is performed by adding impurity atoms. In the present case, it is not to add but to remove some of the Se atoms. So, the doping is done by removing 2 Se atoms from the 4 belonging to the tetrahedron. While the tetrahedron gives 2 Se atoms per unit cell, we have only 1 Se atom per unit cell. In this case, the unit cell constants are $a = 3.6067\text{\AA}$ and $c = 4.8260\text{\AA}$. The Se atoms are not symmetrized with respect to the unit cell of FeSe. They are now located at $(0, 0.5, 0.427)$ and $(1, 0.5, 0.427)$ retaining the memory of the tetrahedron. The k-points are G $(0, 0, 0)$, F $(0, 0.2, 0)$, Q $(0, 0.5, 0.5)$, and Z $(0, 0, 0.5)$. The Fermi energy is found to be -4.52 eV by using polarized orbitals and -4.248 eV by using unpolarized orbitals. Thus there is a small effect of the spin polarization. The band gap is shown in Table 2.2.

TABLE 2.2. The energy gap at various k-points in Fe:Se = 2:1 crystal.

k-point	Energy Gap in Fe:Se = 2:1 (eV)	
	Polarized Orbitals	Unpolarized Orbitals
G	0.45	0.43
F	0.73	0.15
Q	1.02	1.11
Z	0.62	0.61
G	0.45	0.43

The polarized band structure of Fe:Se = 2:1 is shown in Fig. 2.6 and the unpolarized in Fig. 2.7. There is some crossing phenomenon at the F point. The energy between G and F point is affected by the polarization.

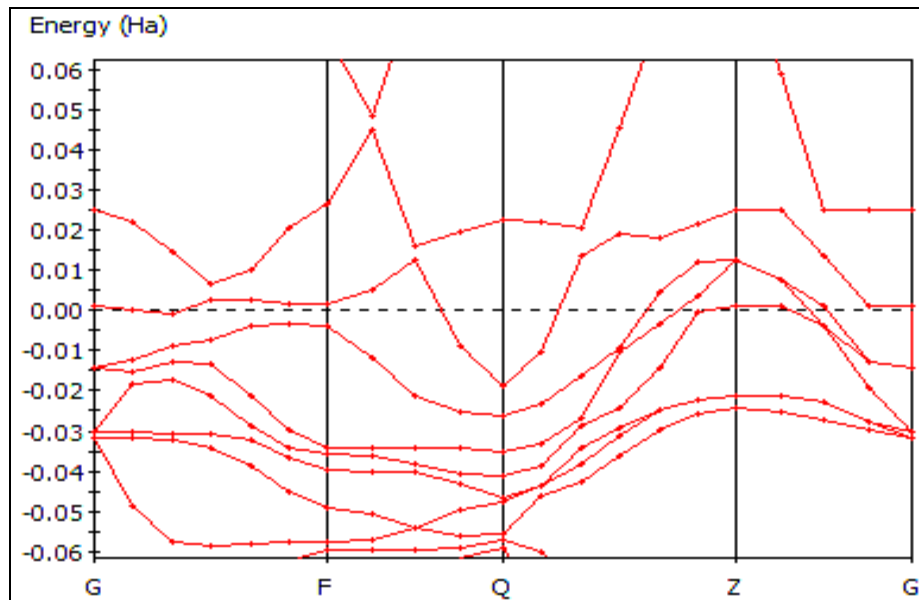


FIGURE 2.6.
The polarized band structure of Fe:Se = 2:1 structure.

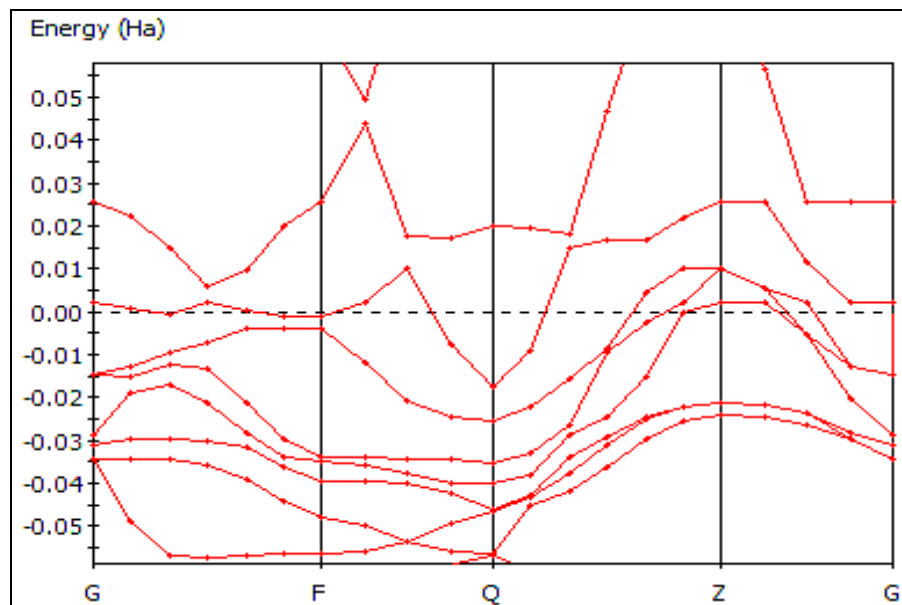


FIGURE 2.7.
The unpolarized band structure of Fe:Se = 2:1 structure.

The DOS calculated by using unpolarized orbitals is shown in Fig. 2.8 and that with polarized orbitals is given in Fig. 2.9. The lack of any major difference clearly indicates that the case of magnetism is very weak.

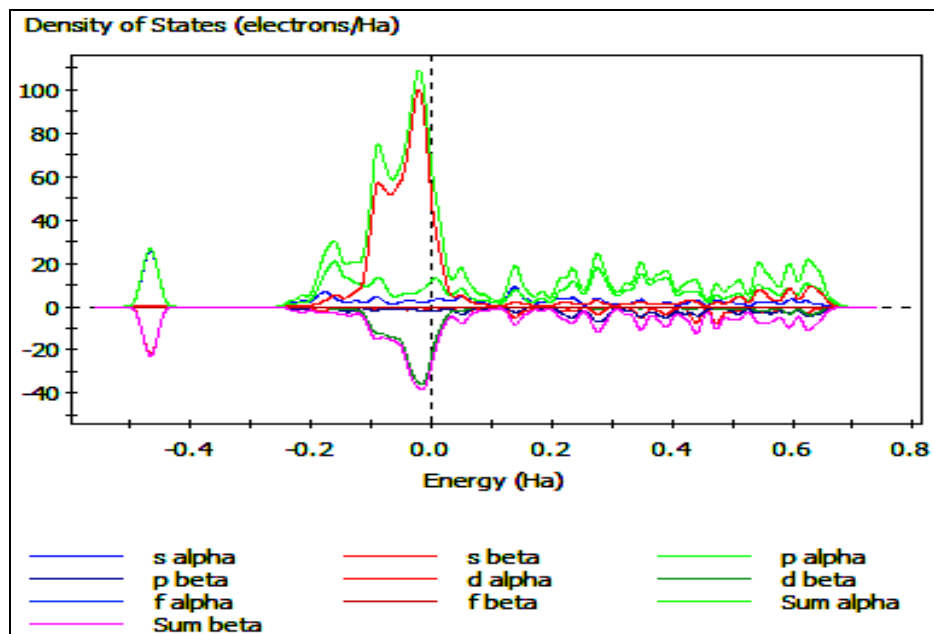


FIGURE 2.8.
The density of states of Fe:Se = 2:1 for unpolarized orbitals

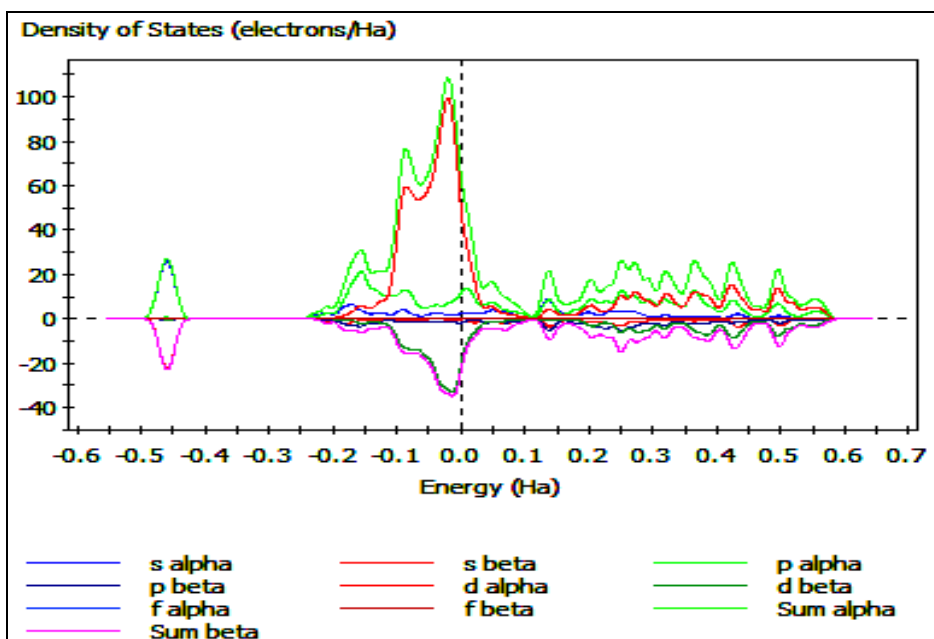


FIGURE 2.9.
The density of states of Fe:Se = 2:1 for polarized orbitals

SECTION 2.3

Binding energy

In the case of the unit cell of FeSe, the binding energy calculated is -31.9 eV for the unpolarized orbitals and -33.0 eV for the polarized orbitals showing only 3% effect of polarization. In the case of Fe:Se = 2:1 , the unpolarized binding energy calculated is given as -26.9 eV and the polarized value is -26.5 eV. So the effect of spin is only 1.2%. This means that upon reducing the Se atom, the effect of spin is reduced. The effect of spin reduction is useful for superconductivity.

SECTION 2.4

Conclusions

One of the important findings is that the magnetization in FeSe is very weak. In fact, the effect of spin polarization is small. The band gap is found to be reduced by a large amount when one Se atom is removed from the unit cell. The reduced band gap induces superconductivity [18]. The superconductivity in FeSe unit cell is thus distinguished by the effect of spin and incomplete Meissner effect. Usually, there are the type-I superconductors which are distinguished by complete absence of magnetic atoms. In this case there is only one critical field which destroys the superconductivity. In the case of type-II superconductors, there is a mixed phase between the two critical fields, the upper critical field at which the superconductivity is completely destroyed and the lower critical field at which vortices appear. The present superconductors containing Fe atoms [19-23] form a class by themselves. They are distinguished by incomplete Meissner effect.

CHAPTER 3

THE MEISSNER EFFECT IN

FeSe SUPERCONDUCTOR

In the zero-field cooled samples, the Meissner susceptibility, $-1/4\pi$, is found to depend on the mass density of the samples so that the experimental value comes out to be less or more than $-1/4\pi$. The change in value of $-1/4\pi$ due to field trapping is determined. In the field cooled samples there is a large effect of the field trapping. The band structure of FeSe, FeSe from which 2 atoms of Se out of 4 per unit cell have been removed and a system in which 2 Te atoms have been substituted for 2 Se atoms in a unit cell are calculated. Large effects are found in the density of states. The normal state gap reduces in the composition which becomes superconducting.

SECTION 3.1

Introduction

The iron atoms have a large magnetic moment and in compounds, such as FeSe, the magnetic moment per Fe atom is very large, such as $2.1\mu\text{B}$ when Fe is surrounded by some vacancies and even $-1.1\mu\text{B}$ in the neighbourhood of Se atoms. The net magnetic moment of Fe $\approx 1.0\mu\text{B}$ is quite large to yield the Meissner effect. It has been found that pure Fe which has the electronic configuration of $3d^64s^2$ is a ferromagnet. When another atom is brought in the neighbourhood of Fe, such as As, there is a likelihood of forming an antiferromagnetic material. FeSe forms a ferromagnet because the down magnetic moment is smaller than the up moment. It turns out that FeAs has a superconducting phase. Similarly, FeSe has a superconducting phase when number of Se atoms is slightly deficient. For example, $\text{Fe}_x\text{Se}_{1-x}$ with $x\approx 0.12$ is a superconductor [7]. Another study showed that FeSeTe with equal amount of Se and Te, is a superconductor [24]. It is possible that some impurities, such as oxygen are present in the sample [25]. Lee et al [26] find that $\text{FeSe}_{0.78}$ is a half metal, i.e., $\frac{1}{4}$ filled conduction bands. In all possibilities, it should be a ferromagnet as pointed out above. As the system goes from normal to the superconducting phase, there is no change in the phonon density of states [27]. Subedi et al [3] find that the ground state of FeS, FeSe and FeTe is a spin-density wave state.

Some time ago, it was found [28-30] that in field cooled samples, the usual Meissner effect is not found and there are magnetic terms in the free energy. It was suggested that currents with phase factor shifted by π occurred [18, 31].

In the present work, the reported value of $-1/4\pi$ for the susceptibility does not occur due to the coordinate but dependent of the mass density. The Meissner effect formulation based on $B = H + 4\pi M$ is found to be too simple because magnetization, M can depend on the coordinates and exhibit nonuniformity and there may be trapped fields. Here B is the magnetic induction inside the sample, H is the external field and M is the magnetization of the sample. The band structure calculation is performed by using density-functional theory; DFT (LDA) from which the gap in Fe_2Se_2 is found to be very large but reduces when some atoms of Se are removed. In particular Fe_2Se has smaller band gap than Fe_2Se_2 . When the Se atoms are replaced by Te atoms, the gap further reduces. The reduced band gap in FeSeTe indicates that the superconducting transition temperature increases as the normal state gap reduces.

SECTION 3.2

The Meissner Effect

The field inside a material, B is given by the external field, H , and the internal field determined by the magnetization, M as,

$$B = H + 4\pi M \quad (3.1)$$

Since $B = 0$, then

$$\chi = \frac{M}{H} = -\frac{1}{4\pi} \quad (3.2)$$

This is the theory of the Meissner effect. Now, consider two modifications, one of which introduces the coordinate dependent density, i.e., the susceptibility, χ is replaced by $\chi_o\rho(x)$ where $\rho(x)$ is the mass density and the quantity χ_o is the susceptibility per unit density. Another modification introduced here, is to use a small field, instead of zero field. This small field works like the London penetration depth which leads to a small resistivity. The susceptibility in the zero field cooled samples is obtained as well as in the field cooled samples. It is found that in $\text{FeSe}_{0.85}$, the magnetization ratio $M_{ac}(T)/M_{ac}(2K)$ approaches ≈ -1 . The typical a.c. susceptibility was found to be -0.015 to -0.017 emu/g. In some of the samples [1] the value is -0.0155 emu/g. This value must be multiplied by the mass density, $\rho = 5.22 \text{ g/cm}^3$. Then, the value found becomes 0.08091 emu/cm^3 which is only slightly different from $-1/4\pi \approx 0.07961$ but the lesson is

that the mass density which depends on the coordinates is needed. The mass near Fe-Se atoms is indeed different from that in between layers. Hence, the Meissner effect has to be modified to,

$$\chi = \chi_o \rho(x) \quad (3.3)$$

$$B = H + 4\pi M(x) \quad (3.4)$$

$$\chi = \chi_o \rho(x) = \frac{M_o \rho(x)}{H} = -\frac{1}{4\pi} \quad (3.5)$$

$$M = M_o \rho(x) \quad (3.6)$$

$$\frac{M_o}{H} = -\frac{1}{4\pi} \frac{1}{\rho(x)} \quad (3.7)$$

Second modification is to introduce a small field instead of zero,

$$B = H + 4\pi M = H_{zero} \quad (3.8)$$

$$\frac{M}{H} = -\frac{1}{4\pi} + \frac{H_{zero}}{4\pi H} \quad (3.9)$$

Where H_{zero} is a small field due to trapped fields and it is very small. It causes a small resistivity which is of the same order of magnitude as the one caused by the London penetration depth. The zero field cooled susceptibility of several Fe containing superconductor is examined and the H_{zero}/H of each samples is evaluated. The results obtained are as given in Table 3.1. The susceptibility of two samples is also shown in Figs 3.1 and 3.2. The superconductors $LiFeAs$, $K_{0.4}Sr_{0.6}Fe_2As_2$, $Cs_{0.4}Sr_{0.6}Fe_2As_2$, $Ba_{0.6}K_{0.4}Fe_2As_2$ and $LaFeAsO_{0.89}F_{0.1}$ have also been studied by several authors [21, 32-

35]. The original definition of Meissner effect [9] is that the field penetrates the superconductor for only a short distance, called the London penetration depth, after which it decays rapidly to zero. In the present result, apparently, the field does not decay to zero but to a small value. In Fig. 3.1 show the susceptibility of zero-field cooled sample of LiFeAs. It is seen that the susceptibility approaches a value which is slightly different from $-1/4\pi$. The field cooled ($H \approx 10\text{G}$) value is also shown which is very different from $-1/4\pi$ due to field trapping near the Fe atoms. The LiFeAs crystallizes in a tetragonal unit cell with $a = 3.7914\text{\AA}$ and $c = 6.364\text{\AA}$ as given by Tapp et al [32]. In Fig. 3.2, show the susceptibility of $\text{K}_{0.4}\text{Sr}_{0.6}\text{Fe}_2\text{As}_2$ as a function of temperature. Here again it is seen that the zero-field cooled susceptibility is slightly off from $-1/4\pi$ value and the finite field ($H=10\text{G}$) cooled value is positive indicating the field trapping.

Table 3.1. The values of $H_{\text{zero}}/4\pi H$ for Fe containing superconductors (zero-field cooled = ZFC)

S. No	Formula	$T_c(\text{K})$	$\chi(T=0)(\text{ZFC})$	$H_{\text{zero}}/4\pi H$
1	$\text{FeAs}_{0.85}$	8.2	-0.0809	+0.0013
2	LiFeAs	18.0	-0.0943	+0.0147
3	$\text{K}_{0.4}\text{Sr}_{0.6}\text{Fe}_2\text{As}_2$	37.0	-0.1146	+0.0350
4	$\text{Cs}_{0.4}\text{Sr}_{0.6}\text{Fe}_2\text{As}_2$	38.0	-0.0931	+0.0135
5	$\text{K}_{0.4}\text{Ba}_{0.6}\text{Fe}_2\text{As}_2$	38.0	-0.0740	-0.00558
6	$\text{O}_{0.89}\text{F}_{0.11}\text{LaFeAs}$	27.0	-0.0589	-0.02070

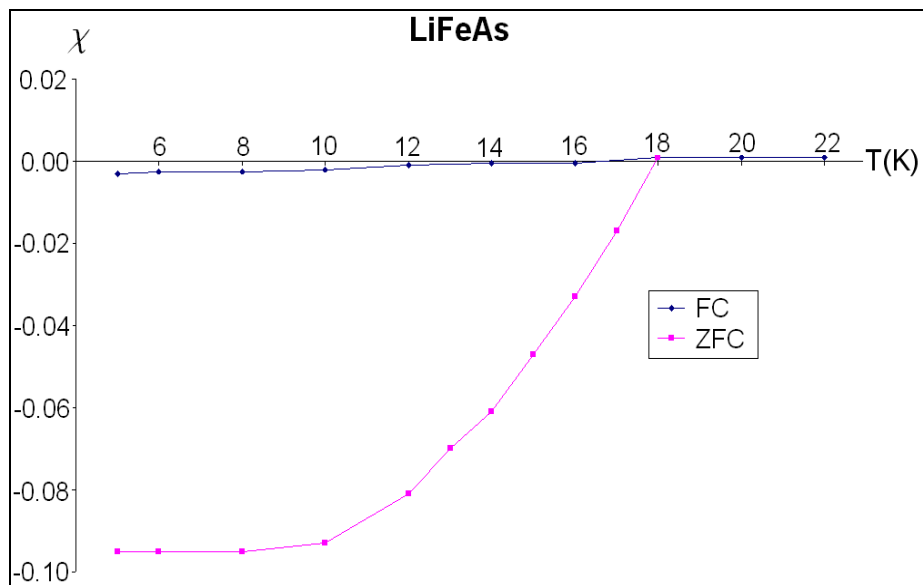


FIGURE 3.1.

The susceptibility of the LiFeAs in zero-field cooled and in finite (10G) field cooled samples showing derivations from $-1/4\pi$

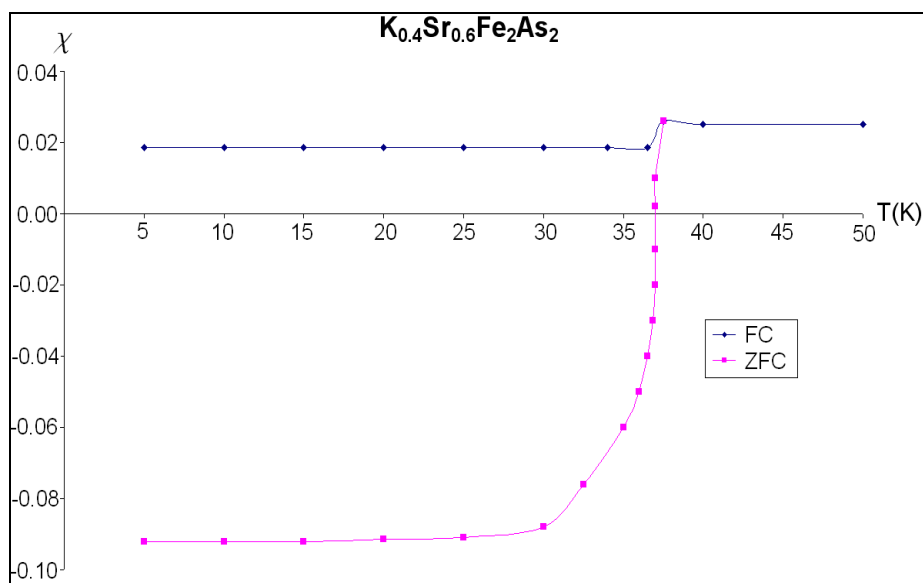


FIGURE 3.2.

The susceptibility of $K_{0.4}Sr_{0.6}Fe_2Se_2$ as a function of temperature for the zero-field as well as the finite (10G) field cooled samples. The lower zero-field cooled (SCF) does not reach the $-1/4\pi$

SECTION 3.3

Band Structure

The transition temperature of FeSe is about $T_c = 8\text{K}$, while that of $\text{FeSe}_{0.85} \approx 8.2\text{K}$. The transition temperature of $\text{Fe}_{1+y}\text{TeSe}_{1-x}$ for equal amount of Se and Te is about 14K . The band gap of these materials is calculated from which we find that the band gap reduces in going from Fe_2Se_2 to Fe_2SeTe which might indicate a relationship between the normal state gap and the superconductivity. The density-functional theory [13, 15, 36] in the local density approximation (LDA) is used in this calculation to obtain the band structure by using polarised as well as the unpolarized wave functions. The band gap found from this calculation is given in Table 3.2. At the z point the reduction in the gap from 0.58eV for Fe_2Se_2 to 0.29eV for FeSeTe is clearly seen. At the G point the reduction from 0.69eV for Fe_2Se_2 to 0.06eV for FeSeTe clearly shows a large reduction in the normal state gap accompanied by increase in the superconductivity transition temperature. The space group of Fe_2Se_2 is $P4/nmm$ with $a = 3.7675\text{\AA}$ and $c = 5.7096\text{\AA}$ upon optimization. When two atoms of Se are removed from the 4 in the unit cell we obtain Fe_2Se_1 with optimised lattice parameter $a = 3.6057\text{\AA}$ and $c = 4.826\text{\AA}$ which shows that the unit cell volume is reduced in going from Fe_2Se_2 to Fe_2Se_1 . When Te is introduced in the Se sites, Fe_2SeTe has a much smaller cell with $a = 3.5504\text{\AA}$ and $c = 5.498\text{\AA}$. As the cell size is reducing, the transition temperature is increasing. For Fe_2SeTe the calculated band structure is shown in Fig. 3.3 and the calculated DOS in

Fig. 3.4. There is a peculiar effect seen in the valence band. The effect of Te is to create a separate peak. In order to investigate this effect further, a large unit cell is made.

A block of 4 unit cells is made so that the ratio of atoms can be varied. For Fe:Se = 8:8 by using the polarised orbitals in the DFT(LDA) the band structure obtained is as shown in Fig. 3.5 and the DOS is shown in Fig. 3.6. In this calculation the k-points are, G(0,0,0), F(0,0.5,0), Q(0,0.5,0.5) and Z (0,0,0.5). The polarized Fermi energy is -4.796eV and the binding energy is -106.8eV. The vacancies are introduced by removing two Se atoms so that Fe:Se = 8:6. In this case the polarised Fermi energy is found to be -4.733eV which in magnitude only slightly lower than when there is no vacancy. The polarised binding energy is -93.91eV which in magnitude is smaller than that for the fully occupied lattice. The polarised band structure of 8:6 cell is shown in Fig. 3.7 and its DOS is given in Fig. 3.8. When Te atoms are introduced in the places vacated by Se, the ratios of atoms becomes Fe:Se:Te = 8:6:2. In this case, the calculated band structure for polarised orbitals given in Fig. 3.9 and the DOS is given in Fig. 3.10. The band gaps obtained from these calculations are given in Table 3.3. It is quite clear that the band gap reduces upon introducing Te and this process is accompanied by an increase in the transition temperature. In the lattice Fe:Se = 8:6 two of the Se atoms have been removed. Upon optimisation for minimum energy, it is found that some of the Fe atoms approached towards the antisites. The Fe atoms moved towards the sites vacated by Se atoms. This antisite motion is accompanied by changes in electron cloud which is more conducive to superconductivity than the rigid fully occupied lattice. The iron atoms in different directions move by 4 percent, 8 percent and 30 percent of the rigid position. The coordinates, (0, 0, 0) became (0, 0, -0.8), the position (0.25, 0.25, 0.0) became (0.25, 0.25, 0.04) and (0.5, 0, 0) became (0.5, 0, 0.3). Thus Fe atoms moved to the positions which later formed the superconducting phase.

The Fermi energy has been calculated for FeSe, FeSe with Se vacancies and with Se vacancies filled with Te atoms as given in Table 3.4. It is known that the superconducting transition temperature increases by creating Se vacancies or by substituting Te for Se. The Fermi energy is seen to reduce as the transition temperature increases.

Table 3.2. The band gap in eV at various K point calculated by using DFT(LDA) (pol=polarised, unpol=unpolarised). The coordinates of the k points are Z(0, 0, 0.5), A(0.5, 0.5, 0.5), M(0.5, 0.5, 0), G(0, 0, 0), R(0, 0.5, 0.5) and X(0, 0.5, 0).

S. No	Formula	Z	A	M	G	R	X
1	Fe ₂ Se ₂ (pol)	0.58	1.21	0.66	0.68	1.58	0.90
2	Fe ₂ Se ₂ (unpol)	0.60	1.20	0.71	0.69	1.61	0.87
3	Fe ₂ Se ₁ (pol)	0.62	0.45	1.02	0.73
4	Fe ₂ Se ₁ (unpol)	0.61	0.43	1.11	0.15
5	FeSeTe(pol)	0.29	0.063	1.99	1.13
6	FeSeTe(unpol)	0.25	0.057	2.05	1.22

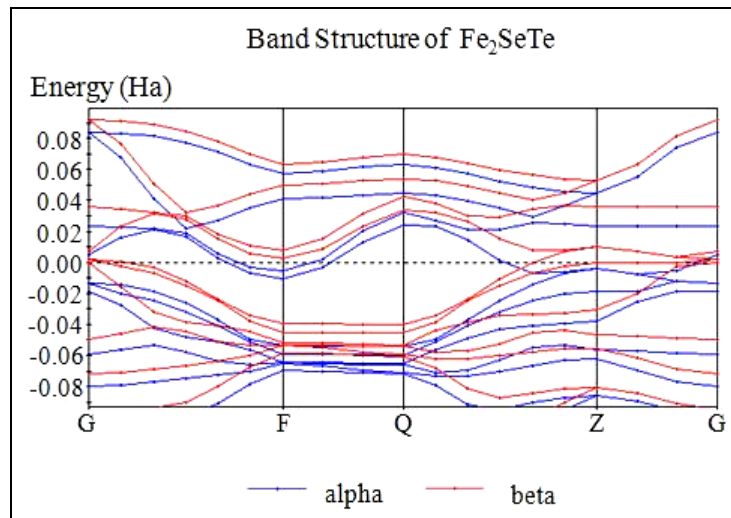


FIGURE 3.3.
The band structure of Fe₂SeTe calculated by using DFT(LDA)

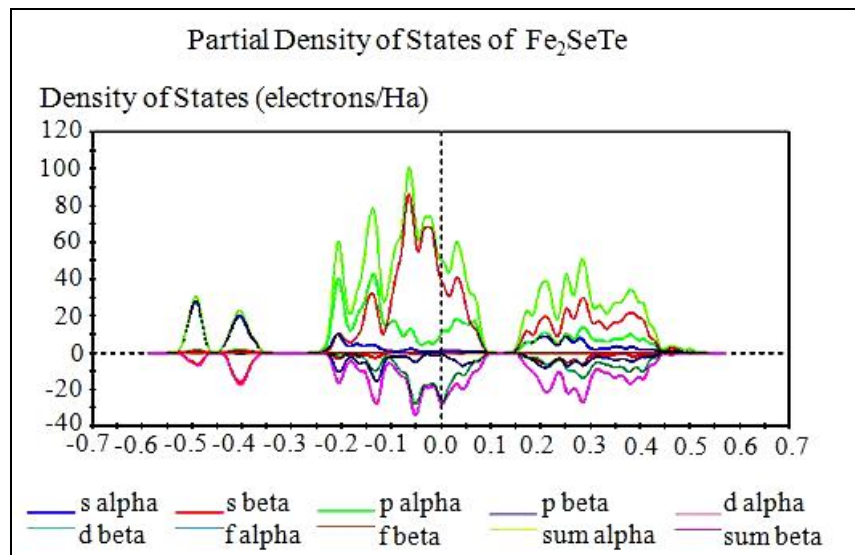


FIGURE 3.4.
The density of electron states (DOS) of Fe₂SeTe calculated from the first principles.

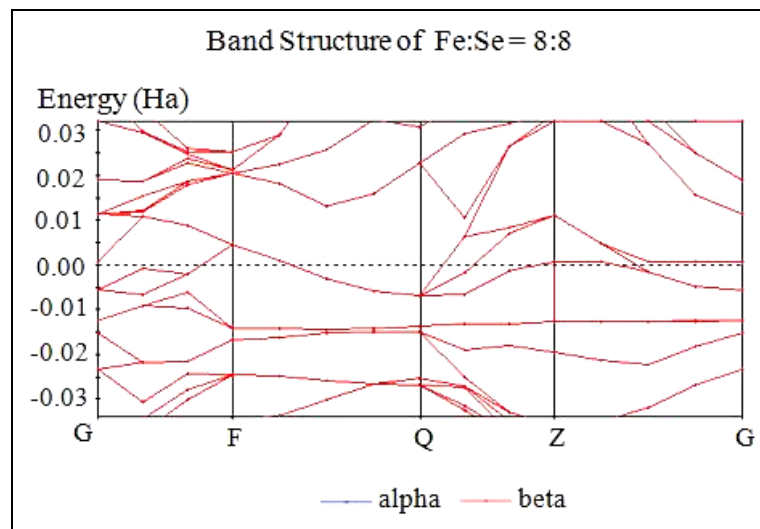


FIGURE 3.5.
The band structure of Fe:Se = 8:8 calculated by using polarised orbitals in the DFT(LDA).

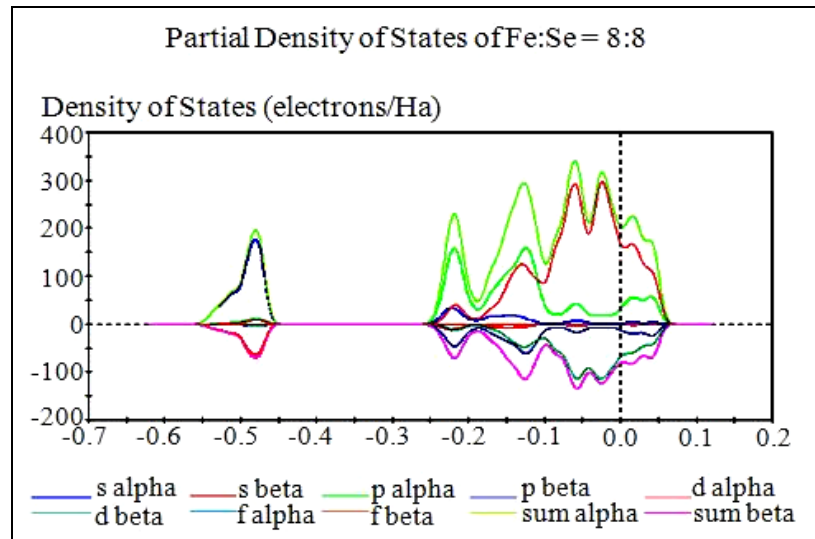


FIGURE 3.6

The density of states of Fe:Se = 8:8 calculated by using the polarised orbitals in the DFT(LDA)

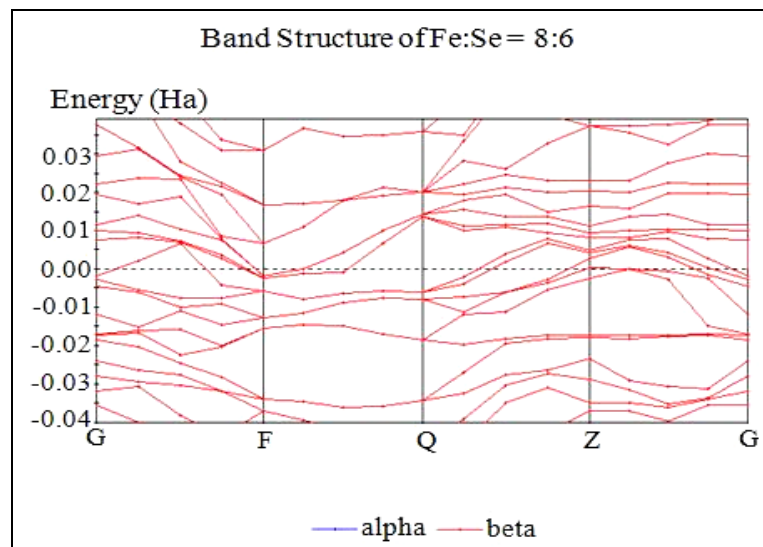


FIGURE 3.7

The polarised band structure of 8:6 cell from which Se atoms have been removed.

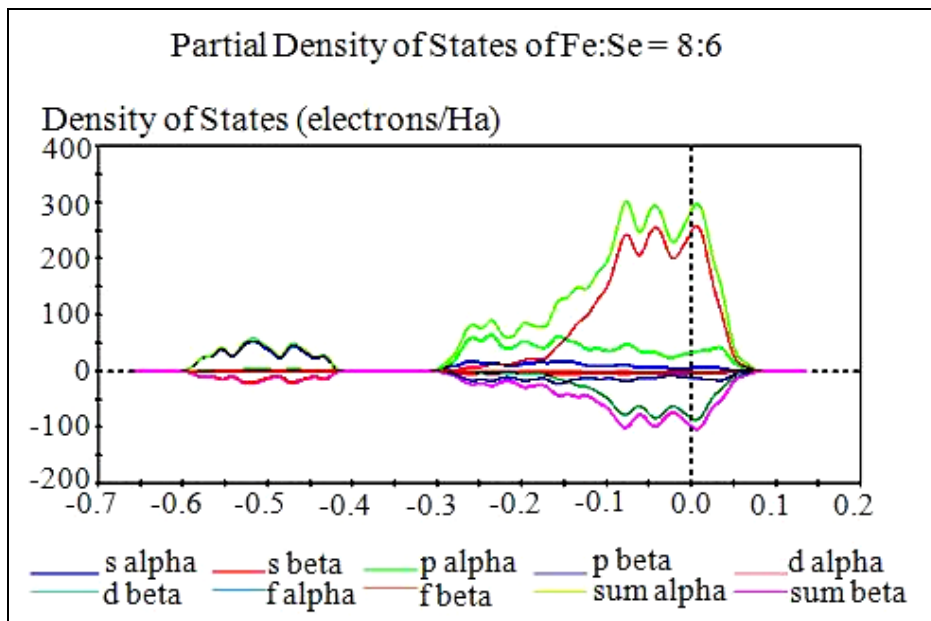


FIGURE 3.8.

The density of states of Fe:Se = 8:6 cell calculated from the DFT(LDA) with polarised orbitals.

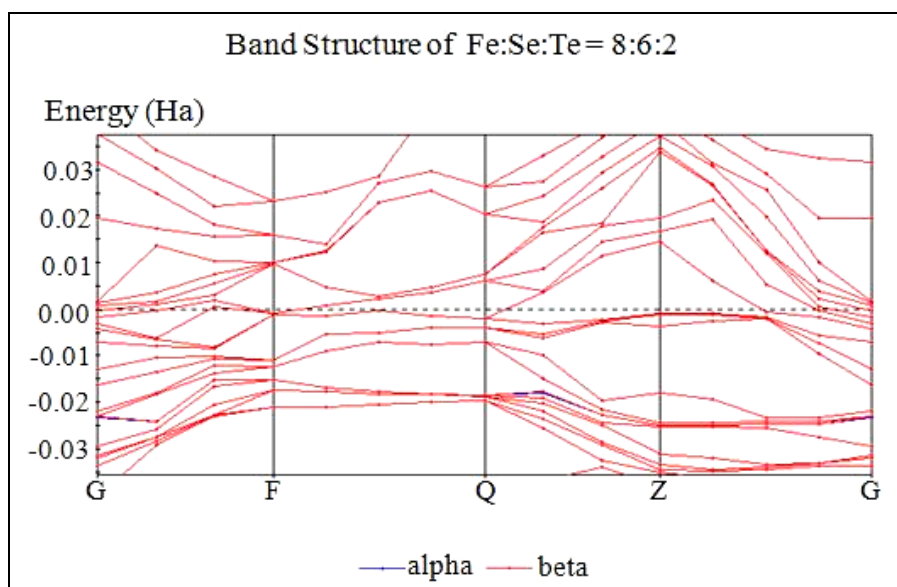


FIGURE 3.9.

The polarised band structure when vacant sites of Se are occupied by Te atoms so that the ratio of atoms is Fe:Se:Te = 8:6:2

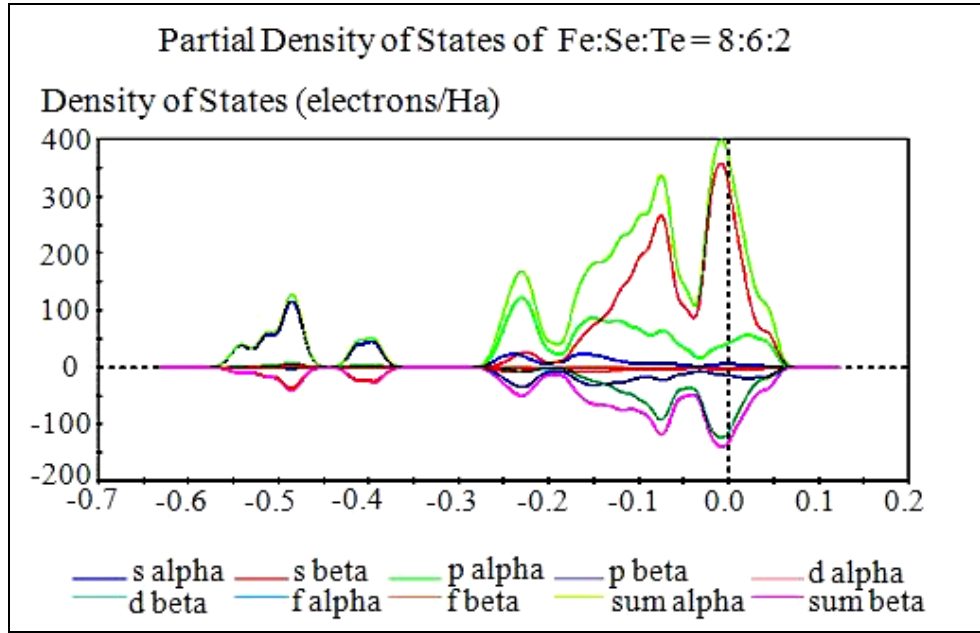


FIGURE 3.10.

The density of states (DOS) of Fe:Se:Te = 8:6:2 calculated by polarised orbitals.

Table 3.3. The band gap in eV at various points with varying ratios of atoms calculated using DFT(LDA).

S. No	Atomic Ratios	G	F	Q	Z
1	Fe:Se = 8:8(pol)	0.182	0.509	0.808	0.365
2	Fe:Se = 8:8(unpol)	0.180	0.522	0.691	0.346
3	Fe:Se = 8:6(pol)	0.250	0.234	0.533	0.076
4	Fe:Se = 8:6(unpol)	0.090	0.190	0.520	0.054
5	Fe:Se:Te = 8:6:2(pol)	0.030	0.286	0.220	0.419
6	Fe:Se:Te = 8:6:2(unpol)	0.044	0.219	0.204	0.416

Table 3.4. The Fermi energy in eV for the three systems

S. No	System	Fermi Energy (pol)	Fermi energy (unpol)
1	Fe:Se = 8:8	-4.80	-4.52
2	Fe:Se = 8:6	-4.73	-4.48
3	Fe:Se:Te = 8:6:2	-4.32	-4.00

SECTION 3.4

Conclusions

The magnetization, M in the Meissner effect should be modified to include the effect of mass density, $M = M_0\rho(x)$ where $\rho(x)$ is the mass per unit volume which depends on the coordinates. In the zero-field cooled samples, the value of $-1/4\pi$ is modified. Extensive calculation of the band gap in Fe_2Se_2 , Fe_2Se_1 and Fe_2SeTe indicates that the transition temperature of the superconductor increases with reduced normal state gap. It seems that doping and non-stoichiometry are important as found by Bednorz and Muller [1, 37] and periodic symmetry is relatively not important for the mechanism of superconductivity. That is why, the BCS theory, which requires periodic symmetry for the electron-phonon interaction is not immediately relevant to the present compounds.

CHAPTER 4

DENSITY-FUNCTIONAL

THEORY COMPUTATION OF

OXIDATION OF FeSe

FeSe with slight deficiency of Se is superconducting. Fe₂SeTe has higher transition temperature than FeSe. The transition temperature further increases upon oxidation. The band gaps of Fe₈Se₆O₂ as well as that of Fe₂Se₂ are calculated in this chapter. The calculated band gap reduces upon oxidation. The density-functional theory is used to optimize the cell parameter of Fe₈Se₆O₂ which are found to be $a = 6.9974\text{\AA}$, $b = 7.3016\text{\AA}$ and $c = 5.2444\text{\AA}$. The Fermi Energy is found to be -4.472eV for the polarized orbitals. The k-points for which the coordinate has been done are G (0, 0, 0), F (0, 0.5, 0), Q (0, 0.5, 0.5) and Z (0, 0, 0.5). The unpolarized band gap varies from 0.19eV at G point to 0.466eV at F point. These gap energies of Fe₈Se₆O₂ are smaller than those of Fe₂Se₂. Hence, in the chapter, the reduced normal state gap is found to have higher transition temperature.

SECTION 4.1

Introduction

FeSe becomes a superconductor when some Se atoms are missing. The magnetic moment of Fe per atom is almost completely neutralized so that the susceptibility is negative corresponding to diamagnetism. The electrons in Fe are strongly paramagnetic and ferromagnetic phase of Fe is well known. Even then upon addition of Se, at a suitable low temperature the ground state is diamagnetic. Because of these reasons, the superconductivity in Fe containing material is of special interest. We have calculated [38] the band structure of FeSe to determine the band gaps and the Fermi energy. The band gap as well as the Fermi energy of FeSe with extra oxygen atoms which replace Se atoms is calculated in this chapter. In this case it is found that the gap reduces which is accompanied with increase in transition temperature of the superconductor [18].

In this chapter, the calculation of the band structure of $\text{Fe}_8\text{Se}_6\text{O}_2$ is reported. The unit cell of Fe_2Se_2 is formed from which the Se atoms are removed and replaced with the oxygen atoms on that a large unit cell. Similarly, the calculation of band structure of $\text{Fe}_8\text{Se}_4\text{O}_4$ is also reported.

SECTION 4.2

Methodology

The method of calculation is to solve the Schrodinger equation in the density-functional theory. In order to make the problem tractable, we use the local density approximation (LDA). We use the spin unpolarized orbitals to calculate the energies. Since, polarization is important for magnetic atoms, we repeat the calculation with polarized orbitals. The density of states for electrons is obtained for both polarized as well as unpolarized orbitals.

4.2.1 Band Structure of $\text{Fe}_8\text{Se}_6\text{O}_2$

The unit cell of FeSe has two atoms of Fe and two atoms of Se. The Fe atoms are shared with other cell at the corner of a cube. The four atoms of Se in a tetrahedron inside the cube constitute only two atoms per cell. In order to dope it with oxygen, a much bigger cell is built. A larger cell which has 26 atoms of Fe located at the coordinates given in table 4.1 is formed. There are ten Se atoms and two oxygen atoms which replace Se sites. Therefore, the oxygen atoms occupy the sites of Se. Thus oxygen atoms are located at the antisites. The coordinate of all the 38 atoms are given in table 4.1. The k

points are G (0, 0, 0), F (0, 0.5, 0), Q (0, 0.5, 0.5) and Z (0, 0, 0.5). The band structure calculated by using the unpolarized orbital is given in Fig. 4.1 and that calculated by using polarized orbitals is given in Fig. 4.2. The gap energies are given in table 4.2. The unpolarized Fermi energy is found to be -4.472eV which changes to -4.450eV for polarized orbitals. The gap at G point is only 0.19eV for unpolarized orbitals which changes to 0.052eV for polarized orbitals. Hence, there is a large effect of spin polarization on the gap energy. The effect of spin polarization is highly anisotropic. At the Q point, the unpolarized gap is 0.446eV which upon polarization changes to 0.465eV. The unpolarized DOS is given in Fig. 4.3 and the polarized DOS is given in Fig. 4.4. Apparently, the DOS is not very sensitive to spin polarization in this system.

Table 4.1. Coordinate of atoms in $Fe_8Se_6O_2$

<i>Atoms</i>	<i>Coordinates</i>		
Fe	0, 0, 0	0, 0, 1	0.5, 0, 0.126
	0, 0.5, 0	0, 0.5, 1	0.5, 0.5, 0.126
	0, 1, 0	0, 1, 1	0.5, 1, 0.126
	1, 0, 0	1, 0, 1	0.5, 0, 1.126
	1, 0.5, 0	1, 0.5, 1	0.5, 0.5, 1.126
	1, 1, 0	1, 1, 1	0.5, 1, 1.126
	0.25, 0.25, 1	0.25, 0.25, 0	0.75, 0.25, 1
	0.25, 0.75, 1	0.25, 0.75, 0	0.75, 0.75, 1
	0.75, 0.25, 0	0.75, 0.75, 0	0.25, 0.5, 0.701
Se	0, 0.25, 0.319	0.25, 0, 0.701	0.75, 0.5, 0.701
	1, 0.25, 0.319	0.25, 1, 0.701	
	0, 0.75, 0.319	0.75, 0, 0.701	
	1, 0.75, 0.319	0.75, 1, 0.701	
O	0.5, 0.25, 0.18	0.5, 0.75, 0.18	

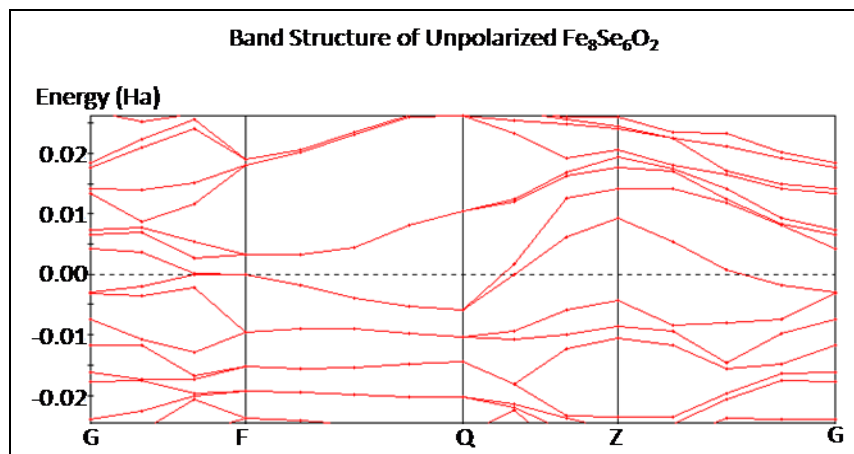


FIGURE 4.1.
The band structure of $\text{Fe}_8\text{Se}_6\text{O}_2$ calculated by using unpolarized orbitals

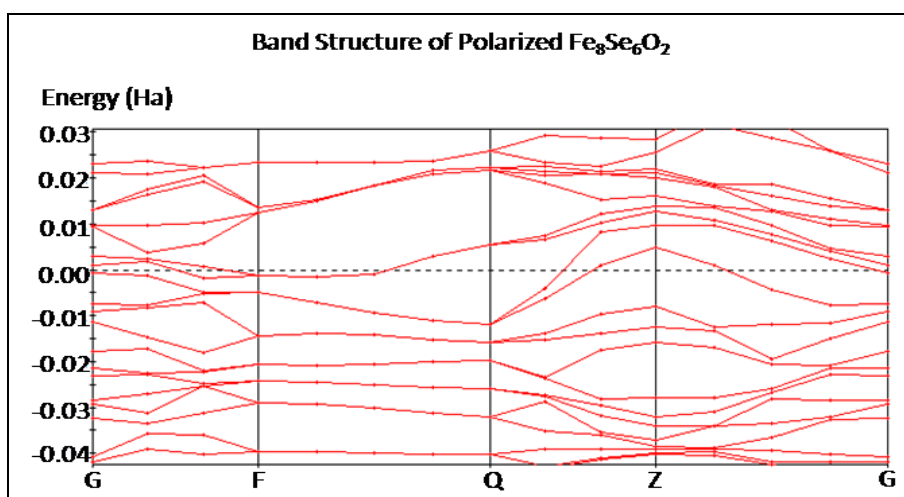


FIGURE 4.2.
The band structure of $\text{Fe}_8\text{Se}_6\text{O}_2$ calculated by using polarized orbitals

Table 4.2. The band gap of for polarized as well as unpolarized orbitals

<i>K</i> points	<i>Band Gap (eV)</i>	
	<i>UNPOLARIZED</i>	<i>POLARIZED</i>
G	0.190	0.052
F	0.264	0.373
Q	0.446	0.465
Z	0.370	0.356

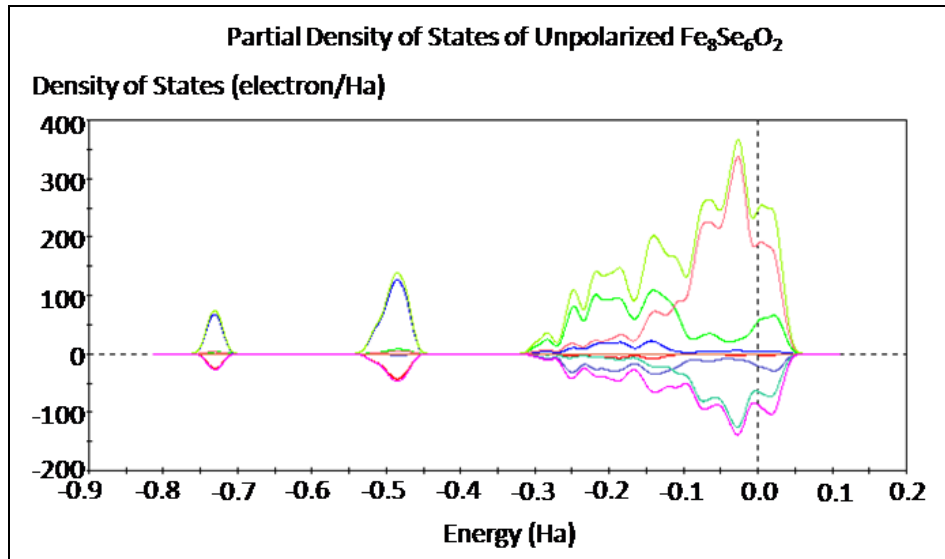


FIGURE 4.3.
The DOS of $\text{Fe}_8\text{Se}_6\text{O}_2$ for unpolarized orbitals.

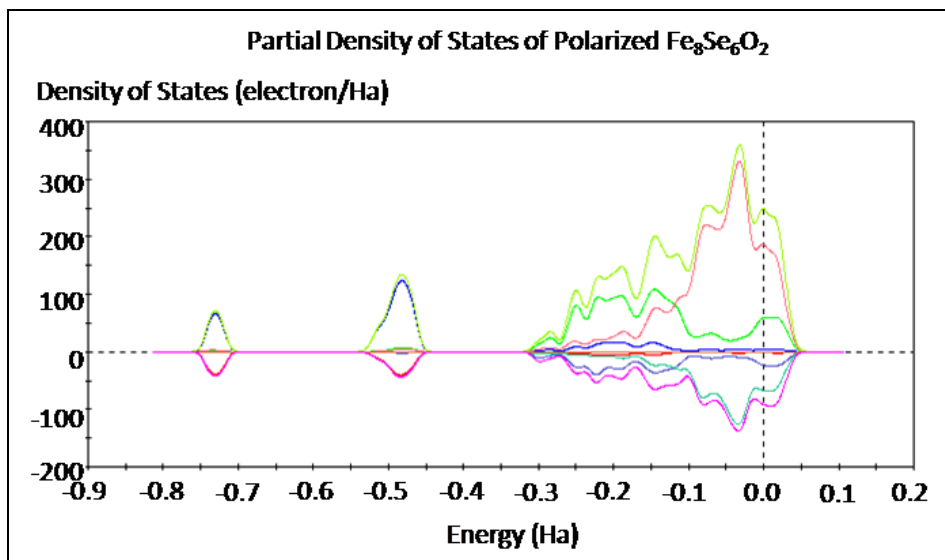


FIGURE 4.4.
The DOS of $\text{Fe}_8\text{Se}_6\text{O}_2$ for polarized orbitals.

4.2.2 Band Structure of Fe₈Se₄O₄

Now four oxygen atoms are located at the Se antisites. Therefore, the unit cell has half the structure of the Se atoms replaced by oxygen atoms. There is a displacement of Fe atoms due to optimization. The movement of Fe atoms might reveal the secret of increased transition temperature in the superconducting state. The coordinates of Fe, Se and O atoms are given in table 4.3. The magnitude of the Fermi energy has increased upon adding extra oxygen atoms. Now for Fe₈Se₄O₄ the Fermi energy is -4.613 eV for unpolarized orbitals and -4.771 eV for the polarized orbitals. The band structure calculated by using the unpolarized orbitals is given in Fig. 4.5 and that for the polarized orbitals is given in Fig. 4.6 and the polarized DOS is given in Fig. 4.7. The effect of spin polarized is much reduced in Fe₈Se₄O₄ compared with that in Fe₈Se₆O₂. This is an important result because it shows the effect of “spin reduction” upon doping the Fe material with oxygen.

Table 4.3. Coordinate of atoms in Fe₈Se₄O₄

Atoms	Coordinates		
Fe	0, 0, 0	0.5, 0, 0	0, 0, 1
	0, 0.5, 0	0.5, 0.5, 0	0, 0.5, 1
	0, 1, 0	0.5, 1, 0	0, 1, 1
	1, 0, 1	1, 0, 0	0.5, 0, 1
	1, 0.5, 1	1, 0.5, 0	0.5, 0.5, 1
	1, 1, 1	1, 1, 0	0.5, 1, 1
	0.75, 0.25, 0	0.75, 0.25, 1	0.25, 0.25, 0
	0.75, 0.75, 0	0.75, 0.75, 1	0.25, 0.75, 0
	0.25, 0.25, 1	0.25, 0.75, 1	
Se	0.25, 0, 0.643	0.25, 0.5, 0.643	0.25, 1, 0.643
	0.75, 1, 0.643	0.75, 0, 0.643	0.75, 0.5, 0.643
O	0.5, 0.25, 0.117	0.5, 0.75, 0.117	0, 0.25, 0.117
	1, 0.75, 0.117	0, 0.75, 0.117	1, 0.25, 0.117

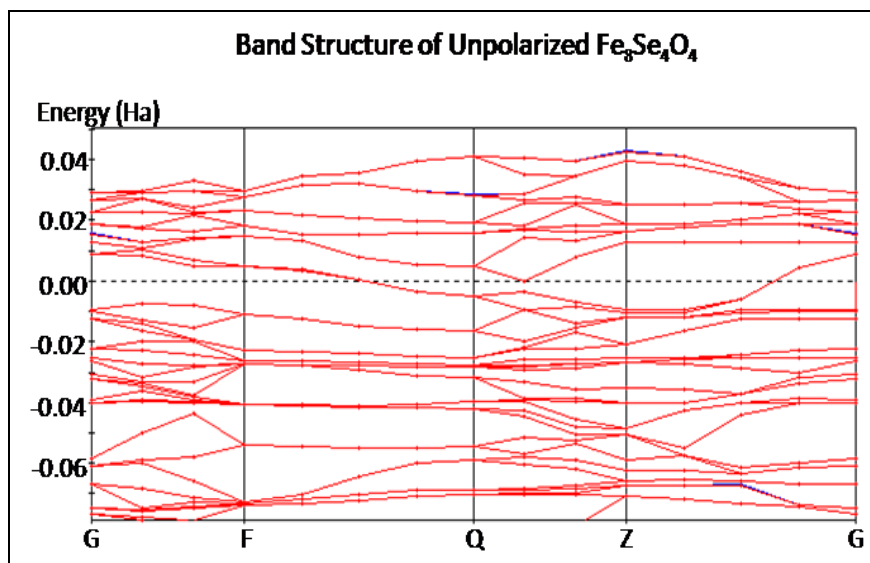


FIGURE 4.5.
The band structure of $\text{Fe}_8\text{Se}_4\text{O}_4$ calculated by using unpolarized orbitals

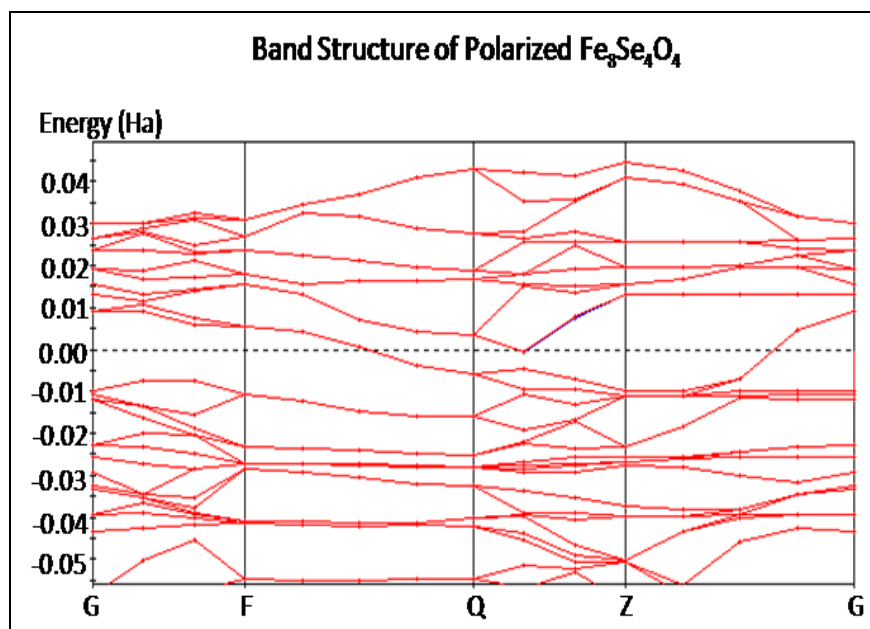


FIGURE 4.6.
The band structure of $\text{Fe}_8\text{Se}_4\text{O}_4$ calculated by using polarized orbitals

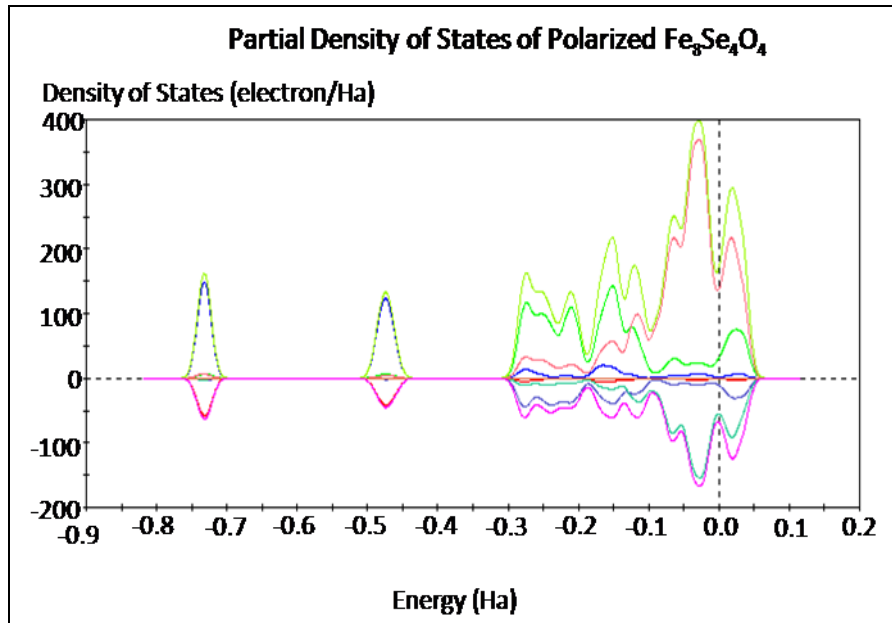


FIGURE 4.7.
The DOS of Fe₈Se₆O₂ for polarized orbitals.

Table 4.4. The band gap of for polarized as well as unpolarized orbitals

<i>K</i> points	<i>Band Gap (eV)</i>	
	<i>UNPOLARIZED</i>	<i>POLARIZED</i>
G	0.498	0.506
F	0.427	0.444
Q	0.269	0.253
Z	0.672	0.620
G	0.498	0.506

SECTION 4.3

Binding Energy

The binding energy of $\text{Fe}_8\text{Se}_6\text{O}_2$ for unpolarized orbitals is found to be -118.77eV and for polarized orbitals is -137.43eV . The effect of spin is thus seen to be only about 17 percent. When oxygen is increased to form $\text{Fe}_8\text{Se}_4\text{O}_4$ the binding energy is reduced to -109.78eV for unpolarized and -112.77eV for the polarized orbitals. The bonds have thus become weaker upon oxidation. The weaker bonds have higher transition temperature.

SECTION 4.4

Conclusions

The oxidation of FeSe is found to produce a large effect on the normal state gap energy. The weaker bonds in the oxide have larger transition temperature. The iron containing superconductors found recently [25, 27, 39] require deeper theoretical understanding than is available at this time.

CHAPTER 5

ELECTRONIC BAND

STRUCTURE OF FeSeTeO

SUPERCONDUCTOR

The $\text{Fe}_{1.068}\text{Te}$ exhibits a first order structural transition at 67K which is not a superconductivity phase but such distortions are seen in the superconductors. The lattice of FeTe is monoclinic P21/m which changes to P4/mmm above T_N . The doped system $\text{Fe}_{1+y}\text{Se}_x\text{Te}_{1-x}$ is superconducting at about 14K. $\text{Fe}(\text{Se}_{1-x}\text{Te}_x)_{0.82}$ has a superconducting phase for $0.3 < x < 1.0$. The superconducting transition temperature increases upon oxidation. Hence, the band structure of FeSeTeO I calculated in this chapter and it is compared with FeSeTe structure. We find that onset of superconductivity is related to the reduced gap energy of the normal state.

SECTION 5.1

Introduction

Recently it has been reported by Fang et al [40] that $\text{Fe}(\text{Se}_{1-x}\text{Te}_x)_{0.82}$ is superconducting with the maximum value of the transition temperature of $\sim 14\text{K}$ for $0.3 < x < 1.0$. Li et al [42] find that there is an antiferromagnetic phase. It is known that oxidation in similar systems stabilises superconductivity [42, 43] and increase the transition temperature. A study of the normal state of the superconductor is needed to understand the origin of superconductivity in these unusual Fe containing materials. According to Meissner effect, there is no magnetic field in the superconducting state. Hence, the way magnetic moment of Fe is neutralized is to be understood.

The band structure of FeSeTeO is calculated to investigate the change in the band gap upon oxidation of FeSe to which Te has already been added.

SECTION 5.2

The Band Structure

The larger cell of FeSeTe is built by 26 Fe atoms as given in Table 5.1. There are 9 Se atoms placed at $z = 0.759$ and another 9 Te atoms at $z = 0.275$. The coordinates of the Fe, Se and Te atoms after optimisation are given in table 5.1. The introduction of oxygen is obtained by removing two Te atoms and two oxygen atoms to replace the Te vacancy. Since, the configuration of atoms is optimised for the minimum energy; Fe atoms are found to move upon optimization. The coordinate of all the atoms of FeSeTeO in the optimised configuration are given in Table 5.2. It is found that the optimised cell has $a = 6.5855\text{\AA}$, $b = 7.3511\text{\AA}$ and $c = 5.2279\text{\AA}$. The band structure with unpolarised orbitals as well as with polarised orbitals is calculated. When unpolarised orbitals are used the Fermi energy of FeSeTeO is found to be -4.177eV and it becomes -4.439eV for polarised orbitals. The binding energy is -104.28eV for the unpolarised and -108.49eV for the polarised orbitals.

Table 5.1. Coordinate of atom in FeSeTe

Atoms	Coordinate		
Fe	0, 0, 0	0.5, 0, 0	1, 0, 0
	0, 0.5, 0	0.5, 0.5, 0	1, 0.5, 0
	0, 1, 0	0.5, 1, 0	1, 1, 0
	0, 0, 1	0.5, 0, 1	1, 0, 1
	0, 0.5, 1	0.5, 0.5, 1	1, 0.5, 1
	0, 1, 1	0.5, 1, 1	1, 1, 1
	0.25, 0.25, 0	0.25, 0.25, 1	0.75, 0.25, 0
	0.25, 0.75, 0	0.25, 0.75, 1	0.75, 0.75, 0
	0.75, 0.25, 1	0.75, 0.75, 1	
Se	0.25, 0, 0.759	0.25, 0.5, 0.759	0.25, 1, 0.759
	0.75, 0, 0.759	0.75, 0.5, 0.759	0.75, 1, 0.759
Te	0, 0.25, 0.275	1, 0.25, 0.275	0, 0.75, 0.275
	1, 0.75, 0.275	0.5, 0.25, 0.275	0.5, 0.75, 0.275

Table 5.2. Coordinate of atoms in FeSeTeO

Atoms	Coordinate		
Fe	0, 0, 0	0.5, 0, 0.312	1, 0, 0
	0, 0.5, 0	0.5, 0.5, 0.312	1, 0.5, 0
	0, 1, 0	0.5, 1, 0.312	1, 1, 0
	0, 0, 1	0.5, 0, 1.320	1, 0, 1
	0, 0.5, 1	0.5, 0.5, 1.320	1, 0.5, 1
	0, 1, 1	0.5, 1, 1.320	1, 1, 1
	0.25, 0.25, 0	0.25, 0.25, 1	0.75, 0.25, 0
	0.25, 0.75, 0	0.25, 0.75, 1	0.75, 0.75, 0
		0.75, 0.25, 1	0.75, 0.75, 1
Se	0.25, 0, 0.705	0.25, 0.5, 0.705	0.25, 1, 0.705
	0.75, 0, 0.705	0.75, 0.5, 0.705	0.75, 1, 0.705
Te	0, 0.25, 0.369	1, 0.25, 0.369	0, 0.75, 0.369
	1, 0.75, 0.369		
O	0.5, 0.25, 0.245	0.5, 0.75, 0.245	

The band structure of FeSeTeO obtain for unpolarised orbitals is given in Fig. 5.1 and that obtained for the polarised orbitals is given in Fig. 5.2. The energy gap for FeSeTe is given in table 5.3 as well as FeSeTeO at various k-points is given in Table 5.4. From the results obtained for FeSeTeO, it is clear that G point has a special position. At this point the gap gives a minimum value while it is almost constant at other points. This is also the point which is maximum affected by polarization. The unpolarised gap at this point is 0.101eV which reduces to 0.046eV upon polarisation. The gap at F, Q and Z points is almost equal to 0.3eV and not much affected by the spin polarization. The gap is thus having a dip at G point and three times higher value at other point. It is also seen that

the energy gap for FeSeTe reduces upon oxidation. The density of states (DOS) for the unpolarised wave functions is given in Fig. 5.3 and for the polarised wavefunctions in Fig. 5.4. It is showing only small qualitative effect of spin polarisation. The system is not sensitive to spin polarization. The Fe atoms in this material have very weak magnetic moment per atom. Apparently, weak magnetization is taken over by the superconducting state.

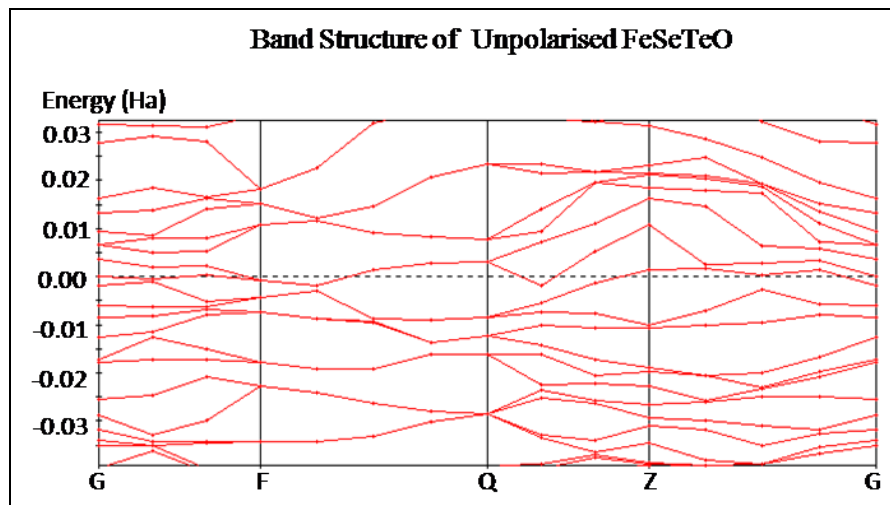


FIGURE 5.1.

The band structure of FeSeTeO calculated by using unpolarised orbitals

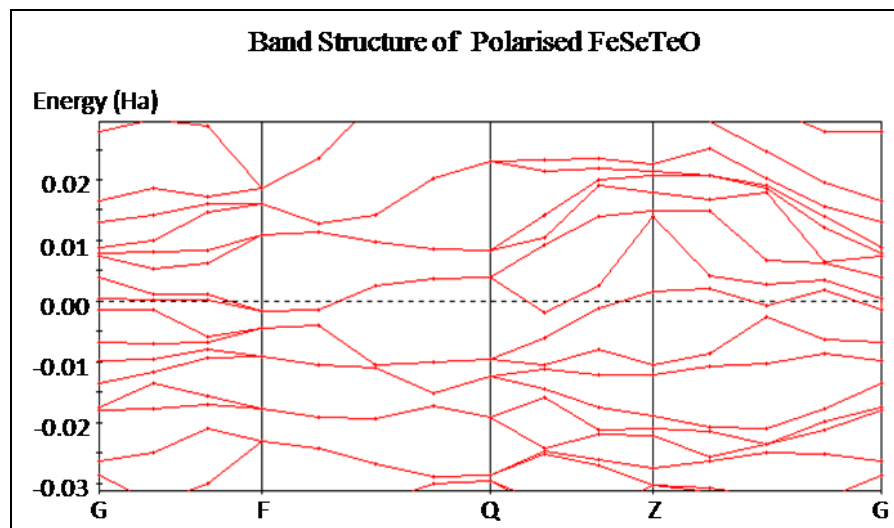


FIGURE 5.2.

The band structure of FeSeTeO calculated by using polarised orbitals

Table 5.3 The energy gap of various point in FeSeTe

K-point	Coordinate	Energy Gap (eV)	
		Unpolarised	Polarised
G	0, 0, 0	0.199	0.250
F	0, 0.5, 0	0.302	0.272
Q	0, 0.5, 0.5	0.321	0.259
Z	0, 0, 0.5	0.321	0.395

Table 5.4. The energy gap of various point

K points	Energy gap (eV)	
	UNPOLARIZED	POLARIZED
G	0.101	0.046
F	0.313	0.343
Q	0.316	0.365
Z	0.316	0.329

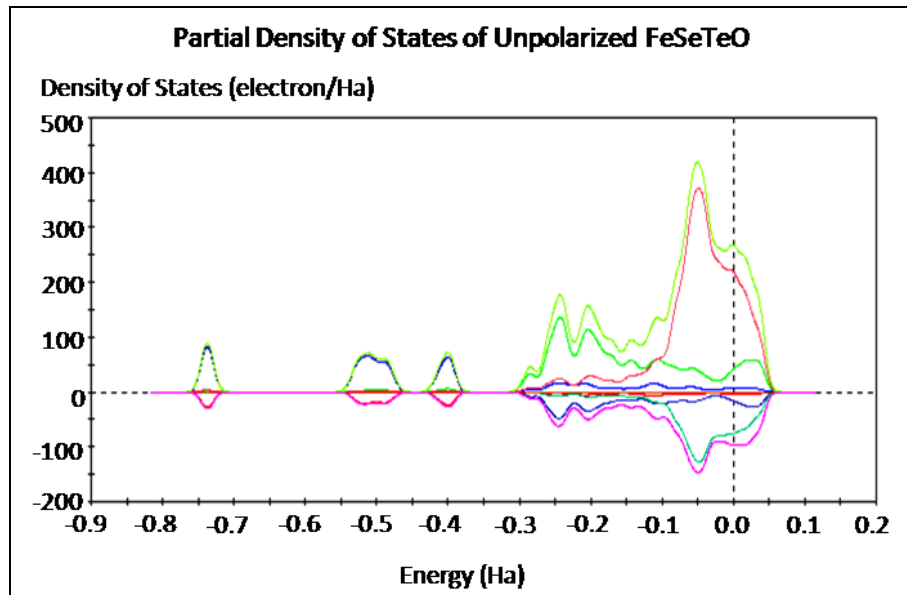


FIGURE 5.3.
The DOS of FeSeTeO for unpolarised orbitals.

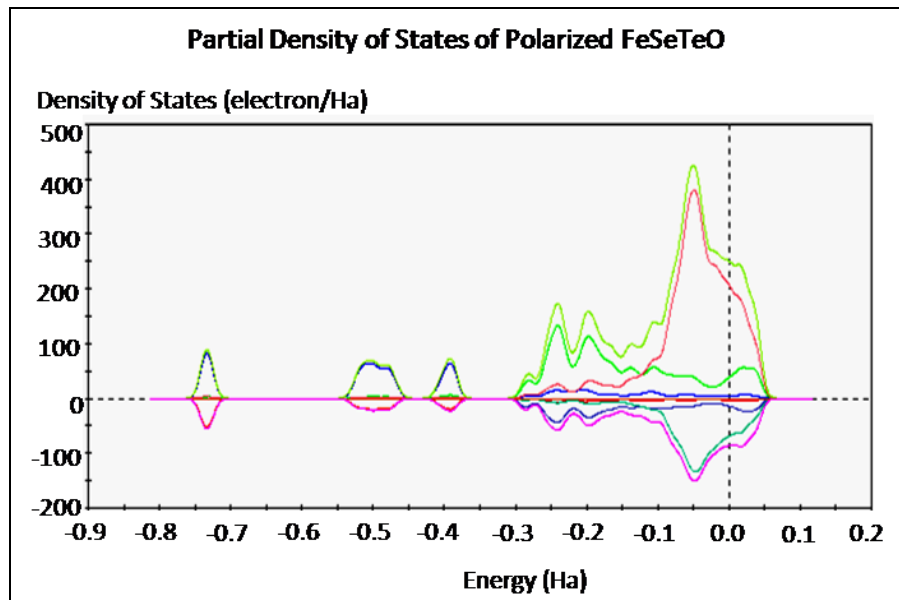


FIGURE 5.4.
The DOS of FeSeTeO for polarised orbitals.

SECTION 5.3

Conclusions

This study found that oxidation reduces the normal state gap. At point G, the polarised gap of FeSeTe is calculated to be 0.250eV reduces to 0.046eV upon oxidation. The effect of spin polarisation of wavefunctions on the DOS is small and only qualitative. The smaller gap in the oxygen containing material is accompanied with larger transition temperature of the superconductivity state.

CHAPTER 6

BAND STRUCTURE OF FeSe WITH LAYERS OF SAMARIUM AND TELLURIUM ATOMS

In this chapter, the band structure of FeSe with layers of Te and Sm atoms is reported. By adding Te atom to FeSe increases the transition temperature of the superconductor. Adding Sm further increases the T_c up to 55K in the As compound. The experimental values are available for the As compound but for Se compound, the experiments have yet to be done. The band structure of four different compounds has been calculated (a) FeSeSmO, (b) Fe₂SeSm₂O₂, (c) FeSeTeSmO and (d) FeTeSmO. The Fermi energy and the binding energy have been calculated in each case. The band gap has been found at various wave vectors with unpolarised as well as polarised orbitals.

SECTION 6.1

Introduction

Recently, it has been reported by Fang et al that Fe (Se_{1-x}Te_x)_{0.82} (0.3<x<1.0) is superconducting with the minimum transition temperature of ~14K [40]. In the analogous As compound, addition of Sm leads to increased transition temperature as shown in Table 6.1. FeSe_{0.82} has a PbO type structure with tetragonal space group, P4/nmm which is superconducting with transition temperature of 8K. The hexagonal FeSe_{1.14} is a ferromagnet. The addition of Te in FeSe leads to increase in the transition temperature from 8K to nearly 14K. Similarly, we expect that T_c will increase upon addition of rare earth atoms. Since, it is known that chemical composition is important to produce a superconducting compound; this chapter point out that normal state can also be studied by changing composition. It may be possible to predict the superconducting state by means of changes in the band gap of the normal state. Therefore, the study of normal state band gap is taken up.

Table 6.1. Some of the Sm containing compounds which have a superconducting phase. Some are magnetic

<i>S. No</i>	<i>Formula</i>	<i>T_c (K)</i>	<i>Ref.</i>
1	Sm _{1.85} Ce _{0.15} CuO _{4-x}	23	[44]
2	SmBa ₂ Cu ₃ O _{7-δ}	Magnetic	[45]
3	Sm ₃ Co ₄ Sn ₁₃	Magnetic	[46]
4	SmFePO	3	[47]
5	SmFeAsO _{0.82} F _{0.18}	55	[48]
6	SmO _{1-x} F _x FeAs	26	[43]

The density functional theory is used to calculate the normal state band gap of four compounds, FeSeSmO, Fe₂SeSm₂O₂, FeSeTeSmO and FeTeSmO. The Fermi energy as well as the chemical binding for unpolarised as well as the spin polarised orbitals is also calculated.

SECTION 6.2

Methodology

The method of calculation uses the ordinary quantum mechanics with density functional theory in the local density approximation first develop by Kohn and Sham.

6.2.1 FeSeSmO

The unit cell for FeSeSmO has a layer of Fe atoms, then a layer of Se atoms, then Sm, then O, then Sm, then Se and Fe again. The top and bottom layers are on the Se sites. Thus, there are 10 Fe atoms, 4 Se atoms, 4 Sm and 5 O atoms in the large unit cell. When optimised, it has a large $c = 7.2092\text{\AA}$ and $a = b = 3.7833\text{\AA}$ as shown in Fig. 6.1. The coordinates of Fe, Se, O and Sm atoms are given in table 6.2. The Fe and Se are on their own sites while O and Sm are on antisites. The Fermi energy is calculated to be -

7.897eV for the unpolarised wave functions and -8.062eV for the polarised orbitals. Thus the effect of spin polarisation on the Fermi Energy is only ~1.2 per cent. Similarly, the binding energy is found to be -42.812eV for unpolarised orbitals to -44.686eV for polarised orbitals. The points in the wave vector space are Z (0, 0, 0.5), A (0.5, 0.5, 0.5), M (0.5, 0.5, 0), G (0, 0, 0), R (0, 0.5, 0.5) and X (0, 0.5, 0). The band structure calculated by using polarised orbitals is given in Fig. 6.2. The gap energies are Zero at the X point and largest at the A point as seen in Table 6.3. The effect of spin polarisation on the gap energies is small. For example, at the Z point the energy gap calculated for the unpolarised orbitals is 0.57eV which becomes ~0.53eV for polarised orbitals.

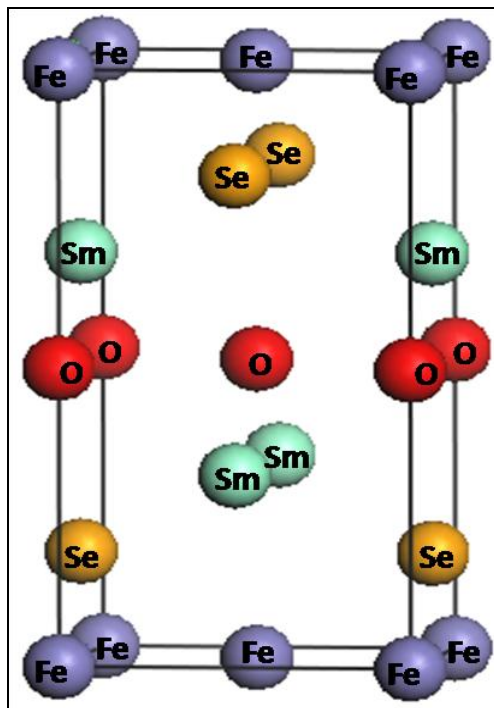


FIGURE 6.1.
The unit cell of FeSeSmO stack of atoms.

Table 6.2. The coordinates of FeSeSmO atoms in a unit cell.

Atoms	Coordinates				
Fe	0, 0, 0	0.5, 0.5, 0	1, 0, 0	0, 0, 1	1, 0, 1
	0, 1, 0	0.5, 0.5, 1	1, 1, 0	0, 1, 1	1, 1, 1
Se	0, 0.5, 0.176	1, 0.5, 0.176	0.5, 0, 0.824	0.5, 1, 0.824	
O	0, 0, 0.5	0, 1, 0.5	0.5, 0.5, 0.5	1, 0, 0.5	1, 1, 0.5
Sm	0.5, 0, 0.322	0.5, 1, 0.322	0, 0.5, 0.678	1, 0.5, 0.678	

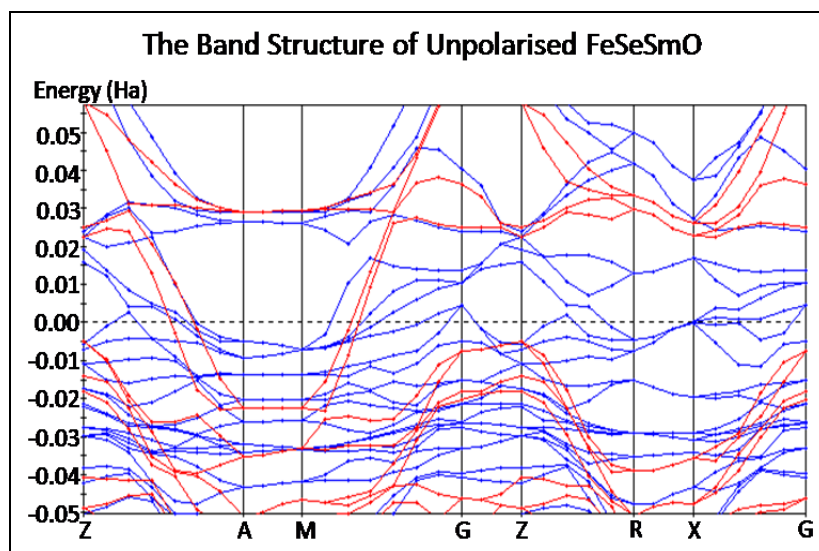


FIGURE 6.2.

The band structure of FeSeSmO calculated by using unpolarised orbitals.

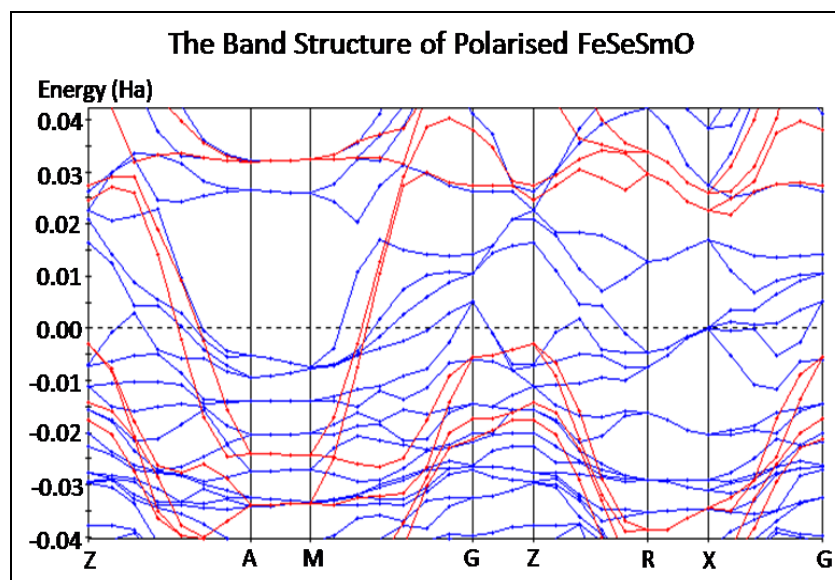


FIGURE 6.3.

The band structure of FeSeSmO calculated by using polarised orbitals.

Table 6.3. The energy gap for various k points.

K- point	Coordinates	Energy gap (eV)	
		unpolarized	Polarized
Z	0, 0, 0.5	0.5714	0.5279
A	0.5, 0.5, 0.5	0.8544	0.8653
M	0.5, 0.5, 0	0.9034	0.9034
G	0, 0, 0	0.2503	0.2912
Z	0, 0, 0.5	0.5714	0.5279
R	0, 0.5, 0.5	0.4789	0.4708
X	0, 0.5, 0	0	0
G	0, 0, 0	0.2503	0.2912

The density of states (DOS) for the unpolarised orbitals is shown in Fig. 6.4 while that for polarised orbitals is given in Fig. 6.5. In the positive energy part there is clearly some effect of polarised orbitals which shows that the Fe spins are important in the conduction band.

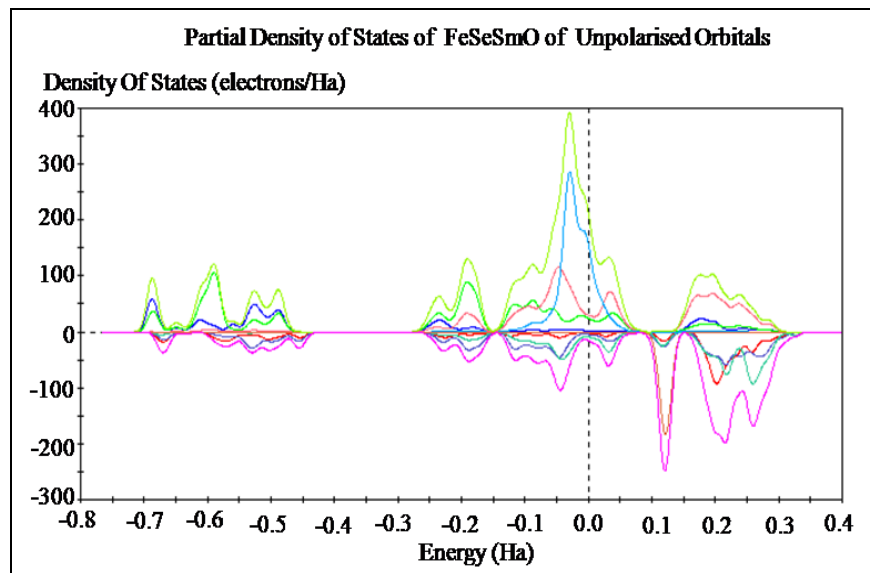


FIGURE 6.4.
The DOS of FeSeSmO for unpolarized orbitals.

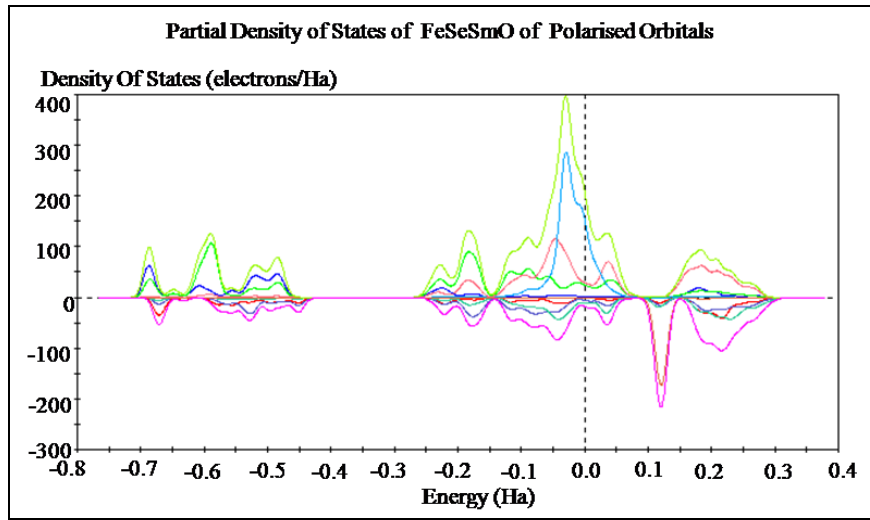


FIGURE 6.5.
The DOS of FeSeSmO for polarized orbitals.

6.2.2 $\text{Fe}_2\text{SeSm}_2\text{O}_2$

One layer of Se atoms are removed so that the unit cell becomes slightly smaller than in Fig. 6.1. We show this magnified cell in Fig. 6.6. The optimized cell constant are now $a = 3.9958\text{\AA}$ and $c = 6.7255\text{\AA}$. The coordinates of various atoms are given in Table 6.4. The Fermi energy for the unpolarised orbitals is found to be -4.154eV and for the polarized orbitals it is -4.24eV showing only about 2 percent effect of using the polarized orbitals. The binding energy for the unpolarised orbitals is -72.26eV which becomes -73.00eV for polarized orbitals. The wavevector points are G (0, 0, 0), F (0, 0.5, 0), Q (0, 0.5, 0.5) and Z (0, 0, 0.5). The unpolarised largest gap of 0.61eV is found at the G point which is not affected by the polarized orbitals. Similarly, the gap energy of 0.378eV at F point is not affected by the polarized orbitals. However, at Q point the unpolarised gap is 0.185eV which changes to 0.163eV when polarized orbitals are used. At the Z point also the unpolarised gap of 0.5143eV is changed to 0.495eV for the polarized orbitals. The band structure calculated by using the polarized orbitals is given

in Fig. 6.7 and that calculated by using polarized orbitals is given in Fig. 6.8. The DOS for the unpolarised wavefunction is given in Fig. 6.9 and for the polarized wave functions is given in Fig. 6.10. Somehow, the DOS is not very sensitive to spin polarized wave functions.

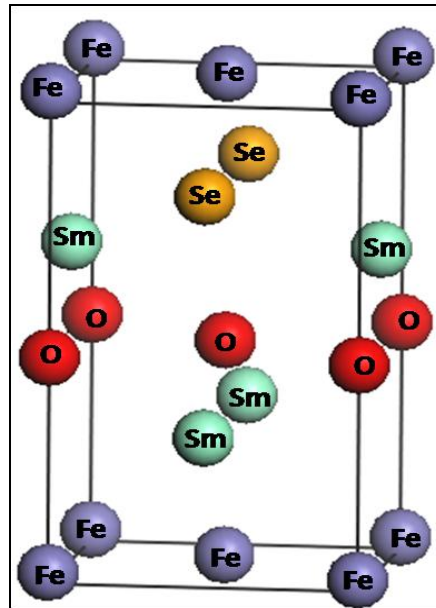


FIGURE 6.6.
The unit cell of $\text{Fe}_2\text{SeSm}_2\text{O}_2$ stack of atoms.

Table 6.4. The coordinates of $\text{Fe}_2\text{SeSm}_2\text{O}_2$ atoms in a unit cell.

Atoms	Coordinates				
Fe	0, 0, 0	1, 0, 0	1, 1, 0	0, 1, 0	0.5, 0.5, 0
Se	0.5, 0, 0.788	0.5, 1, 0.788			
O	0, 0, 0.446	1, 0, 0.446	1, 1, 0.446	0, 1, 0.446	0.5, 0.5, 0.446
Sm	0.5, 0, 0.287	0, 0.5, 0.643	0.5, 1, 0.287	1, 0.5, 0.643	

Table 6.5. The energy gap for various k points

K -point	Coordinates	Energy gap (eV)	
		Unpolarized	Polarized
G	0, 0, 0	0.6095	0.6095
F	0, 0.5, 0	0.3782	0.3728
Q	0, 0.5, 0.5	0.1850	0.1633
Z	0, 0, 0.5	0.5143	0.4952
G	0, 0, 0	0.6095	0.6095

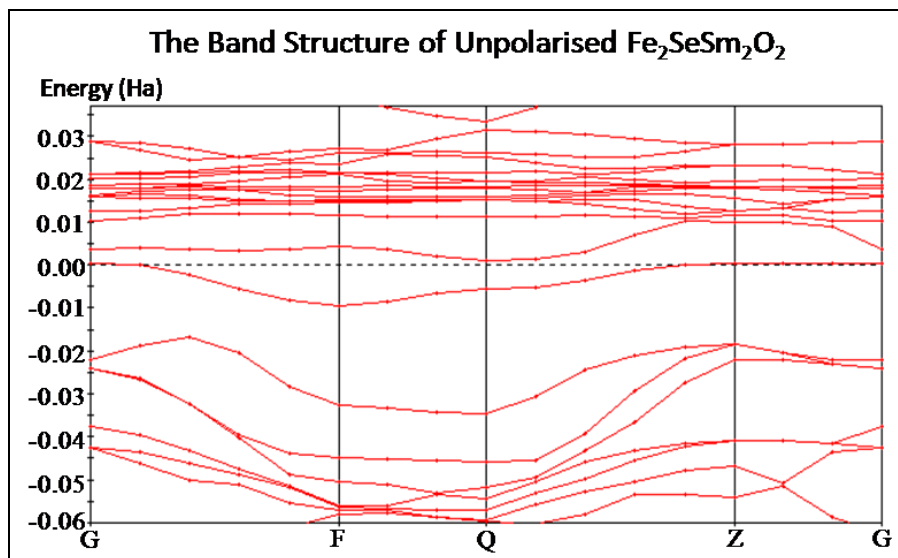


FIGURE 6.7.
The band structure of Fe₂SeSm₂O₂ calculated by using unpolarised orbitals.

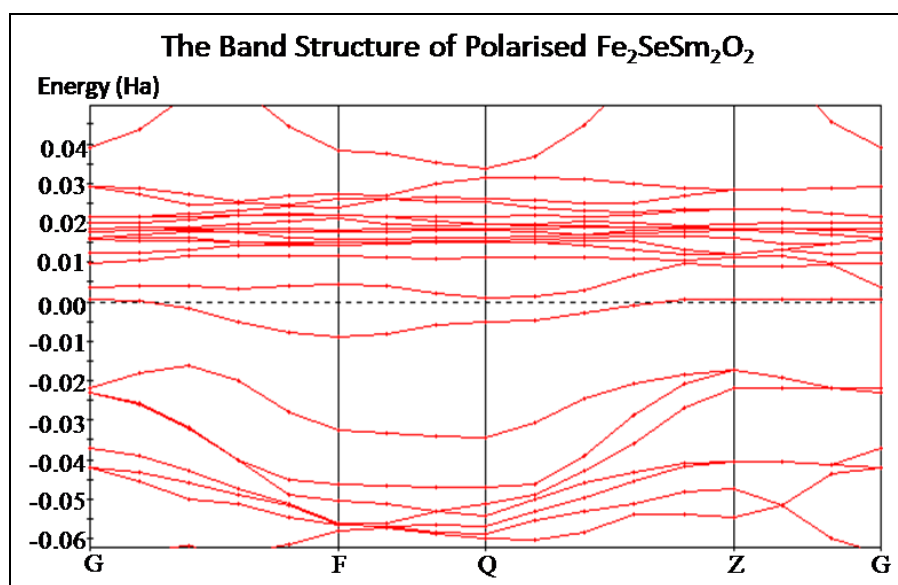


FIGURE 6.8.
The band structure of Fe₂SeSm₂O₂ calculated by using polarised orbitals.

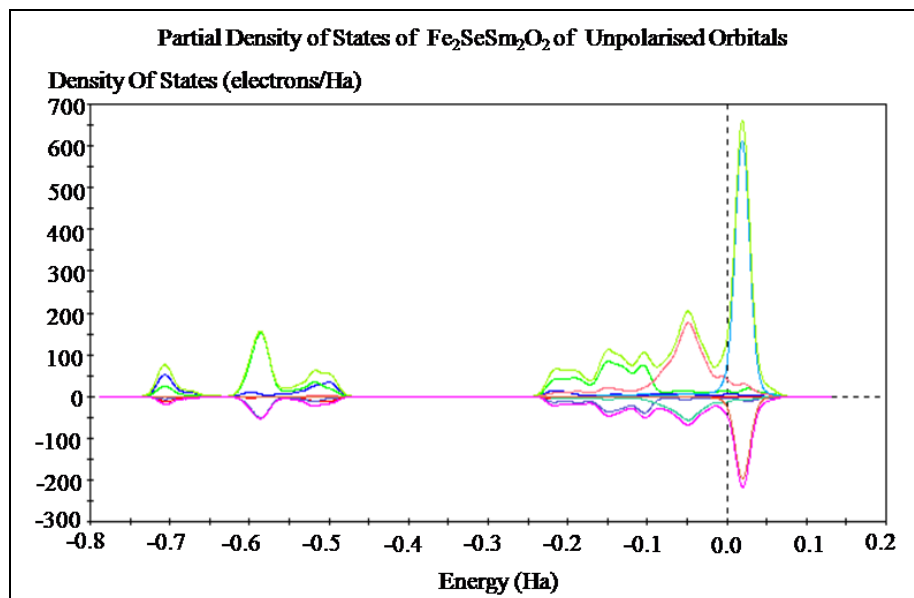


FIGURE 6.9.
The DOS of $\text{Fe}_2\text{SeSm}_2\text{O}_2$ for unpolarized orbitals.

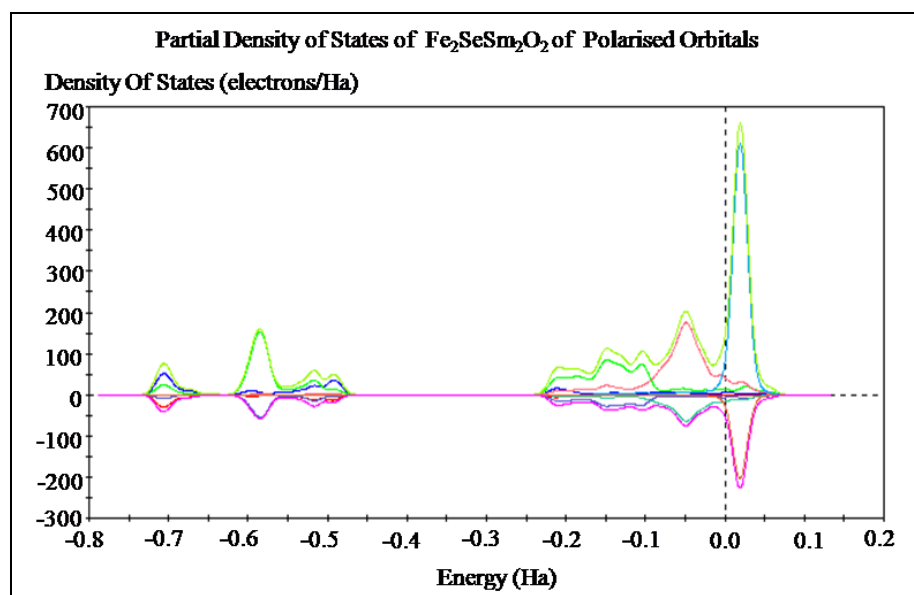


FIGURE 6.10.
The DOS of $\text{Fe}_2\text{SeSm}_2\text{O}_2$ for polarized orbitals.

6.2.3 FeSeTeSmO

The unit cell of FeSeTeSmO has layers of atoms in the sequence Fe Se Sm O Sm Te Fe. The top layer of Fe as well as the bottom layer of Fe is on the usual Fe sites. The Se atoms are on their own sites. The Te is on the Se sites. The O atoms are on the Fe antisites as shown in Fig. 6.11. The unit cell constants are $a = 4.2233\text{\AA}$ and $c = 6.0213\text{\AA}$. The coordinates of all these atoms are given in Table 6.6. The band structure is calculated by using spin unpolarised as well as spin polarised orbitals. The unpolarised Fermi energy is found to be -3.849eV and the polarised value is -4.008eV . Thus the effect of polarisation is only about 4 percent. The binding energy for the unpolarised orbitals is -74.187eV and it is -75.64eV for the polarised orbitals showing only 1.2 percent effect of polarisation of the orbitals. The wave vector points are G (0, 0, 0), F (0, 0.5, 0), Q (0, 0.5, 0.5) and Z (0, 0, 0.5). The gap energies calculated for the polarised as well as the unpolarised orbitals are given in Table 6.7. Very large effect of spin polarisation is clearly visible. The F and Z points are not very sensitive to spin polarised orbitals but the effect is largest at Q point. The calculated band structure for unpolarised orbitals is given in Fig. 6.12 and that of the polarised orbitals is given in Fig. 6.13. The unpolarised DOS is given in Fig. 6.14 and the polarised is given in Fig. 6.15.

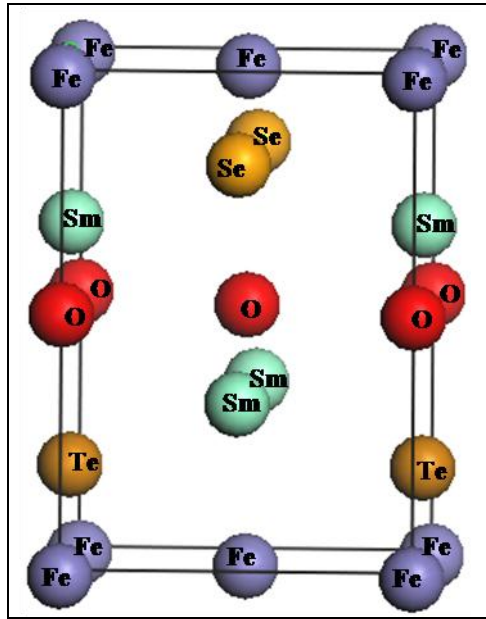


FIGURE 6.11.
The unit cell of FeSeTeSmO stack of atoms.

Table 6.6. The coordinates of FeSeTeSmO atoms in a unit cell.

Atoms	Coordinates				
	Fe	0, 0, 0	1, 0, 0	0, 1, 0	1, 1, 0
Te	0, 0.5, 0.187	1, 0.5, 0.187			
Se	0.5, 0, 0.813	0.5, 1, 0.813			
O	0, 0, 0.511	1, 0, 0.511	0, 1, 0.511	1, 1, 0.511	0.5, 0.5, 0.511
Sm	0.5, 0, 0.335	0, 0.5, 0.673	0.5, 1, 0.335	1, 0.5, 0.673	

Table 6.7. The band gap energies at various k points

K- point	Coordinate	Energy gap (eV)	
		unpolarized	Polarized
G	0, 0, 0	0.0898	0.5959
F	0, 0.5, 0	0.3728	0.3456
Q	0, 0.5, 0.5	0.0027	0.1796
Z	0, 0, 0.5	0.8245	0.8218
G	0, 0, 0	0.0898	0.5959

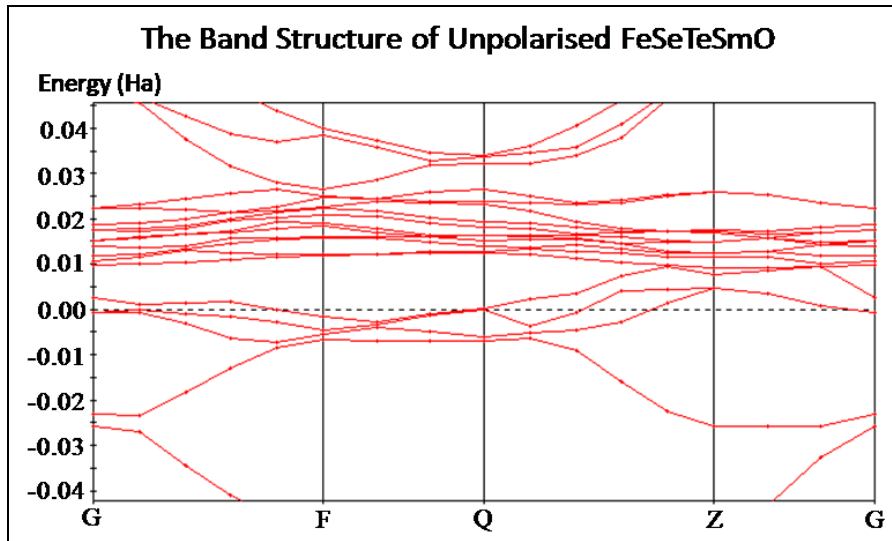


FIGURE 6.12.
The band structure of FeSeTeSmO calculated by using unpolarised orbitals.

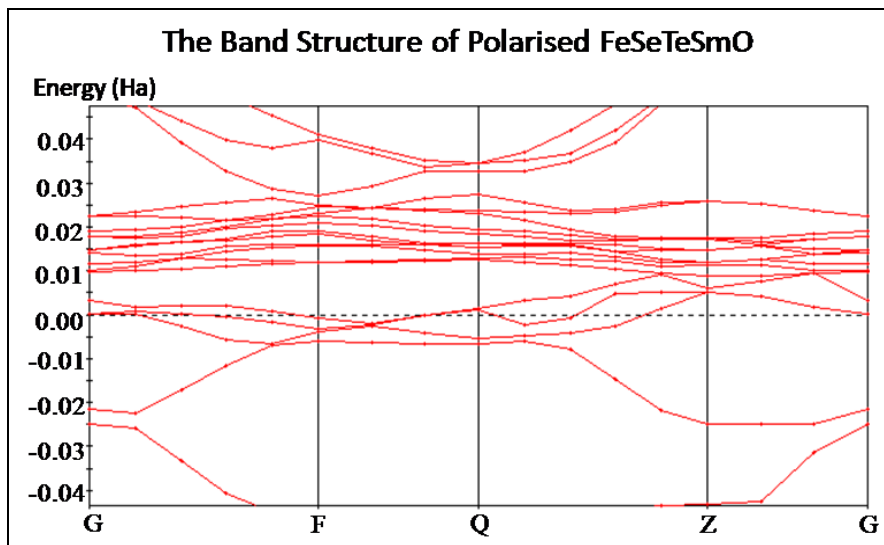


FIGURE 13.
The band structure of FeSeTeSmO calculated by using polarised orbitals.

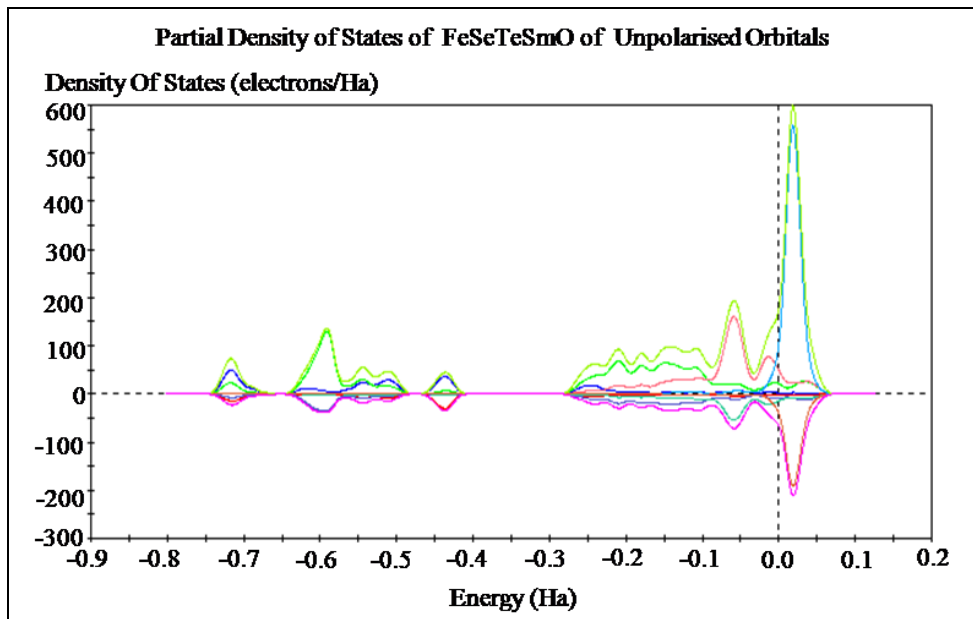


FIGURE 6.14.
The DOS of FeSeTeSmO for unpolarized orbitals.

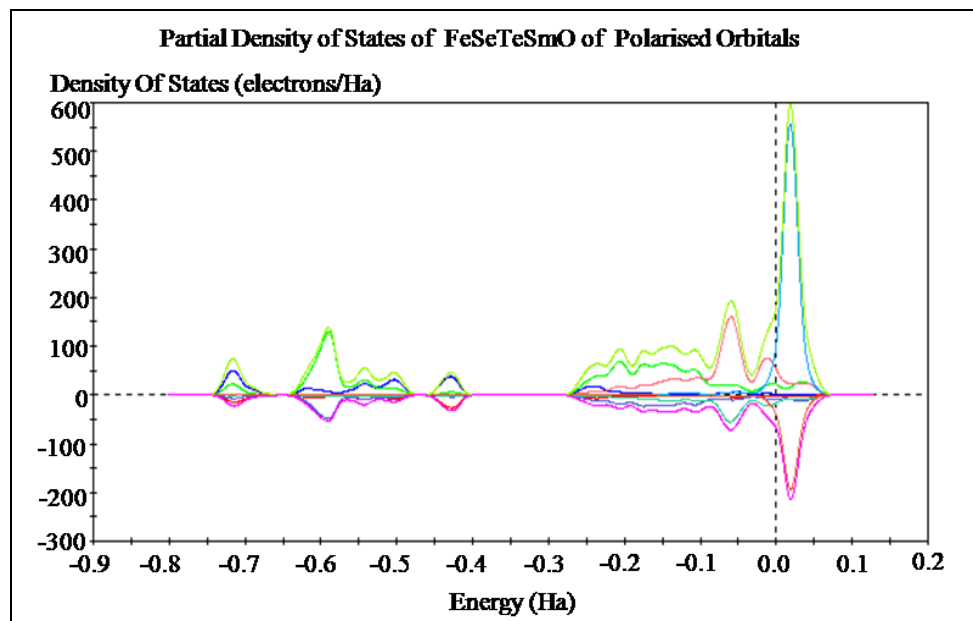


FIGURE 6.15.
The DOS of FeSeTeSmO for polarized orbitals.

6.2.4 FeTeSmO

In this lattice all of the Se sites have been occupied by the Te atoms and there is no Se at all. There are 4 tellurium atoms on the Se sites and 4 Sm atoms are also on the Se sites. The oxygen atoms are on Fe antisites as shown in Fig. 16. The lattice constants are $a = 4.3327\text{\AA}$ and $c = 6.1340\text{\AA}$. The coordinates are given in Table 6.8 and the gap energies are given in Table 6.9.

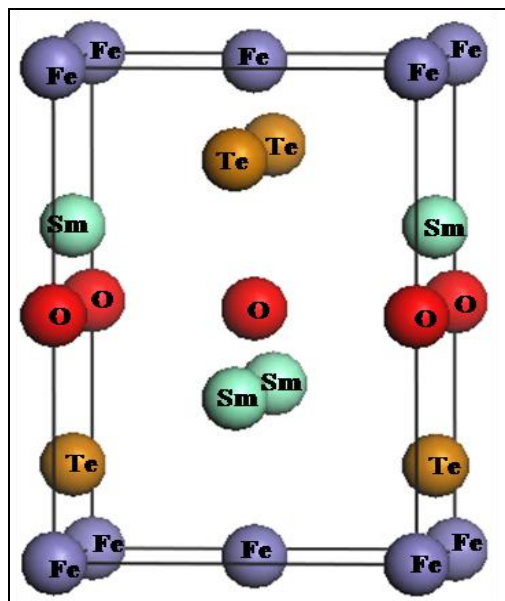


FIGURE 6.16.
The unit cell of FeTeSmO stack of atoms.

Table 6.8. The coordinates of FeTeSmO atoms in a unit cell.

Atoms	Coordinates				
Fe	0, 0, 0	1, 0, 0	0, 1, 0	1, 1, 0	0.5, 0.5, 0
Te	0, 0.5, 0.184	0.5, 0, 0.816	1, 0.5, 0.184	0.5, 1, 0.816	
O	0, 0, 0.5	1, 0, 0.5	0, 1, 0.5	1, 1, 0.5	0.5, 0.5, 0.5
Sm	0.5, 0, 0.334	0, 0.5, 0.666	0.5, 1, 0.334	1, 0.5, 0.666	

Table 6.9. The band gap energies at various k points

<i>K- point</i>	<i>Coordinate</i>	<i>Energy gap (eV)</i>	
		<i>unpolarized</i>	<i>Polarized</i>
Z	0, 0, 0.5	0.9660	0.9660
A	0.5, 0.5, 0.5	0.9578	0.9197
M	0.5, 0.5, 0	1.0394	0.9959
G	0, 0, 0	0.7020	0.6857
Z	0, 0, 0.5	0.9741	0.9606
R	0, 0.5, 0.5	0.1578	0.3048
X	0, 0.5, 0	0.3945	0.3836
G	0, 0, 0	0.7020	0.6857

The unpolarised Fermi energy is -3.692eV and the polarised value is -3.864eV. The transition temperature increases by doping FeSe with Te and Sm.

Table 6.10. Fermi energy decreases upon doping with Te and Sm atoms

S. No	Formula	Unpolarised (eV)	Polarised (eV)
1	FeSeSmO	-7.897	-8.062
2	Fe ₂ SeSm ₂ O ₂	-4.154	-4.240
3	FeSeTeSmO	-3.849	-4.008
4	FeTeSmO	-3.692	-3.864

It is seen that there is a systematic decrease in the magnitude of the Fermi energy upon adding the Te and Sm atoms. The binding energy is -74.291eV for unpolarised orbitals and -75.731eV for the polarised orbitals. The effect of polarization of the orbitals on the binding energy is thus quite small. The unpolarised band structure is given in Fig. 6.17 and the polarised band structure is given in Fig. 6.18. The corresponding DOS is given in Figs. 6.19 and 6.20. It is seen in Table 6.9 that at most of the k points the polarised and the unpolarised band gap differ by a small amount except that at the R (0, 0.5, 0.5) point, where the effect is very large.

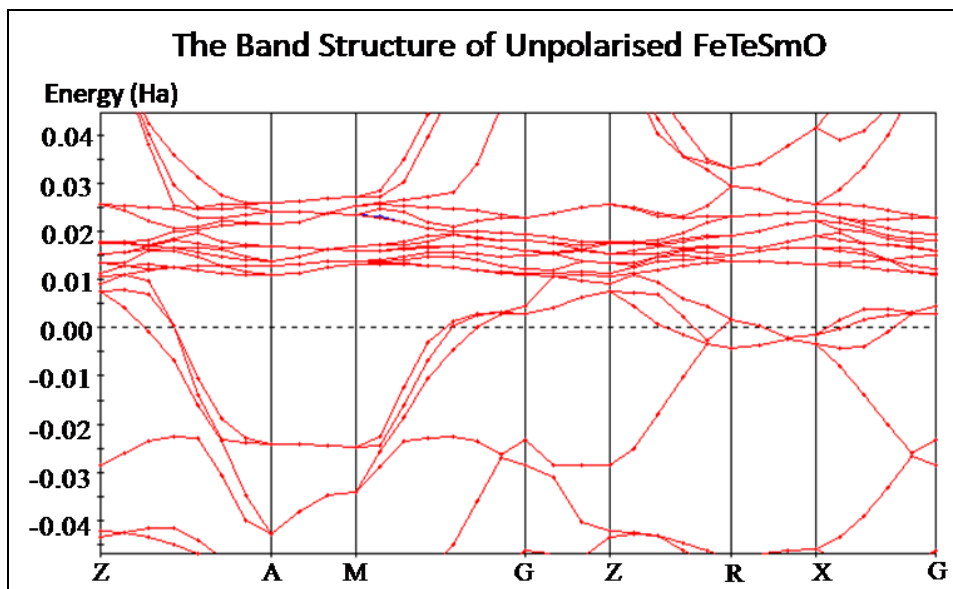


FIGURE 6.17.
The band structure of FeTeSmO calculated by using unpolarised orbitals.

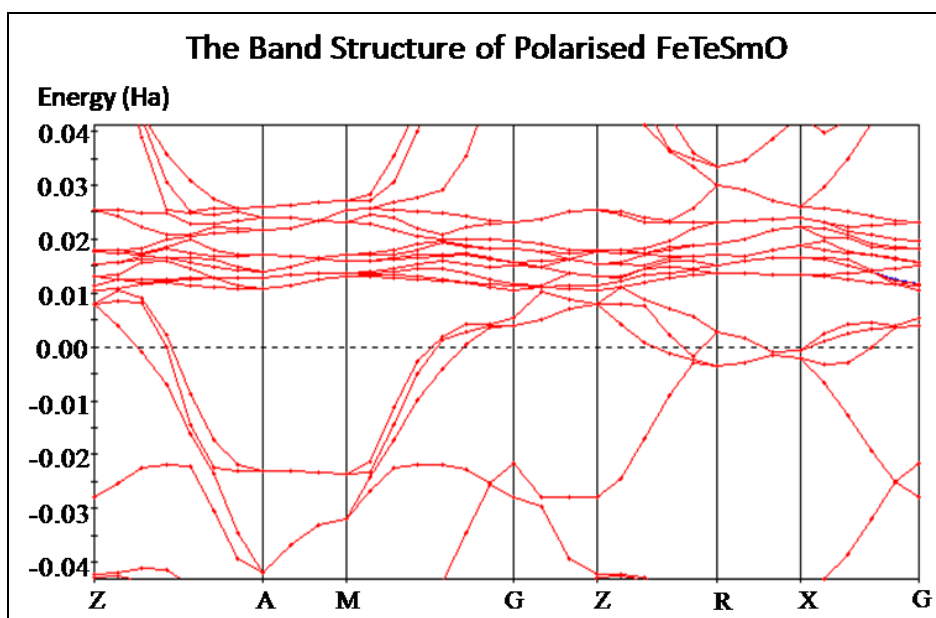


FIGURE 6.18.
The band structure of FeTeSmO calculated by using polarised orbitals.

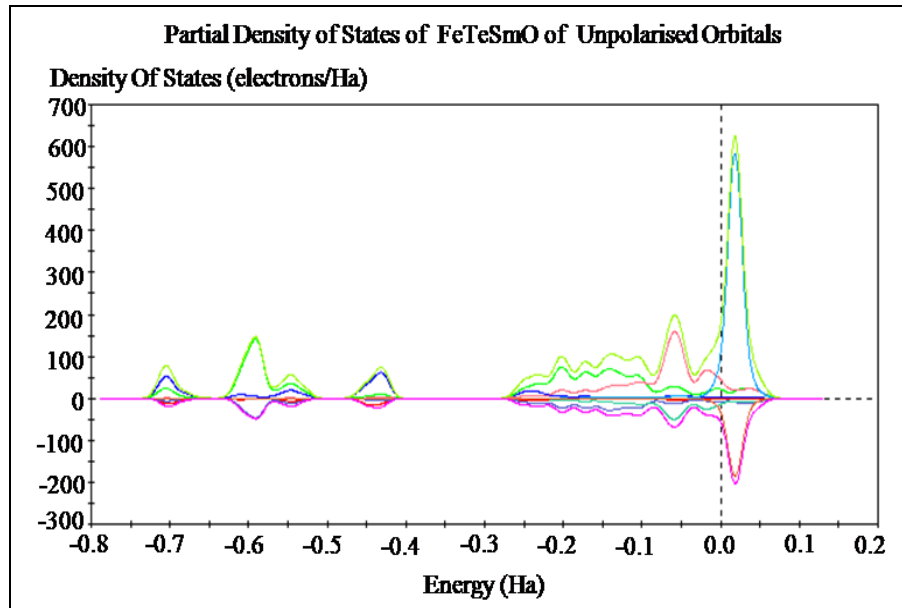


FIGURE 6.19.
The DOS of FeTeSmO for unpolarized orbitals.

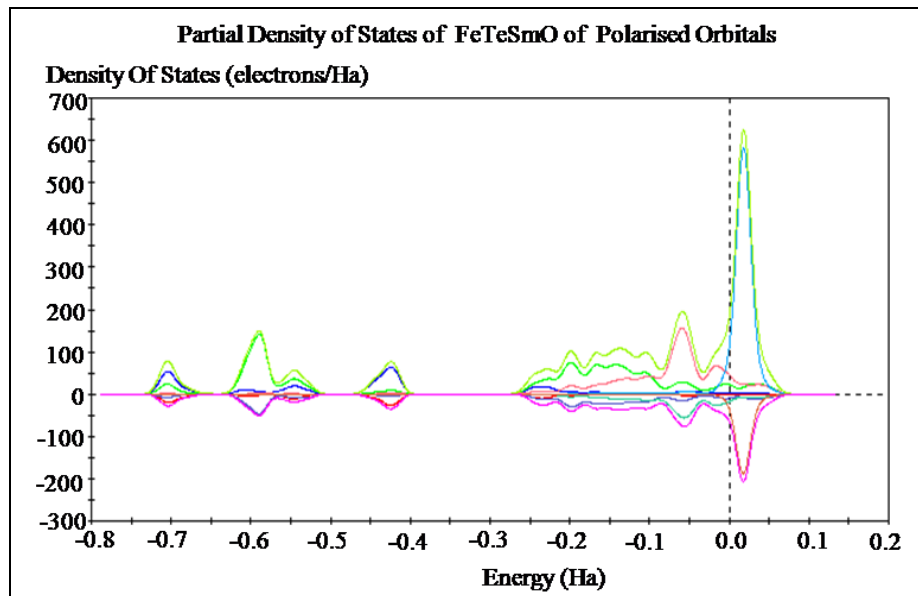


FIGURE 6.20
The DOS of FeTeSmO for polarized orbitals.

SECTION 6.4

Conclusions

We have calculated the band structure of several FeSe based compounds. Those compounds are superconducting with their transition temperature increasing with the addition of Te, O and Sm atoms. We find that (i) the magnitude of the normal state energy gap reduce upon doping FeSe with these atoms. (ii) The Fermi energy also reduces when the additional atoms are mixed. The normal state gap thus indicates the increase in the transition temperature. The increase in the transition temperature is achieved by doping which is not a characteristic of translational symmetry needed for the B.C.S. theory [18].

CHAPTER 7

CONCLUSIONS

Chapter 1 gives an overview of superconductivity by first giving the historical background on the development of superconductivity from the discovery of Onnes in 1911 in section 1.1 and section 1.2. The theoretical explanation of the mechanism such as the Meissner effect and the BCS theory in the superconducting material is thus explained. The chapter is closed with a brief discussion on the general application of superconductors in today's industry. Section 2 in this chapter explains the ab initio calculation method used to calculate the energy gap in this research. In this chapter, the development of the density functional theory (DFT) is explained by first looking at the initial approach made by the Hartee-Fock approach by explaining the interaction of single electrons. The approach was then corrected by the Hohenberg-Kohn theorem by using many-body system and was successfully modelled by Kohn-Sham approach by using a system of interacting particles. The exchange-correlation was then discussed together with the local density approximation (LDA) and the generalised gradient approximation (GGA).

The materials studied in this research are reported from chapter 2 to chapter 6. In chapter 2, the unit cell of FeSe and that of Fe:Se = 2:1 are studied. The energy gap for FeSe lattice and Fe:Se = 2:1 lattice were obtained from the calculation and was compared. It was found that the energy gap for the Se deficient cell is smaller compared to the FeSe lattice. There is a small change in the density of states due to weak magnetization. The effect of spin polarization upon the reduction of Se atoms is very small, giving only 1.2% of change. The reduction in normal state energy gap as well as the spin effect induces superconductivity in the Se deficient lattice. Upon studying the results obtained from the polarised and unpolarised calculation there were changes in band gaps and Fermi level, but there were no significant effects on spin on the band diagram (splitting of bands forming the spin up and spin down bands). However, there upon polarization, the band gap of FeSe between Z and A point vanishes. Whereas, there is a crossing phenomenon upon polarisation in FeSe = 2:1 along the F point.

The Meissner effect is explained in chapter 3 by studying several superconducting iron-based compounds, namely Fe₂SeTe, Fe₈Se₆ and Fe₈Se₆Te₂ with Fe:Se = 8:8 lattice as the reference. The energy gap obtained from the calculation shows a decrease in normal state energy in Fe₂SeTe, Fe₈Se₆ and Fe₈Se₆Te₂ compared to the pure FeSe lattice. This gives an indication of the increase in the superconducting transition temperature with the reduced energy gap. In this chapter, the inclusion of the effect of mass density in the Meissner effect was suggested to explain the incomplete Meissner effect in the iron-based superconductor. This chapter also shows that doping and non-stoichiometry compounds are important for the mechanism of the high-temperature superconductor as found by Bednorz and Muller and the periodic symmetry is relatively not so important. Hence, the BCS theory which explains according to the periodic symmetry is currently not relevant in the present compounds.

The FeSe based superconductor was also found to superconduct upon oxidation. In chapter 4, the oxidation of FeSe was studied by placing the oxygen atoms at the Se vacancies forming $\text{Fe}_8\text{Se}_6\text{O}_2$ and $\text{Fe}_8\text{Se}_4\text{O}_4$. By taking the polarised calculation, the binding energy calculated for $\text{Fe}_8\text{Se}_6\text{O}_2$ is -137.43eV and -109.78eV for $\text{Fe}_8\text{Se}_4\text{O}_4$. It is seen that upon increasing the number of oxygen atoms, the binding energy is reduced. A weaker bond gives a higher transition temperature. Similarly in chapter 5, the energy gap for FeSeTe varies from 0.250 at point G to 0.395 at point Z. Whereas, the energy gap for FeSeTeO reduced to 0.046eV at point G and 0.329eV at point Z. The oxidation in FeSeTe compound gives a reduction in normal state gap which gives an increase in transition temperature.

In chapter 6, the lattices of FeSe, FeSeTe and FeSe with layers of samarium oxide sandwich in between were built and the band structure for each compound was calculated. It was found that there is a reduction of the normal state energy gap upon doping the FeSe lattice with samarium and tellurium atoms. The reduction in the normal state energy gap indicates the increase in the superconducting transition temperature.

In the research done on different compounds of FeSe structure above, in all cases, the normal state gap reduces upon doping. The normal state energy gap reduces when Se atoms are removed from FeSe lattice. Similarly, doping of FeSe lattice with oxygen atoms, tellurium atoms, and samarium atoms reduces the normal state gap. This shows that upon removing Se atoms and doping, the magnetic effect of Fe atoms is reduced by reducing the scattering of electrons belonging to Fe and the compound becomes a diamagnetic. This explains the superconductivity in the FeSe superconductor. This transition cannot be explained by the B. C. S. theory. Hence, the BCS theory does not

successfully explains the conduction in the iron-based superconductors. The reduction in energy gap increases the superconducting transition temperature.

There are also visible changes in the binding energy of FeSe, FeTe and FeSeTe lattices upon oxidation. The binding energy weakens as the number of oxygen atoms increases. This also causes the transition temperature to increase in FeSe superconductor. Upon comparing the computational results obtained with the experimental results, the reduction of energy gaps agrees with the superconducting state. However, the susceptibility obtained by the experimental results does not agree with the Meissner susceptibility of $-1/4\pi$. Hence, this report suggests that there are small fields trapped in the superconductor instead of zero fields. This suggests that the superconductivity of iron-based superconductor is distinguished by the incomplete Meissner effect.

This thesis, reports the calculation of band structure of several iron based superconductors. The structures are successfully optimized for the minimum energy of the Schrödinger equation. In all of the cases, the normal state band gaps at various zone wave vectors are calculated. The Fermi energy is calculated in all of the systems and the binding energy has been calculated. The effect of doping as well as that of the vacancies has been determined. There were no significant changes upon polarisation in the density of states obtained. This is due to the low magnetization of the iron based superconductors. The usage of LDA and GGA approach in solving the DFT may underestimate the exact value of the calculated band gaps; however it is sufficient to make comparisons for the changes of the energy gaps upon doping in the iron based superconductors.

LIST OF PUBLICATIONS

- [1] Teh Yee Lin, Lee Li Ling, Hasan Abu Kassim and Keshav N. Shrivastava
"Electron energy bands in graphene,
3rd MPSGC, p4py-1, p.201-204(2007).

- [2] Teh Yee Lin, H. A. Kassim and K. N. Shrivastava,
DFT Computation of the Electronic Band Structure of FeSe,
AIP Conf. Proc. **1169**, 283-288(2009).
SCOPUS

- [3] Teh Yee Lin, H. A. Kassim and K. N. Shrivastava,
Density-Functional Theory Computation of Oxidation of FeSe
AIP Conf. Proc. (under publication).
SCOPUS

- [4] Teh Yee Lin, H. A. Kassim and K. N. Shrivastava
The Meissner effect and the normal state gap in FeSe based superconductors.
Materials Chem. Phys. (Elsevier) (SUBMITTED)
ISI Web of Science.

Conferences:

- (a) DFT Computation of the Electronic Band Structure of FeSe,
AMNRE Jakarta, June 2009.

- (b) DFT Computation of Oxidation of FeSe
PERFIK2009.

REFERENCES

- [1] J.G. Bednorz and K.A. Mueller, *Z. Phys.* **B64** (2), 189–193 (1986)
- [2] Hiroki Takahashi, Kazumi Igawa, Kazunobu Arii, Yoichi Kamihara, Masahiro Hirano, Hideo Hosono, *Nature* **453**, 376–378 (2008).
- [3] A. Subedi, L. Zhang, D. J. Singh and M. H. Du. *Phys. Rev. B* **78**, 134514(2008)
- [4] F. C. Hsu, J. Y. Luo, K. W. Yeh, T. K. Chen, T. W. Huang, P. M. Wu, Y. C. Lee, Y. L. Huang, Y. Y. Chu, D. C. Yan, and M. K. Wu, *PNAS*, **105**, 38 (2008)
- [5] K.-W. Lee, V. Pardo and W. E. Pickett, *Phys. Rev. B* **78**, 174502 (2008)
- [6] T. Imai, K. Ahilan, F. L. Ning, T. M. McQueen and R. J. Cava, *Phys Rev Lett.* **102** (2009).
- [7] R. Khasanov, K. Conder, E. Pomjakushina, A. Amato, C. Baines, Z. Bukowski, J. Karpinski, S. Katrych, H.-H. Klauss, H. Luetkens, A. Shengelaya and N. D. Zhigadlo, *Phys. Rev. B* **78**, 220510 (2008).
- [8] H.K. Onnes, *Commun. Phys. Lab. Univ. Leiden* **12**, 120 (1911)
- [9] W. Meissner and R. Ochsenfeld, *Naturwiss.* **21**, 1787 (1933)
- [11] J. Bardeen, L.N. Cooper, and J.R. Schrieffer, *Phys. Rev.* **108**, 1175–1205 (1957)
- [10] V.L. Ginzburg and L.D. Landau, *Zh. Eksp. Teor. Fiz.* **20**, 1064 (1950).
- [12] D. R. Hartree. *Proc. Cambridge Philos. Soc.* **24**, 89(1928).
- [13] P. Hohenberg and W. Kohn, *Phys. Rev.* **136**, 8864 (1964).
- [14] W. Kohn and L. J. Sham, *Phys. Rev.* **137**, 1697-1705 (1965)
- [15] W. Kohn and L. J. Sham, *Phys. Rev.* **140**, 1133-1137 (1965).

- [16] L. J. Sham and W. Kohn, Phys. Rev. **145**, 561-567 (1966).
- [17] W. Kohn, Rev. Mod. Phys. **71**, 1253-1265 (1998).
- [18] K. N Shrivastava, Superconductivity: Elementary Topics, World Scientific, Singapore, 2000.
- [19] K. Sasmal, B. Lv, B. Lorenz, A. M. Guloy, F. Chen, Yu-Yi Xue and Ching-Wu Chu, Phys. Rev. Lett. **101**, 107007(2008).
- [20] P. Richard, T. Sato, K. Nakayama, S. Souma, T. Takahashi, Y.-M. Xu, G. F. Chen, J. L. Luo, N. L. Wang and H. Ding, Phys. Rev. Lett. **102**, 047003(2009).
- [21] A. S. Sefat, M. A. McGuire, B. C. Sales, R. Jin, J. Y. Howe and D. Mandrus, Phys. Rev. B **77**, 174503(2008).
- [22] Jian-Ping Lv and Qing-Hu Chen, Phys. Rev. B **78**, 144507(2008).
- [23] P. J. Baker, H. J. Lewtas, et al, Phys. Rev. B **78**, 212501 (2008).
- [24] B. C. Sales, A. S. Sefat, M. A. McGuire, R. Y. Jin, D. Mandrus and Y. Mozharivskyj, Phys. Rev. B **79**, 094521 (2009)
- [25] T. Imai, K. Ahilan, F. L. Ning, T. M. McQueen and R. J.Cava, Phys. Rev. Lett. **102**, 177005 (2009)
- [26] K. -W.Lee, V. Pardo and W. E. Pickett, Phys. Rev. B **78**, 174502 (2008)
- [27] D. Phelan, J. N. Millican, E. L. Thomas, J. B. Leao, Y. Qiu and R. Paul, Phys. Rev. B **79**, 014519 (2009)
- [28] K. N. Shrivastava, Phys. Lett. A**188**, 182. (1994)
- [29] K. N. Shrivastava, Solid State Commun. **90**, 589 (1994)
- [30] N. M. Krishna, L. S. Lingam, P. K. Ghosh and K. N. Shrivastava, Physics C **29**, 4243 (1998)
- [31] M. Sigrist and T. M. Rice, Rev. Mod. Phys. **67**, 503 (1995)
- [32] J. H. Tapp, Z. Tang, B. Lv, K. Sasmal, B. Lorenz, P. C. W. Chu and A. M. Guloy, Phys. Rev. B **78**, 060505 (2008).
- [33] M. Rotter, M. Tegel and D. Johrendt, Phys. Rev. Lett. **101**,107006 (2008).

- [34] Y. Kamihara, M. Hirano, H. Yanagi, T. Kamiya, Y. Saitoh, E. Ikenaga and K. Kobayashi, *Phys. Rev. B* **77**, 214515 (2008).
- [35] K. Sasmal, B. Lv, B. Lorenz, A. M. Guloy, F. Chen, Yu-Yi Xue and C. W. Chu, *Phys. Rev. Lett.* **101**, 107007 (2008)
- [36] D. Lopez-Duran, M. P. de Lara-Castells, G. Delgado-Barrio, P. Villarreal, C. Di Paola, F. A. Gianturco and J. Jellinek *Phys. Rev. Lett.* **93**, 053401 (2004)
- [37] K. A. Mueller, *J. Phys.:Condens. Matter* **19**, 251002 (2007)
- [38] Teh Yee Lin, H. A. Kassim and K. N. Shrivastava, *AIP Conf. Proc.* **1169**, 283-288 (2009)
- [39] U. Shiliang et al, *Phy. Rev. B* **79**, 054503 (2009)
- [40] M. H. Fang, H. M. Pham, B. Qian, T. J. Liu, E. K. Vehstedt, Y. Liu, L. Spinu and Z. Q. Mao, *Phys. Rev. B* **78**, 224503 (2008)
- [41] S. Li, C. De la Cruz, Q. Huang, Y. Chen, J. W. Lynn, J. Hu, Yi-Lin Huang, Fong-Chi Hsu. Kuo-Wei Yeh, Maw-Kuen Wu and P. Dai, *Phys. Rev B* **79**, 054503 (2009)
- [42] B. Lorenz, K. Sasmal, R. P. Chandhury, X. H. Chen, R. H. Liu, T. Wu and C. W Chu, *Phys. Rev. B* **78**, 012505 (2008)
- [43] L. Ding, C. He, J. K. Dong, T. Wu, R. H. Liu, X. H. Chen and S. Y. Li, *Phys. Rev. B* **77**, 180510 (2008)
- [44] R. Prozorov et al, *Phys. Rev. Lett.* **93**, 147001 (2004)
- [45] B. W. Lee, et al, *Phys. Rev. B* **37**, 2368 (1988)
- [46] G. Zhong, et al, *Phys. Rev. B* **79**, 094424 (2009)
- [47] Y. Kamihara, et al, *Phys. Rev. B* **78**, 184512 (2008)
- [48] A. Dubroka, et al, *Phys. Rev. Lett.* **101**, 097011 (2008)